NTNU – Trondheim
Norwegian University of
Science and Technology

Modelling and optimization of a Gas-to-Liquid plant

Kristine Tomte Knutsen

Chemical Engineering and Biotechnology
Submission date: June 2013
Supervisor: Magne Hillestad, IKP
Co-supervisor: Paris Klimantos, IKP

Norwegian University of Science and Technology
Department of Chemical Engineering

Preface

This thesis on Optimization of a Gas-to-Liquid plant is the result of the work conducted during the fifth year master course in Chemical Engineering at the Norwegian University of Science and Technology (NTNU).

I would like to thank my supervisor, Professor Magne Hillestad for all his help, encouragement and valuable discussions along the way. I would also like to thank Professors Hilde Venvik, Edd Blekkan and Hallvard Svendsen for taking the time to discuss various topics and give input.

I declare that this is an independent work according to the exam regulations of the Norwegian University of Science and Technology(NTNU).

Kristine Tomte Knutsen

Date, Place

Abstract

This thesis investigates the operational performance and optimization of a Gas-to-Liquid plant based on autothermal reforming (ATR) and a multi tubular fixed bed (MTFB) reactor together with a cobalt catalyst. This is achieved through simulation of the process in Unisim Design R400. The simulations were based on a feed designed for a 17000 $\frac{bbl}{d}$ train and does not incorporate the upgrading unit. The work is divided in three main sections; parameter study, optimization on syncrude flow, carbon- and thermal efficiency and optimization with consideration to economics including heat integration through pinch analysis. The optimized process was found to produce 19940 $\frac{bbl}{d}$ of syncrude with a carbon efficiency of 82.41% and thermal efficiency of 65.93%, when not taking economics into consideration. The inclusion of economics changed the operational optimum to a syncrude production of 18620 $\frac{bbl}{d}$ and efficiencies of 77.25% and 61.77% respectively. Ultimately a production cost of 16.10 $\frac{USD}{bbl}$ and revenue of 59.89 $\frac{USD}{bbl}$ was obtained. With current crude oil price at 98.90 $\frac{USD}{bbl}$ it indicates a good economical environment for the Gas-to-Liquid process.

Contents

Chapter 1

Introduction

The energy demand in the world is continuously increasing and from 2011 to 2012 it increased with 2.5% [1]. The single most important energy source is oil and contributes with 33.1% of the overall energy needed [1]. However oil is a finite energy resource, meaning it will run out at a future point. Exactly when that will occur is a debated topic and subject to projections based on consumption rates. The International Energy Agency, IEA, projects the oil to peak earliest in 2035, based on the current consumption rates, however a study by Sorrell et al. indicates risks of it peaking before 2020 while Rajab Khalilpour and I.A. Karimi states that the peak is already past [2, 3, 4]. Nevertheless with the increase in energy demand and reduction in the most important source it becomes evident that there is a need for alternative fuels. With oil being the feed stock used for production of transportation fuels this sector will be especially affected [5].

Gas-to-liquids, GTL, is a process that can provide an alternative for the conventional petrochemical transportation fuels, by substitution with synthetic fuels derived from the Ficher-Tropsch process[6, 7, 8, 5]. The GTL process is based on the Fischer-Tropsch reaction and the process was first applied for coal as feed stock in Germany during the 1920's and 1930's [9]. The main principle is conversion of natural gas to syngas in a reforming step, followed by a conversion to long chained hydrocarbons through the Fischer-Tropsch reaction. Finally, the long chained hydrocarbons are cracked into products with desired chain length in an upgrading unit [10, 11].

The fuels produced with the GTL technology is considered to outper-

form traditional fuels due to higher cetane number and less or no sulphur, NO_x, particulates and aromatics present[10, 12]. Another major advantage is its ability to be used in existing fuel systems and in combination with traditional fuels [7, 10, 12]. The increased interest for GTL is also contributed to its potential for monetizing stranded gas, a resource previously considered lost. The increasingly stricter legislation on flaring and re-injection also provides increased potential for GTL in handling of this gas.

Natural gas is an abundant energy resource and even though GTL offers many potential promising possibilities, there are only a few commercial plants to date [1, 10]. This is related to the conception of GTL being an expensive process and highly dependent on the price of crude oil, consequently making it risk associated [13]. Current estimates indicate $20\frac{USD}{bbl}$ in crude oil price for GTL to be an alternative economically[14]. In addition to directly competing with petroleum based products the natural gas feed stock might also in some cases be considered more suitable for other processing routes such as LNG, which provides a higher utilization of the feedstock[8]. Nevertheless there is an increased commercial effort in GTL with Qatar playing a major role. The two latest, and to date, largest GTL plants are located here with three of the most important industrial players, Shell, Sasol and Qatar Petroleum represented. There is also a large GTL plant coming on line in Nigeria during 2013 [12].

For GTL to become even more competitive it is important that the process is as close to optimal as possible both in terms of efficiencies and economics. This is closely related to operating conditions, but also as to choice of main processing steps in the process, such as reformer technology, reactor type and catalyst, as they result in somewhat different products and process performances.

Chapter 2

Natural gas as a resource

2.1 Natural Gas

Natural gas is a nontoxic, odourless and colorless gaseous mixture of hydrocarbons consisting mainly of methane[15]. However ethane, butane and propane is usually also present in various degrees, depending on the origin of the natural gas [15, 16]. Table 2.1 gives an overview over the compounds normally found in natural gas and to what extent they are present.

Table 2.1 – Overview over the percentage component distribution normally found in natural gas[17]

Component	Formula	Percentage
Methane	CH_4	70-90
Ethane	C_2H_6	0-20
Propane	C_3H_8	
Butane	C_4H_{10}	
Carbon Dioxide	CO_2	0-8
Oxygen	O_2	0-0.2
Nitrogen	N_2	0-5
Hydrogen Sulphide	H_2S	0-5
Rare gases	A, He, Ne, Xe	trace

Natural gas is a fossil fuel and there exist a range of different theories on how fossil fuels are formed, however the organic or thermogenic formation is the most widely accepted one [18, 19]. This theory explains the formation of fossil fuels as plant and animal material that has decayed for millions of years in an environment with high temperatures and pressures [19]. During this process, the carbon molecules degrades into hydrocarbon compounds which can lead to the formation of oil and gas if the accumulated volumes are large enough [19]. The ratio of the formation of oil versus gas is dependent on temperature, pressure and the duration of time at these conditions[18]. Figure 2.1 shows an illustration over probable locations of the different fossil fuels as a function of depth and temperature [18]. The temperature increases with increasing distance beneath the ground and at higher temperatures the formation of gas is generally preferred over the formation of oil[17]. In a very simplified generalization, it can be said that oil and gas is different stages of the same process [18]. All sedimentary rocks able to form oil is also able to form natural gas and it is at these locations the natural gas is referred to as associated gas, which is further explained later in this chapter. However not all sedimentary rocks able to form natural gas can also produce oil and in these sites the gas is classified as non-associated natural gas [18].

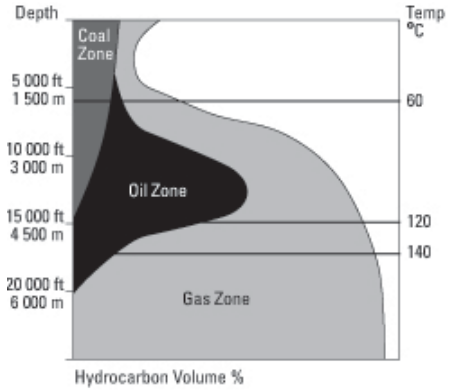

Figure 2.1 – Illustration of the most probable location for coal, oil and gas as a function of depth and temperature [18]

2.1.1 Classifications

Natural gas can be divided into different subclasses based on the location of the reservoir, its composition and its characteristics. Based on location one primarily differs between conventional and unconventional natural gas. The

conventional gas is characterized as being economically feasible to extract and easily accessible [19]. It can further be classified as either associated or non-associated depending on whether the gas is found at the same reservoir as oil or the reservoir is pure natural gas respectively [20]. Unconventional gas is recognized by being more difficult to extract and less accessible with current technology. At present it is commonly divided into four subclasses dependent on its reservoir qualities; shale gas, coal bed methane (also known as coal seam gas), tight gas and methane hydrates [21, 19]. Shale gas is gas trapped between layers of impermeable sedimentary shale rocks, whereas coal bed methane is methane located at the seams of coal deposits underground. Tight gas is characterized by it being trapped under various impermeable rock formations and methane hydrates, can be found in ocean sediments and permafrost areas in the Arctic[19]. However as technology develops, what is recognized as unconventional today might be classified as conventional in the future[21, 19].

Further it is common to differentiate between various types of natural gas based on its chemical composition. Dry natural gas refers to natural gas of almost pure methane, often 95% or more, that does not produce much, or any, liquid when brought to surface [22]. When other hydrocarbons than methane are present, liquid hydrocarbons are usually produced during the production and hence it is referred to as wet gas. If the content of H_2S and/or CO_2 exceeds 1 and 2 vol% respectively, the gas is considered as sour. In the opposite case the gas is classified as sweet [20].

2.1.2 Locations, reserves and markets

It is impossible to state by certainty exactly how much natural gas that exist. As the technology continuously develops and the exploration of reserves expands, more natural gas is discovered [23]. However, there exists estimates for the proven reserves of natural gas and at the end of 2011 this estimates was 208.4 trillion cubic meters of natural gas on a world basis[1, 24]. Figure 2.2 shows the geographic location of these proven reserves. Russia is the country with the largest proven shares of the reserves with 21.4% of the global estimate followed by Iran with 15.9 %. On a regional basis, Europe, Eurasia and the Middle East together, has 76.2% of the total proven reserves in the world [1].

At the end of 2011 the annual consumption of natural gas in the world was reported to be 3222.9 billion m^3 [1]. The United States has the highest consumption with 21.5% followed by Russia with 13.2% [1]. It is conse-

Figure 2.2 – Display of the geographic location of the proven reserves of natural gas in m^3. [25]

quently not necessarily the regions with the largest reserves of natural gas that also are the largest consumers. This creates a market for selling natural gas and natural gas derived products. The distance from exploration to consumption is an important factor for the price and the technology applied to exploit these natural gas reserves. This will be further investigated in the following section.

Table 2.2 gives an overview over the markets for natural gas within consumption, export, imports and where the proven reserves are located.

Table 2.2 – Overview over the five largest countries within proven reserves, consumption, import and export of natural gas in the world [1]

Reserves		**Consumption**		**Imports (pipeline)**		**Exports (pipeline]**	
Country	**size** $[10^{18}\ m^3]$	**Country**	**size** $[10^{18}\ m^3]$	**Country**	**size** $[10^{18}\ m^3]$	**Country**	**size** $[10^{18}\ m^3]$
Russia	1575.0	United States	690.1	United States	88.1	Russia	207.0
Iran	1168.6	Russia	424.6	Germany	84.0	Norway	92.8
Qatar	884.5	Iran	153.3	Italy	60.8	Canada	88.0
Turkmenistan	858.8	China	130.7	Ukraine	40.5	Netherlands	50.4
United States	299.8	Japan	105.5	Turkey	35.6	United States	40.7

2.2 Natural gas processing, production alternatives and GTL's market position

Natural gas is a very versatile feedstock and there is a range of possible processing routes after the gas has been extracted. It can be transported as gas through pipelines, volumetrically reduced to liquefied or compressed natural gas or be chemically converted. The scenario of stranded gas has also prompted increased research in new technologies and will be elaborated further in this section. Which one of these alternatives that are chosen however depends on a range of factors among distance from extraction point to market, quality and volume of the gas. This section aims to give an overview over the various processing alternatives and where their application is desirable.

2.2.1 Conventional natural gas

For the easily accessible natural gas there are three main processing options, pipeline, liquefied natural gas and chemical conversion.

Pipeline

Trade and transportation of natural gas was in the start limited to pipelines and trade between neighbouring countries[4]. Today there exists a range of transportation alternatives, however pipeline is still the most used transportation technology, and onshore it is also the most effective way to transport natural gas [26]. Offshore however, pipelines are limited as its cost is ten times the onshore cost, and in addition distance to market, depth, and underwater terrain offers great challenges for this type of technology[26].

Liquefied natural gas, LNG

During the 1960's other transportation alternatives than pipeline was explored as a consequence of an energy shortage in countries remote from supply sites, such as Japan [4]. This lead to the development of a transportation technology where the natural gas was liquefied before transportation. This technology is today known as liquefied natural gas, LNG, and is principally a reduction in the volume of the gas by a factor of 600 [27]. This is accomplished by cooling the gas to -159 to -162 °C at atmospheric pressure[28, 29]. This allows larger volumes of gas to be transported over longer distances by the use of special LNG tankers [27]. Hence it became economically possible

to ship natural gas to locations where pipeline either was uneconomically or technologically difficult[4]. The main market for LNG trade has traditionally been the Far East, and especially Japan, which is responsible for over half of the annual LNG trade[30, 8].

Chemical conversion

Both pipeline and LNG technology is mainly focused on the natural gas market, however there is also an option to chemically convert the natural gas and target other markets [27]. One of a range of possibilities is to target the transportation fuel markets as an utilization alternative or as part of a diversified production portfolio[11]. Gas to liquid, or commonly abbreviated GTL, is such a process. The natural gas is first converted to syngas through a reforming step and then further processed to Fischer Tropsch products, which are hydrocarbons of various chain length normally sold as LPG, naphta, gasoline, diesel and wax[31]. The products produced are however dependent on the production method and the range of alternative ways to produce Fischer Tropsch products through GTL are outlined in Chapter 4.

The GTL products are sold in the transportation fuel market and competes with traditional fuels made from refinery oil and petrochemicals [8]. The technology for GTL has been available and in use for coal, CTL, as a feedstock since 1920's, nevertheless GTL experiences an increased interest today and in particular for natural gas as feedstock. There are several reasons for this.

First, it is believed that the crude oil industry is close to or already has past its peak[2, 3, 4]. Considering that this is the primary source of transportation fuels today, and that the demand is not declining, there will eventually be a need for alternative transportation fuels [5, 13]. Second, it is desired to use more environmentally friendly fuels to try to slow down global warming and reduce the environmental impacts on air quality [10].

Low temperature Fischer Tropsch process maximizes the production of GTL diesel, which is a fuel with qualities to satisfy the two challenges stated above [11]. This process can use both coal, CTL, and natural gas, GTL, as feedstock. Resources that at present exceeds the proven resources of crude oil with 25 and 1.5 respectively[13]. GTL hence offers a technology to pro-

vide fuels for a long time to come.

GTL diesel is also considered a very clean fuel, with no sulphur content, low aromatics content and lower emissions of hydrocarbons, CO, NO_x and particulates upon combustion, when compared to traditional diesel[32, 33]. In addition it has a superior cetane number compared to regular diesel with 70 and 45 respectively [13]. Essentially this means that GTL diesel has a higher energy density and performance than regular diesel [13]. It should however be mentioned that even though the actual fuel does give environmental benefits over traditional when combusted, the production process of traditional and GTL diesel have about the same pollution level [14].

GTL diesel can be blended with traditional petroleum products making it possible to transport with current technology without need for special tankers such as LNG requires [10]. Another advantage is its ability to be used in the current market and its infrastructure, supply systems and engines [7]. Consequently a transition between traditional diesel and GTL diesel could be carried out without extra incurred costs. This gives it a large advantage compared to other alternative fuels that need different supply systems than those used today. With GTL diesel being blendable with products from crude oil, it also offers a possibility of upgrading low grade conventional diesel and hence an increased utilization of the crude oil based products[10]. GTL diesel hence offers a solution to both the expected fuel switch and the increased environmental concerns.

Viability of processing alternatives

Pipeline and LNG rarely compete for the same resources, as they serve the same markets and the difference in required investment is large [26, 34]. LNG is normally applied where it is technically or economically difficult to use pipeline. Generally it can then be said that pipeline is the main technology for large reserves at short distances, whereas LNG is considered to be the preferred option for large volumes at long distances [30].

GTL and LNG however serve different markets and are more similar in investment requirements, making the preferred choice a more complex matter[8]. In terms of industrial experience, LNG supplies the power sector and has been commercially applied for over 40 years, while GTL generally supplies the transportation fuel sector and large scale plants, based on nat-

ural gas, was not commissioned before late 1990's and early 2000's [8, 5, 27].

As with all technology development there are elements of risks. For LNG there are projections for the supply to exceed the demand in short to medium term and hence the market is very competitive [8]. This could drive down the price of LNG, potentially reducing the return of the investment. The market for GTL diesel however is considered to be unhindered as there is a very large, and increasing, demand for diesel products, and with GTL having superior environmental properties and it being a small player in the large transportation fuel market it does not risk oversupply [8, 4]. However the price of GTL diesel and the profitability of the GTL process is highly dependent on the crude oil price [5, 13]. As the GTL products directly compete with oil and refinery products a low oil price could drive down the price of GTL products and consequently reduce the investment return[8]. From a historical perspective, as will be outlined in Chapter 3, the oil price can directly determine the viability of the plant as the construction takes time and the market environment can change in the meantime. The estimates for profitability for GTL as a function of crude oil price varies some depending on source, but nevertheless a crude oil price above $20\frac{USD}{bbl}$ is considered the norm for GTL to be profitable [14]. Figure 2.3 shows the variation of crude oil price from 1960-2013[35]. It shows that the price has steadily been above $20\frac{USD}{bbl}$ since early 2000's even though the price has fluctuated. It can also be seen that the oil price has increased significantly from about year 2000, with exception of year 2008 when the price dropped significantly. Even though it dropped the lowest price was $41.3\frac{USD}{bbl}$ which still is well above the benchmark of $20\frac{USD}{bbl}$ for GTL profitability. After 2008 the price increased again and currently is at $98.9\frac{USD}{bbl}$[35]. Given the increased environmental benefits of GTL fuels compared to traditional fuels could also lead to a premium on these fuels, or potentially a tax on conventionally fuels, making it less dependent on crude oil prices and more economically favourable.

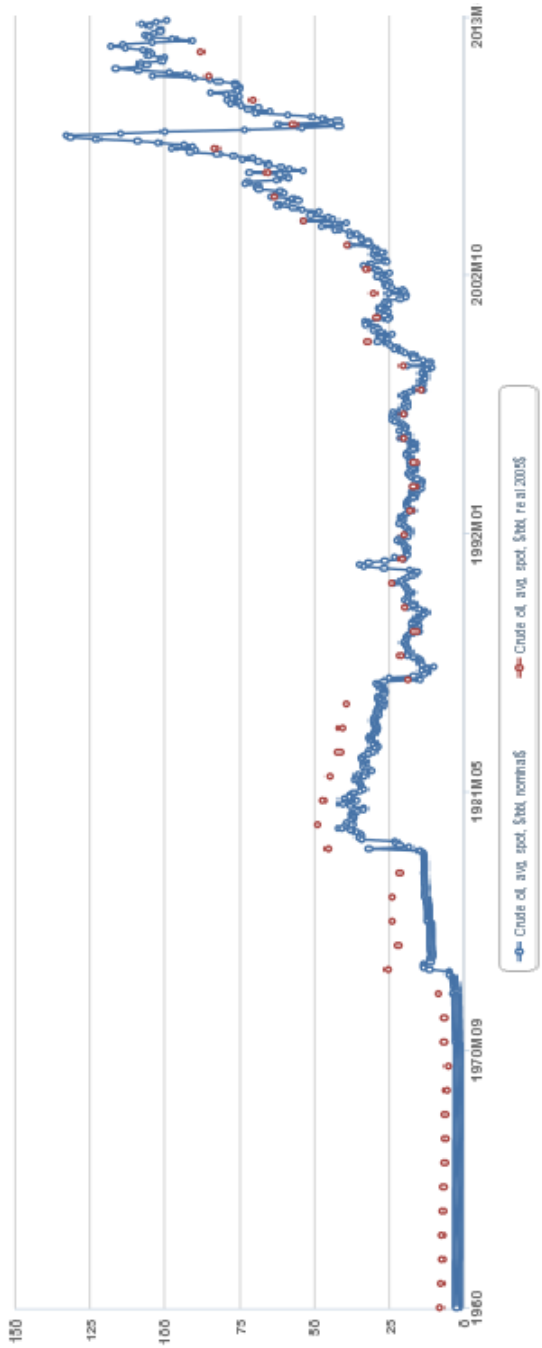

Figure 2.3 – Average spot price of crude oil from 1960-2013[35]

The two processes also differs from each other in complexity, with GTL being the most complex of the two [8, 27]. Besides the current market potential and complexity of the two plants the overall efficiencies are often also compared. LNG has a thermal efficiency of up to 92% whereas GTL is reported to have about 60% thermal efficiency. For carbon efficiency the numbers are 92 and 77% respectively (The efficiencies are defined in section 7.1)[14]. Hence the utilization of the feedstock is better in the LNG process than the GTL[8]. The capital cost for similar LNG and GTL plants are about equal and the choice of process is dependent on the current market situation for oil, GTL diesel and the power market respectively. This is outlined in Figure 2.4 which shows the profitability of LNG and large scale GTL as a function of natural gas prices and oil and refined petroleum prices [11]. From the figure it can be seen that the profitability of GTL is mainly dependent on a high oil price while LNG is more dependent on high natural gas prices.

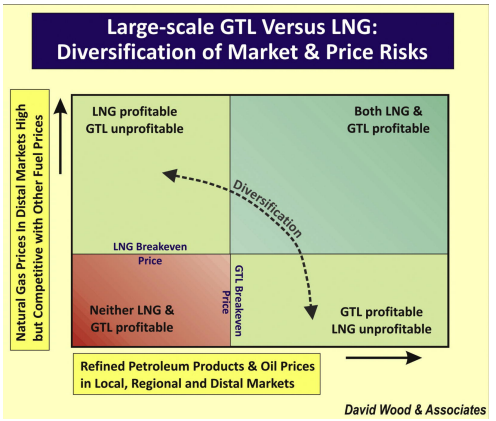

Figure 2.4 – Graphical display of the scenarios where LNG and GTL are considered the best option respectively, none of them are viable and where they can coexist as a function of natural gas price and oil and refinery prices [11]

2.2.2 Stranded gas

More than one third of the proven natural gas reserves are today considered as stranded natural gas[4, 11]. This refers to natural gas that is either located too far from existing markets and pipelines, or are too small to justify developing the reservoir from an economical or technical perspective[4, 8, 30, 34]. Figure 2.5 shows the geographical location of the

stranded gas, and as can be seen from the figure, the main locations are the Middle East, Europe and the Commonwealth of Independent States, CIS.

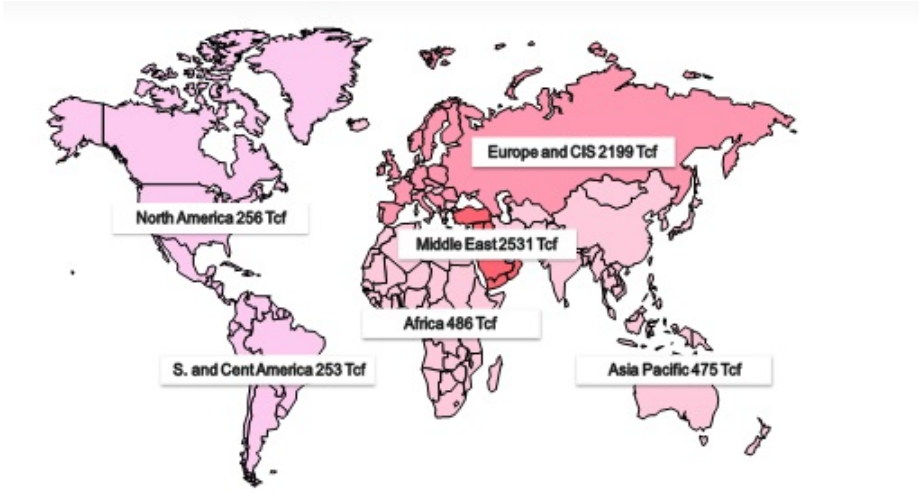

Figure 2.5 – Overview of the locations of stranded gas per region in trillion cubic feet[36]

The increased interest in stranded gas originates from two main perspectives. First, this gas represents a large energy resource and combined with increasing energy demand worldwide, assumed diminishing oil resources and more focus on environmentally friendly energy resources, it has become highly important to find options for utilizing this gas. Second, associated gas that previously were flared, vented or re-injected is now often subject to legislations, bans, environmental related taxes and penalties as a consequence of an increased knowledge of the environmental impact of flaring [4, 14]. Hence these practices are no longer an alternative and this type of stranded gas must be dealt with in a different manner. These two aspects has consequently lead to an increased commitment for the development of new technologies in an attempt to monetize these stranded gas reserves, both those that is an option to develop and those that are a necessity [14].

These "new" technologies include GTL, Compressed-Natural-Gas,CNG, Gas-to-wire, GTW, and Gas-to-solids, GTS. In addition to these new technologies LNG is also considered for stranded gas when the scale of the reservoir is large enough [30]. Figure 2.6 and Figure 2.7 outlines where each of the different natural gas processing technologies have their niche markets as a function of the distance to the market and the size of the production

and the following sections discuss their viability.

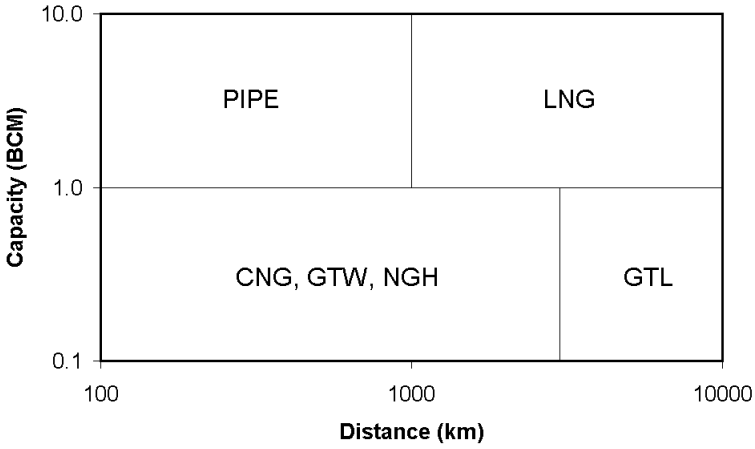

Figure 2.6 – Graphical display of competing technologies for natural gas processing as a function of capacity in BCM and distance in km. [30]

GTL

Many of the arguments for the use of GTL technology was outlined in section 2.2.1 for the purpose of large scale GTL produced from conventional gas. These are however also valid when considering GTL for the potential of monetizing stranded gas. Special interest for the case of stranded gas however is the potential of it being able to be shipped through the use of standard Clean Petroleum Product, CPP, vessels and mixing with crude oil or other petroleum products are considered unproblematic [4]. This eases the transportation process and as stranded gas often is located at associated gas fields this offers a great advantage for development of the oil present.

CNG

This technology is today in use for small scale applications such as buses and cars, but have not yet been tried out for large-scale projects[30]. This technology, like LNG, aims to reduce the volume of the gas for transportation purposes, but unlike LNG, CNG remains in the gaseous state [34]. CNG reduces the gas volume by a factor of 200 and is thereby not as effective in volume reduction as LNG, however it is considered a lot less costly and

hence could offer a potential for certain volumes and distance to market criteria, given it can be successfully scaled up from where it is today[34].

GTW and GTS

Gas to solids is a concept of transportation and storage of natural gas as hydrates and has been widely tested in laboratory and pilot plant scale. The development has however not continued past this point due to its complexity, costs and rate of hydrate formation[14].

Gas to wire is a technology that transforms the natural gas into electric power in high voltage DC transmission lines. Compared to other alternatives for stranded gas this is not yet competetive in cost or efficiency[14].

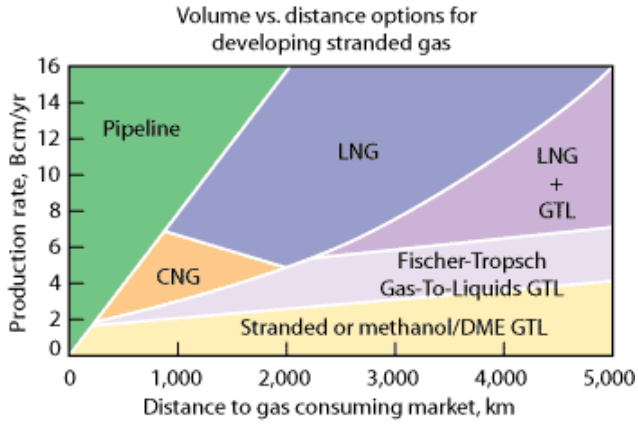

Figure 2.7 – Graphic outline of the optimal technology for monetizing stranded gas as a function of the production rate and distance to market[14]

From the discussion above it can be seen that there are multiple application routes based on natural gas, for both for conventional and stranded gas. Figure 2.8 shows the main options and the route investigated in this report is outlined in red.

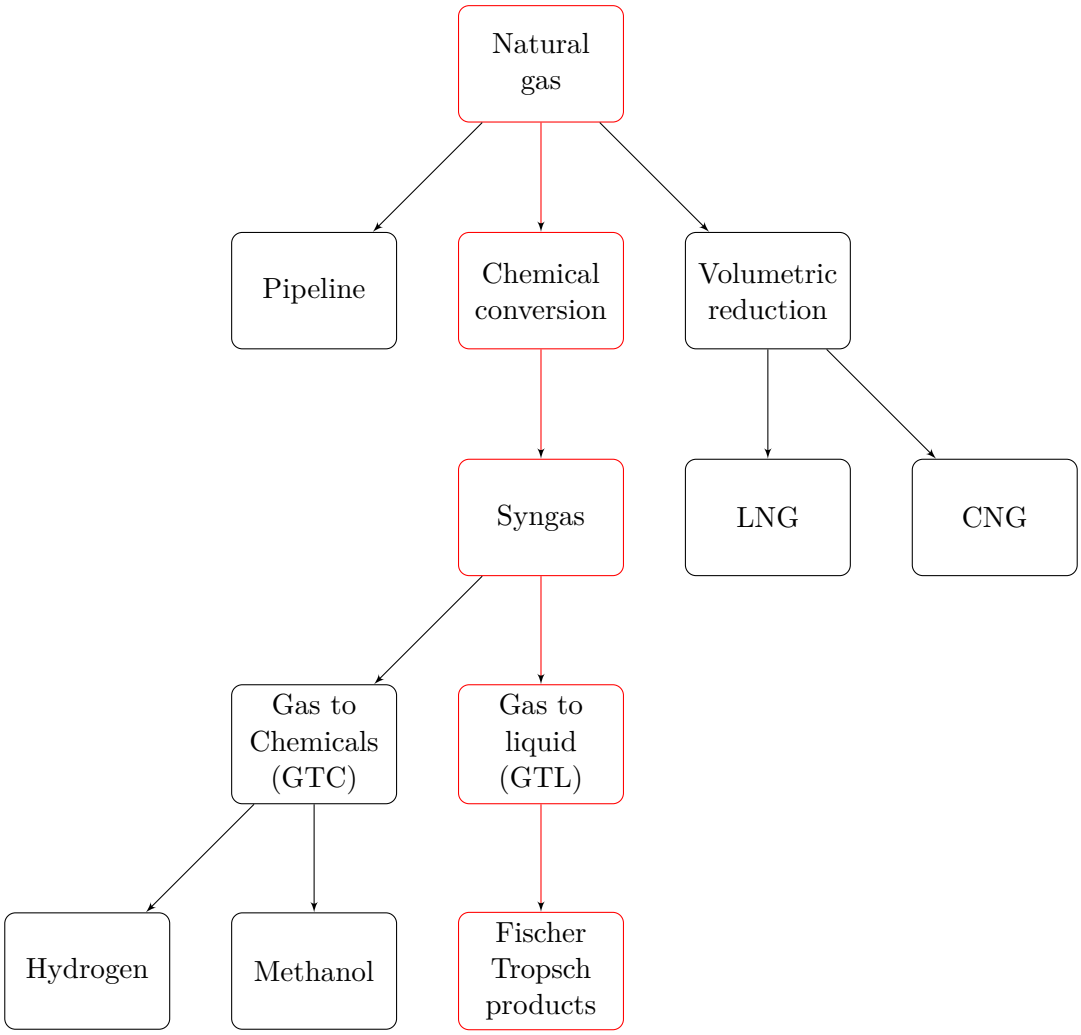

Figure 2.8 – Overview of the main processing alterntives for natural gas

Chapter 3

History of GTL

The GTL process is as outlined in section 2.2.1 a process where natural gas is chemically converted to synthetic fuels such as diesel and gasoline through the Fischer Tropsch process. The Fischer Tropsch process can however also be applied to a range of other feedstocks such as coal and biomass, then referred to as CTL and BTL respectively[5]. This process was invented in Germany in the 1920's and to get an indication of the history and development of GTL it is necessary to review the history of the Fischer Tropsch process. The history of CTL in South Africa is also included as some of these plants has converted to natural gas feedstock in recent times and as much of the same technology is used in syngas generation and for reactors. Sasol, South-African based company is one of the leading actors in GTL today and bases much of their experience on their CTL operations, which again emphasizes the importance of including this part.

3.1 Fischer Tropsch process

The high interest for development of synthetic fuels in Germany relates back to World War I. During this war the British fleet imposed a blockade from overseas to Germany, leading to a shortage of many supplies including petroleum and fuels [37, 38]. World War I also left Germany in a poor economic state, making it difficult to purchase foreign oil. This illustrated Germany's dependency and vulnerability in regards to fuels and importation of oil. Combined with the perception at the time of depleting oil

reserves, Germany put large resources into attempting the production of liquid petroleum fuels from coal [38].However the chemical processes that the Fischer Tropsch reactions are based on was discovered before World War I.

3.1.1 Chemical background

In 1902 Sabatier and Sanderens produced methane by passing CO and H_2 over nickel, iron and cobalt catalysts and about the same time hydrogen was produced by steam reforming synthesis gas [39]. Following this development, Franz Fischer and Hans Tropsch at the Kaiser Willhelm Institute of Coal Research in Mälheim an der Ruhr in Germany, developed a process for production of liquid hydrocarbons from synthesis gas passed over an iron catalyst in 1923[39]. The technology of producing liquid hydrocarbons from CO and H_2 using metal catalysts was followingly patented in 1925 and in 1935 the first industrial reactor was constructed [38, 9]. By 1938 there was nine Fischer-Tropsch plants with coal as feedstock in operation in Germany with a combined capacity of 660 000 tons a year of Fischer Tropsch products[10, 9]. This increased commercialisation of the technology was strategically motivated to provide the fuel needed to operate the German war forces during World War II as a result from the WW I experience [40, 32, 10]. The plants in Germany ceased however to operate after World War II ended, but the interest for Fischer-Tropsch processes was maintained after the second World War due to perceptions of decreasing oil reserves and consequently increasing oil prices[13]. This lead to the construction of a Fischer-Tropsch plant in Brownsville, Texas, in the 1950's that was based on methane and to the construction of Sasol I in Sasolburg in South-Africa in 1955 [13]. The plant in Brownsville was however forced to shut down after a short period of operation due to a severe increase in the price of methane [13]. Sasol I, based on coal, was not affected by the price increase in methane, but by the discovery of large oil fields in the Middle East which occurred before the plant was completely constructed [9]. The period from 1955-1970 is commonly referred to as the oil age and was characterized by cheap oil spupplies as a result of the large reservoirs discovered and consequently the world-wide interest for Fischer-Tropsch, created by a fear of increased oil prices, disappeared [13, 9]. The only country where the interest was maintained was in South Africa [9].

3.1.2 South Africa

South Africa has almost no oil reserves, small natural gas reserves, but with the ninth largest proven reserves of coal in the world they have an abundant energy resource[41]. With the post war rise in oil prices and the continuous institutionalizing of the apartheid regime, South Africa had a desire of being less dependent on oil imports and increase their energy security [42, 43]. As a result it was started both a search for domestic oil, and the possibility of converting the large coal reserves to synthetic fuels through the Fischer Tropsch process was explored[42]. No significant oil reserves were however located and in 1950 the South African Coal, Oil and Gas Corporation Limited, SASOL, was founded and the first synthetic fuel plant, Sasol I, was constructed in Sasolburg in 1955[42, 43]. The plant had a capacity of 6 million tons per year of Fischer Tropsch products and was considered a success [32].

In 1973 the oil crisis started, when OPEC increased the price of crude oil by 70 % as a reaction to the Yom Kippur War, and in addition posed an oil embargo on the export to the United States and other allies of Israel[44]. This prompted the interest in Fischer-Tropsch technology again and in South Africa, together with trade sanctions and disinvestment initiatives from among others the UN and OPEC, as a reaction to South Africa's increasingly stricter and brutal apartheid regime, it led to the construction of Sasol II and Sasol III in Secunda in 1980 and 1982 respectively[42, 11, 45]. It was also in 1973 Shell started to develop their GTL process, Shell Middle Distillate Synthesis[9]. By the end of the oil crisis in 1974 the price of crude oil was four times the price existing before the crisis[44].

3.1.3 Recent commercial development

As the history of Fischer-Tropsch process describes, most of the development have been driven by strategical reasons during war and political conflicts rather than from an economic perspective[39, 11]. In more recent time however the process has gained renewed interest as a result of need for more clean burning fuels, probability of increased oil prices due to reduced crude oil reserves, the potential of monetizing stranded gas and taxes and legislations put on flaring[39].

The Mossgas plant in South Africa, producing Fischer Tropsch products through the high temperature process, came on line in 1992 and in 1993 Shell opened a GTL plant in Bintulu, Malaysia, based on their SMDS process[9, 32]. More recently the Oryx GTL plant, a cooperation between

Qatar Petroleum and Sasol was commissioned and the worlds currently largest GTL plant, the Pearl project from Shell and Qatar petroleum, came on line in 2011[46, 47, 48].

Currently there are five commercial scale GTL plants in operation on a world wide basis. The location for four of the five plants is focused around Qatar and South Africa. Qatar has the third largest proven reserves of natural gas, as outlined in Section 2.1.2 and as also outlined in Chapter 2 there is also a large quantity of stranded gas in the Middle East. Qatar is hence a natural actor in the GTL market and has been the center for the development of the new generation GTL plants in recent time. South Africa on the other hand does not have the same reserves for neither oil or natural gas and in 2006 they were ranked as number 104 on the list over proven reserves of natural gas and number 88 on the list over proven reserves of crude oil [24]. Their position in GTL technology is due to long operation of CTL, which was developed for strategic reasons during the apartheid regime as explained in the previous section.

Table 3.1 gives an overview over both the present GTL plants as well as Sasols plants based on coal and their main features. Additionally it should be noted that Sasol also has started to use natural gas as supplementary feedstock at Secunda, and they have stated that for future increases in production it will likely use natural gas over coal[49]. Consequently, plants that today is classified as CTL might be converted to GTL plants in the future.

Table 3.1 – Overview over Sasols CTL plants and the commercial GTL plants today with location and process information (NA indicates that a value was not located) [10, 9, 5, 31, 11, 50, 51, 52, 49, 53]

Plant	**Location**	**Company**	**Feed stock**	**Capacity**	**Reactor**	**Catalyst**	**Since**	**Notes**
Sasol I	Sasolburg	Sasol						
1955-1993			Coal	2500	CFB & MTFB	Fe	1955	HTFT
1993-2004			Coal	NA	SBC	Fe	1993	LTFT
2004 →			NG	5000		Fe	2004	LTFT
Sasol II	Secunda	Sasol	Coal	85000	SAS (CFB)	Fe	1980	HTFT
Sasol III	Secunda	Sasol	Coal	85000	SAS (CFB)	Fe	1982	HTFT
Mossgas/ PetroSA GTL	Mossel Bay	Petro SA prev. Sasol	NG	25000	SAS(CFB)	Fe	1992	HTFT
Bintulu	Bintulu	Shell	NG	14700	MTFB	Co	1993	LTFT
Oryx GTL	Qatar	Sasol & Qatar Petroleum	NG	34000	SBC	Co	2007	LTFT
Pearl GTL	Qatar	Shell & Qatar Petroleum	NG	140000	MTFB	Co	2011	LTFT

In addition to the existing plants outlined in Table 3.1 there are several more in development at different stages. This includes studies, pilot plants, FEEDs and under construction [50]. The one closest to realization is probably the Escravos plant estimated for completion in 2012 in Nigeria, a cooperation between Sasol and Chevron[54].

Chapter 4

Process and alternative configurations

The GTL process consists of three main parts, production of synthesis gas from natural gas, Fischer-Tropsch reactions to produce long chained hydrocarbons and upgrading of products to hydrocarbons with desired chain lengths. The process chain is ilustrated in Figure 4.1 [31].

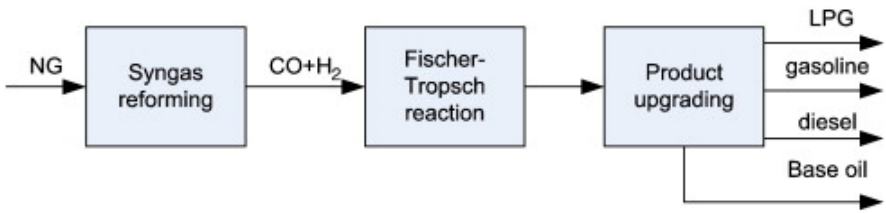

Figure 4.1 – Illustration of the three main sections in the GTL process [10]

Within each of these three sections there is a wide variety of alternative process routes and configurations. The following sections aims to outline these alternatives, their main features and applications.

4.1 Syngas production

The first main part of the GTL process is the syngas production. In this section the natural gas is converted into a mixture of hydrogen and carbon monoxide known as synthesis gas, or syngas in short. This step can contribute to over 50% of the overall capital costs of a GTL plant and hence it is of great economic importance to choose the right type of technology [55]. Given that it is such an expensive part of the GTL technology, there is extensive research in this area in order make GTL more economically favourable. This has resulted in a wide variety of possible technologies available and in several future possible technologies being developed.

4.1.1 Pre-reforming

As outlined in Chapter 2, the feed of natural gas consists mainly of methane but there is also usually some ethane, propane and butane present as well. To avoid these heavier hydrocarbons to crack and produce olefins in the reformer, a pre-reformer is often applied as a first step in production of syngas[31]. This has been common procedure in reforming of naphta for years, but have presently also gained interest in use for production of syngas from natural gas, where it has shown to be able to increase capacity of the plant with 10-20% and hence make the plant more economically feasible[56].

A pre-reformer is an adiabatic fixed bed reactor, and the catalyst used is often a highly active steam reforming nickel catalyst[56]. The feed of natural gas and steam is normally heated to 420-500 °C and fed to the pre-reformer where all hydrocarbons with more than one carbon atom in the chain is converted to hydrogen and carbon monoxide as described by Equation 4.1 [56, 57]. The higher the inlet temperature, the greater the reaction rates, as reaction 4.1 is endothermic for natural gas as feedstock, and hence less catalyst needed and greater energy savings are experienced[56].

$$C_nH_m + nH_2O \longrightarrow \left(n + \frac{m}{2}\right) H_2 + nCO \qquad \text{for } n \geq 2 \tag{4.1}$$

Besides from prevent cracking, a pre-reformer can trap what is left of sulphur as the chemisorption of sulphur on nickel is favourable at the low temperature in the pre-reformer[58, 56].

In addition to the cracking of heavier hydrocarbons, methanation reaction and shift reaction as described in Equation 4.2 and 4.3 respectively,

also occurs. These reactions are assumed to go to equilibrium in the pre-reformer[31, 56, 57]

$$CO + 3H_2 \leftrightarrow CH_4 + H_2O \tag{4.2}$$

$$CO + H_2O \leftrightarrow CO_2 + H_2 \tag{4.3}$$

The reaction enthalpy for ethane, propane and butane from Equation 4.1 is 350, 500 and 650 $\frac{kJ}{mol}$ respectively. Even though the methanation reaction and shift reaction are both exothermic reactions, with reaction enthalpies of -210 and -41 $\frac{kJ}{mol}$ respectively, the overall process in the pre-reformer is of endothermic nature when natural gas is used as feedstock[57]. Consequently a temperature drop is experienced after the pre-reforming section. To reduce the load on the main reforming step, the pre-reformed gas can be brought up in temperature by a fired heater before this step [58].

There are several processing alternatives for the main syngas production with steam methane reforming, SMR, autothermal reforming, ATR, partial oxidation, POX, two step reforming and heat exchange reforming, HEX, the most considered technologies. They all have their strengths and weaknesses and the optimal choice is determined by the process in question.

4.1.2 Steam methane reforming, SMR

Steam methane reforming has been and still is the most widely used technology for syngas production on a commercial level [59]. The main principle of the technology is catalytic, endothermic conversion of steam and methane to hydrogen and carbon monoxide [59].

The reactions taking place in the SMR are the steam methane reforming reaction, water gas shift reaction, WGS, and the steam reforming of higher hydrocarbons[60]. These reactions are given below as Equation 4.4, 4.5 and 4.6 respectively. Comparing these reactions with the ones from the pre-reformer it can be seen that both the WGS reaction occurs in both reactors as well as the steam reforming of higher hydrocarbons. However the third and last reaction for the two processes are opposites of each other. In the pre-reformer carbon monoxide and hydrogen produces methane through the exothermic methanation reaction, while in the steam reformer the reaction

goes in the opposite direction producing syngas from methane through the endothermic steam methane reforming reaction[57, 56].

$$CH_4 + H_2O \leftrightarrow CO + 3H_2 \tag{4.4}$$

$$CO + H_2O \leftrightarrow CO_2 + H_2 \tag{4.5}$$

$$C_nH_m + nH_2O \longrightarrow \left(n + \frac{m}{2}\right) H_2 + nCO \qquad \text{for } n \geq 2 \tag{4.6}$$

The WGS reaction is the only one of the three that is exothermic with natural gas used as feedstock and hence renders this a net endothermic process as for the pre-reforming[60]. Hence it is necessary to provide a heat source in order for the reactions to occur and in SMR this heat is supplied by an external source, often by utilizing a part of the feedstock as fuel [59].

The steam methane reformer is a type of packed tubular reformer, meaning that the reactor consists of a large quantity of tubes filled with catalyst [11]. The catalyst commonly applied in SMR is nickel, for the same reasons as the pre-reformer [60]. The pre-reformed natural gas is fed into these tubes together with steam, while burners are heating them up from the outside. The operating temperature is usually in the range 850-920 °C and at pressures up to 30 bar [11, 60]. There are several different arrangements possible the burners, such as top-fired, bottom fired or side fired reformers [60]. Figure 4.2 gives an illustration of a top fired steam methane reforming process.

SMR has two large advantages in its extensive industrial experience and in not requiring oxygen, which is very costly[59]. However it produces syngas with a $\frac{H_2}{CO}$ ratio in the range 3-5[60]. As GTL production requires a ratio of approximately 2, SMR is considered unsuitable for this process[59]. Its economy of scale is also poorly suited for GTL processes and in addition it requires great amounts of heat[62]. Steam methane reforming is more commonly used in hydrogen production where the higher ratio is beneficial and this mainly also accounts for its position as benchmark syngas technology [59, 60].

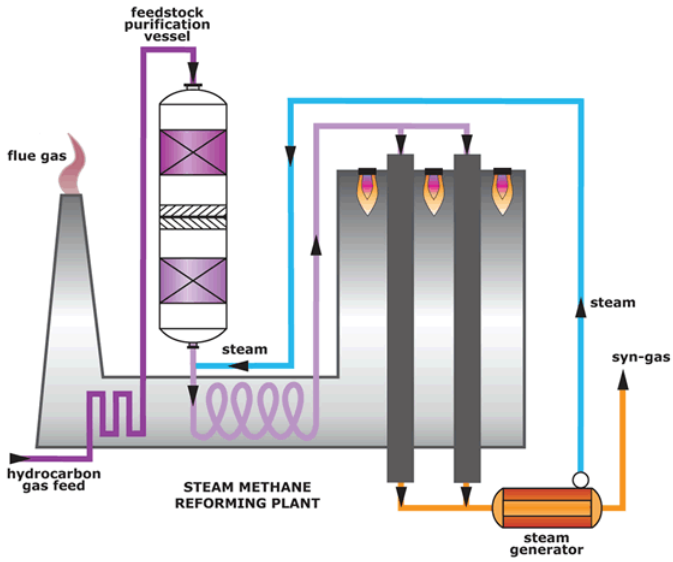

Figure 4.2 – Illustration of a top-fired steam methane reformer including the feedstock purification process [61]

4.1.3 Partial oxidation, POX

Partial oxidation is an exothermic, non-catalytic reforming process for production of syngas [59]. Figure 4.3 shows the partial oxidation reformer. As a consequence of operating without a catalyst the operating temperature is very high and about 1200-1400 °C[63]. This produces soot and a scrubber is needed if POX is used as reformer technology [63]. As for ATR, methane and oxygen are the feed streams in on the reformer, but little or no steam. Partial oxidation produces syngas with a hydrogen to carbon monoxide ratio under 2, which is lower than the desired level for GTL applications and is caused by the low use of steam [59]. In addition to low $\frac{H_2}{CO}$ ratio and the need of a scrubber, POX uses more oxygen than ATR [63]. Hence this technology is not often used for syngas generation for GTL alone, but could be applied in combination with other technologies[59]. The Shell Gasification Process, SGP, is however based on the partial oxidation reforming[47].

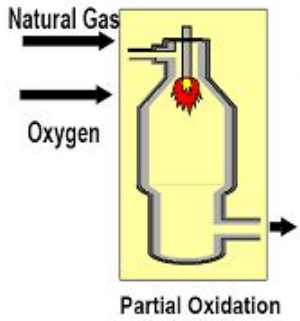

Figure 4.3 – Illustration of a partial oxidation reformer[64]

4.1.4 Autothermal reforming, ATR

Autothermal reforming is a combination of steam reforming and non-catalytic partial oxidation in one reactor[7]. Like in partial oxidation, methane and oxygen are the two feed streams, but the reactions are endothermic and catalytically driven as for steam methane reforming[7]. The ATR is divided into three main sections as illustrated by Figure 4.4, a burner section, a combustion section and catalyst bed [60, 55].

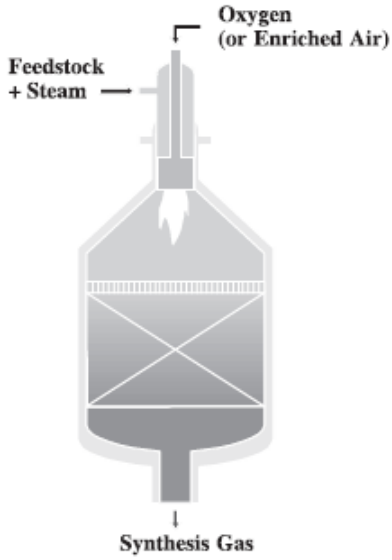

Figure 4.4 – Illustration of an autothermal reformer [55]

Pre-reformed natural gas and oxygen enters the burner zone where it

is burned with a sub-stoichiometric flame and mixed[60, 55]. In the combustion section a fraction of the methane is partially oxidised and another fraction of the methane is completely combusted[7]. This oxidation is shown in Equation 4.7. The partial oxidation reaction and combustion of methane are exothermic reactions and the heat released serves as energy source for the endothermic steam reforming reaction occurring in the catalytic bed as shown in Equation 4.8 [7]. It is this ability to supply heat for the endothermic reactions by internal combustion of a fraction of the feed, making the reforming reaction "automatically" happen that has given name to the process [11, 7]. In addition to the steam reforming reaction, the shift reaction, as shown in Equation 4.9 goes to equilibrium in the catalytic bed. As for the other reformer applications mentioned so far where steam methane reforming is present, nickel is often the preferred catalyst and this is also the case for the ATR[60].

$$CH_4 + \frac{3}{2}O_2 \longrightarrow 2H_2O + CO \tag{4.7}$$

$$CO + 3H_2 \leftrightarrow CH_4 + H_2O \tag{4.8}$$

$$CO + H_2O \leftrightarrow CO_2 + H_2 \tag{4.9}$$

The main advantage of the ATR reforming process is the favourable $\frac{H_2}{CO}$ ratio of the syngas. Figure 4.5 gives an overview over the resulting ratios from the variuos reforming routes. It can be seen that as previously mentioned SMR does not have the potential to reach a low enough ratio while POX does not have the potential to reach a high enough ratio[59]. However ATR spans over the optional range for GTL production.

The range of the ratio is quite wide and the $\frac{H_2}{CO}$ ratio depends on the steam to carbon ration entering the reformer[65]. Figure 4.6 shows this dependency of the ratio of the steam to carbon ratio [55]. From the figure it can be seen that a very low steam to carbon ratios is necessary if the desired ratio a ratio of close to 2 is to be achieved. At about ten years ago it was not common industrially to operate at ratios below 1.3 [63]. At this high ratio a soot free syngas is produced, however it gives $\frac{H_2}{CO}$ ratio of approximately 2.5[63]. In order to come closer to the optimal value for GTL processes of 2.0-2.1, recycling or addition of CO_2 have been common practice [63]. Today, the commercial ratios applied lies between 0.6 to above 1.0 resulting in $\frac{H_2}{CO}$ ratios of 2.3-2.5[65]. Haldor Topsøe is one of the main actors in the syngas reforming industry and during the 1990's they developed a new ATR

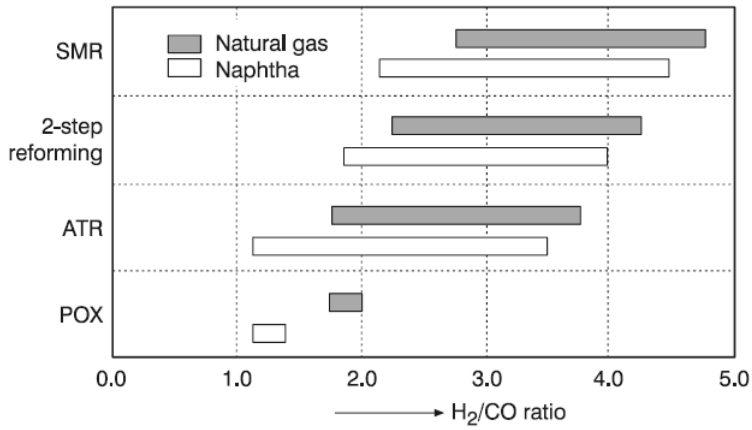

Figure 4.5 – Overviev of the various reforming technologies and their corrsponding $\frac{H_2}{CO}$ ratio for both naphta and natural gas [59]

operation technology where a steam to carbon ratio of 0.5-0.6 was applied [60, 66, 55]. This process has been in use industrially in Sasolburg in South-Africa since early 2004 and in Europe since early 2002[66]. This technology was also chosen for the first large scale GTL plant based on natural gas, The Oryx plant, and is also planned used for the Escravos project in Nigeria[66]. With the lowered ratio, the $\frac{H_2}{CO}$ relation is closer to the desired value for GTL processes, and the recycling need of CO_2 is consequently reduced[55]. This process based on lower steam to carbon ratio has also proved to have a positive effect on the process economics[55].

There are continuous efforts in improving the ATR technology as well as other syngas reforming methods and Haldor Topsøe is for instance looking into further reducing the steam to carbon ratio[66]. Ratios as low as 0.2 has been demonstrated in pilot plants, but not yet been applied commercially [66]. This further reduction has shown to be beneficial economically, but a low steam to carbon ratio increases the risk of soot formation in the ATR and coke formation in the pre-reformer[55].

The ATR technology have several other beneficial attributes in addition to the favourable $\frac{H_2}{CO}$ ratio. First, it does not require an external heat source, and second it is considered to have a favourable economy of scale making it suitable to handle large scale applications[32]. ATR is also a very cost-effective reforming method and is together with two-step reform-

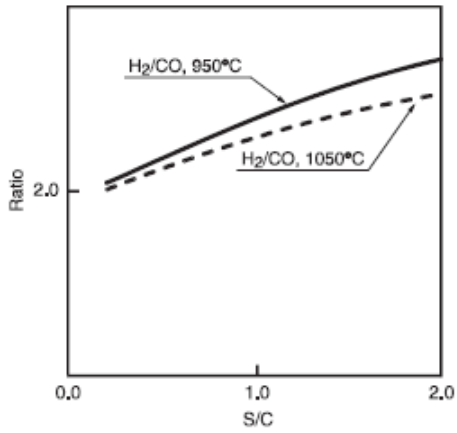

Figure 4.6 – Hydrogen to carbon monoxide ratio as a function of steam to carbon ($\frac{S}{C}$) ratio for the two temperatures 950 °C and 1050 °C [55]

ing generally considered to be the best alternatives for syngas generation for GTL plants [60, 32, 59]. Asberg-Petersen et al. reports the ATR technology in combination with low steam to carbon ratio to be the preferred option for large scale, economic syngas generation for GTL, while a report about syngas alternatives from Bakkerud claims ATR or ATR in combination with a heat exchange reformer will be the preferred technology for the next 5-10 years[55, 67]

However as all other technologies it has its drawbacks. One of the disadvantages of the ATR technology is that there is not much commercial experience with its use, compared to technologies such as SMR [59]. Nevertheless, ATR is currently the preferred choice of reforming technology for new industrial plants for GTL and hence this experience will increase. Another drawback is the use of oxygen as feedstock which requires an air separation unit, which have a considerable cost related to it [59].

4.1.5 Heat exchange reforming, HEX

Heat exchange reforming is a reforming technology where the heat needed for steam reforming is supplied by effluent heat from another reformer. [6, 68]. Hence these type of reformers are always installed in combination with another reformer and the heat exchange reforming can either be accomplished in series or parallel arrangement[6, 62]. The two arrangements

are shown in Figure 4.7.

In series, shown to the right in Figure 4.7, the feed gas first passes through the heat exchange reformer, where heat is supplied by the conventional reformer, before the feed gas then passes through the conventional reformer directly. The conventional reformer may be a tubular reformer or a secondary reformer[6]. In parallel, as shown to the left in Figure 4.7, the feed stream is split and one fraction passes through the conventional reformer while the rest passes through a heat exchange reformer. The heat for the HEX is supplied by the conventional reformer[6]. The technological principle relates to exploiting the effluent heat from for instance an ATR and use that as heat source instead of using a fired heater for this purpose. This use of effluent heat instead of a fired heater is also what separates this technology from two-step reforming [63]. However, due to this heat integration, there is a risk of metal dusting with the use of heat exchange reforming[6, 66].

Haldor Topsøe has designed a heat exchange reformer that operates in parallel combination with an ATR at Secunda in South Africa. It was started as a revamp for the original process and was meant to run for a 22 month long demonstration[68, 66]. The demonstration project met all expectations and has been running since. It has been shut down a number of times to inspect the material as it operates in a metal dusting prone temperature range, but have been found to operate well[68].

The main attribute of HEX is that it offers a more energy efficient use for the effluent heat from for instance ATR's than generating low value steam[68]. It has however little commercial experience to date and is in its development stage[68].

4.1.6 Two step reforming

Two step reforming is a combination of a primary and a secondary reformer. The primary reformer catalytically converts hydrocarbons and steam in an endothermic process to produce syngas, and an example of this is SMR[69]. The secondary reformers however converts partially converted process gas from the primary reformer by internal combustion. ATR and POX are examples of secondary reformers and both air and oxygen can be used for the internal combustion [69]. The same arrangements as for heat exchange reforming, parallel and series, is possible for two step reforming. Benefits

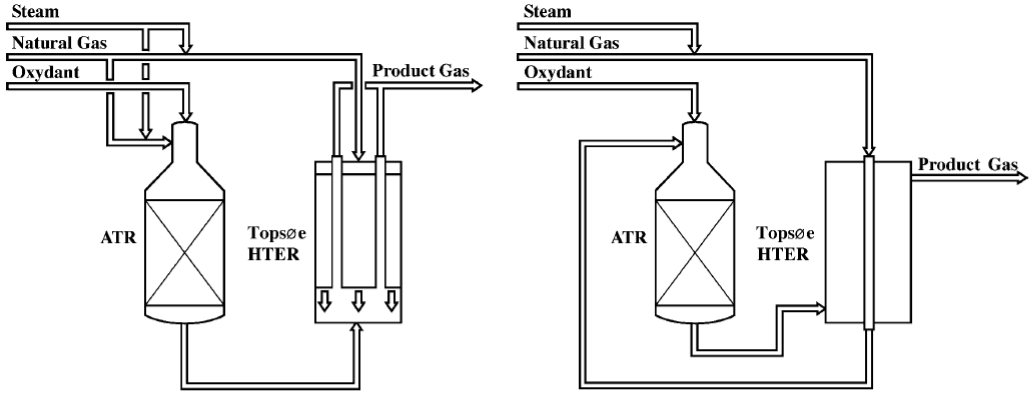

Figure 4.7 – Illustration of parallel (left) and series (right) heat exchange reforming configurations[67]

with this type of technology is a reduced SMR size, lower steam consumption and reduced costs [59]. However the complexity increases when two step reforming is applied and usually oxygen is preferred as internal combustion component which is costly [59, 70]. The combined reforming is also considered more expensive than ATR alone[63].

4.1.7 Metal dusting

Metal dusting is a form of corrosion process of metal and alloys,caused by a carburizing attack, resulting in the metal disintegrating to a powder of fine metal particles and carbon[71, 72, 73]. This powder is easily removed with the gas flowing through the equipment, resulting in formation of pits in the material.[72]. The continuous formation of these pits will eventually degrade the material to such an extent that it will need costly maintenance or could even lead to a severe material failure and hence be a safety issue [73]. The pit formation is however difficult to detect without physically inspecting the equipment and equipment operating in metal dusting prone environment must therefore be inspected regularly, and as this include process downtime it is also very costly[73].

Metal dusting occurs most often in environments with high carbon ac-

tivity and in a small temperature range between 400-800 °C [72, 73]. Below 400 °C the phenomena is hindered by slow kinetics, while above 800 °C the thermodynamical conditions are unfavourable [73]. The degree of the disintegration is dependent on the metal/alloy applied, gas composition, temperature and pressure, however nickel, iron and cobalt are especially prone for metal dusting[71, 73]. Composition wise is carbon monoxide considered the most active metal dusting component and in the presence of hydrogen the effect is reinforced[74, 71]. Metal dusting is hence most often found in processes including syngas or the production of hydrogen and the risk of metal dusting increases with decreasing steam to carbon ratio[73, 75].

Metal dusting can be prevented by changing the process conditions or slowed down by the use of protective coatings and oxide layers[73, 76]. Particularly chromium, silicon and aluminium oxide layers have shown to be effective[71, 76]. However it is also possible for the syngas to get beneath these layers and cause metal dusting from underneath the coating and consequently material failure could occur without one knowing[77]. Care should therefore still be applied even with the use of protective coatings.

An example of how dangerous metal dusting could be is from 1993, when a 200mm diameter hole was formed in a secondary reformer at the Mossgas plant in South Africa. Metal dusting had led to the lodging of a piece in a gas vane at the burner tip, increasing the oxygen to carbon ratio to such an extent that the temperature increased significantly. In only 34 minutes all three refractory layers and the steel shell had melted[78].

Exploiting the heat from the hot syngas after the reforming step could lead to potentially large savings industrially, and is also the idea behind heat exchange reforming, but does as outlined in this section bring with it risk of metal dusting. Normal industrial practice is the use of a waste heat boiler, WHB, or a heat recovery steam generator, HRSG, for steam production or cooling by water quench[63].

4.2 Fischer Tropsch reactors

In the Fischer Tropsch reactor, syngas is converted to long chained hydrocarbons by a form of polymerization reaction where methyl groups are sequentially added to the chain. This can be illustrated by the generalized reaction shown in Equation 4.10 [31]. The length of the hydrocarbon chains are determined by a range of factors and can be described by the Anderson-

Schulz-Flory distribution, ASF, which will be outlined in section 4.4. In addition to this reaction there will also be some formation of methane as displayed in Equation 4.11 and if the applied catalyst is iron, then also the water gas shift reaction, shown in Equation 4.12, will be present [9].

$$nCO + 2nH_2 \longrightarrow (-CH_2-)_n + nH_2O \tag{4.10}$$

$$CO + 3H_2 \longrightarrow CH_4 + H_2O \tag{4.11}$$

$$CO + H_2O \longrightarrow CO_2 + H_2 \tag{4.12}$$

As for the production of syngas, there exists a range of options for this processing stage though in terms of choice of Fischer-Tropsch reactor. The main attributes needed for the reactor is effective heat removal and temperature control, as the Fischer Tropsch reactions are highly exothermic [79, 13]. A sustained high temperature may deter the vessel material, deactivate the catalyst and favour methane production over the long chained FTS products, which is naturally undesirable. [13, 32]. Which other factors considered important are determined by the desired product and type of process.

Fischer Tropsch reactions can be run at either high temperature, HTFT, at about 300-350 °C or at low temperature, LTFT, at about 200-240 °C [13, 80]. The two processes results in different products and also uses different type of reactors. The high temperature process is used for production of gasoline and olefins while the low temperature is usually used for production of wax[13]. For the purpose of utilizing stranded and remote gas, the low temperature process is presently the preferred option[79].

The following sections outlines the different choices for the Fischer Tropsch reactor, their attributes and preferred usage area.

4.2.1 High temperature Fischer Tropsch process

For the high temperature Fischer Tropsch process there will only be two phases present in the reactor as a consequence of the high temperature, gas and solid material (catalyst). The two main reactor options for this case is the circulating fluidized bed, CFB and fixed fluidized bed , FFB reactors. The CFB reactors is commonly known as synthol reactors and is the precursor for the FFB reactors also known as Sasol advanced synthol, SAS, reactors[80].

CFB and SAS rectors

From 1955-2000, 19 synthol reactors were used in Sasols HTFT process in South Africa[80]. The design of this reactor is shown in Figure 4.8. In this reactor large amounts of catalyst is circulated and a separate support system for handling the catalyst is needed[80]. This drawback combined with high pressure drops and erosion problems prompted research activities to improve the reactor design and the Sasol Advanced Synthol reactor was launched as the new and improved reactor [80]. Figure 4.9 shows the SAS reactor concept, and as can be seen from the figure the main feature of the reactor compared to the synthol reactor is that it no longer uses a circulating catalyst system, but rather a fluidised bed. The syngas is bubbled through the bed and gaseous products leave at the top. The internal cyclones in the SAS reactor effectively separates the products and catalyst removing the need for scrubbers associated with catalyst removal in CFB's[80].

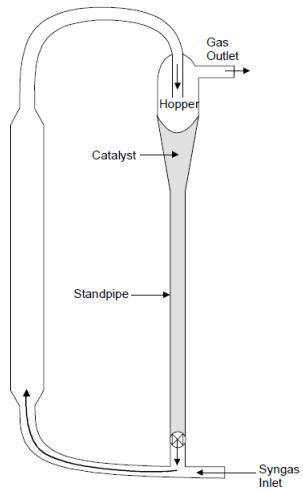

Figure 4.8 – Illustration of a synthol, CFB, reactor [32]

According to Sasol, the SAS reactor out performs the CFB reactor in a range of areas. The catalyst consumption is reduced by 40%, maintenance is reduced by 15 %, cost reduced by 40%, it is easier to operate, has greater capacities and a simpler structure and support[79]. As this reactor is a direct improvement of the CFB reactor there is little point comparing its advantages and drawbacks. In stead a table summarizing the upgrades is outlined in Table 4.1

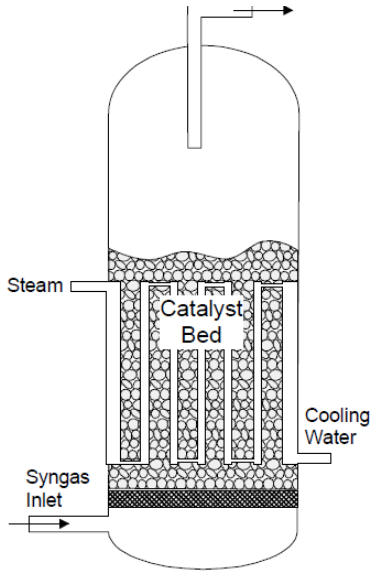

Figure 4.9 – Illustration of a Sasol Advanced Synthol reactor [32]

Given the improved reactor design the 16 synthol reactors in use at Secunda in South Africa was replaced by eight SAS recators between 1998-2000[80]. The improved reactor design showed superior capacities as indicated by halving the number of necessary reactors [13, 80]. The traditional CFB reactors had a capacity of 6500 $\frac{bbl}{d}$ while four of the SAS reactors had a capacity of 11000 $\frac{bbl}{d}$ and the remaining four had capacities of 20000 $\frac{bbl}{d}$[79].

Table 4.1 – Overview of the improvements in the FFB compared to the CFB reactor [13, 80]

Improvements in the FFB compared to CFB reactors
• lower construction cost
• smaller size for same capacity
• higher capacity
• all catalyst in use
• less need for catalyst replacement
• longer time between maintenance

4.2.2 Low temperature Fischer Tropsch process

In the LTFT process liquid is also present due to the lower temperature, resulting in total three phases in the reactor. A theoretically ideal LTFT reactor should have highly efficient gas-liquid mass transfer rates, operate isothermally at highest possible temperature, use a fixed bed catalyst and have high catalyst efficiency[9]. However no such reactor exist to date and industrially it is the multi tubular and slurry bubble column reactors that are in operation today[9]. Both have significant advantages and drawbacks and in the following sections, a presentation of the two type of technologies is given.

Multi tubular fixed bed, MTFB

Traditionally, the fixed bed reactor has been the preferred choice for LTFT processes[80]. It was the reactor of choice for wax production when the Sasolburg plant in South Africa was opened in 1955 and was also the preferred choice for Shells Bintulu plant when it started operating in 1993[73, 13]. The reactors used at Sasol plant is commonly called ARGE reactors and uses an iron catalyst, while Shells fixed bed reactor uses cobalt as catalyst and is often referred to as SMDS reactors after the process used at the Bintulu plant, Shell Middle Distillate Synthesis[9].

The MTFB reactor is as the name indicates,filled with multiple tubes. The tubes are filled with catalyst material and when the syngas is passed through the tubes, the exothermic Fischer-Tropsch reactions proceeds and the produced wax can be drained from the bottom of the reactor [13]. This is illustrated in Figure 4.10. The design of the MTFB reactor is not to different from a tubular heat exchanger and plug flow conditions are obtained in the process[80]. In order to keep the temperature within 200-240°C, boiling water is flowing on the outside of the tubes, removing heat through the production of steam [80]. This way of cooling the reactor leads to both axial and radial temperature gradients which will affect the conversion trough the reactor. The conversion will be at the highest in the beginning of the reactor and will decline with reactor length. The catalyst will therefore be unused to a higher degree at the end of the reactor, where the conversion is lower [80].

Another drawback with this type of reactor is its high capital cost, and its time consuming and difficult to replace the catalyst. Shell reports two weeks time for change of catalyst in the reactor[39]. It is therefore consid-

ered to be a better option to use cobalt than iron catalyst with this reactor due to a much longer lifetime[80].

The MTFB reactor also has some important advantages in a theoretically relatively easy scale up through multiplying the number of tubes and also there is little problems associated with separating the liquid and the solid, due to the catalyst being packed inside the tubes [39].

The capacity for the SMDS reactors was originally 3000 $\frac{bbl}{d}$. As the technology has developed Shell has reported capacities of 9000 $\frac{bbl}{d}$ for these reactors and launched potential future capacities of 10-15000 $\frac{bbl}{d}$ [80].

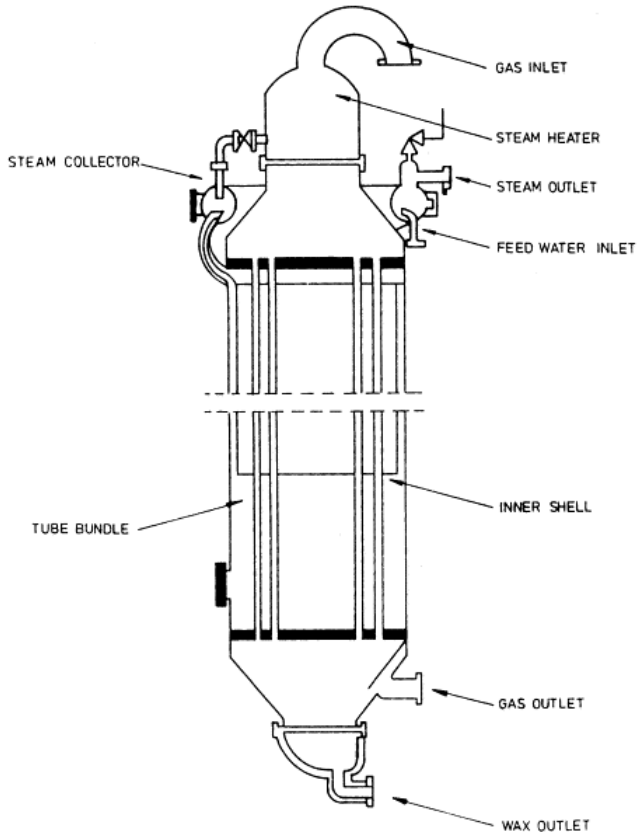

Figure 4.10 – Illustration of a multi tubular fixed bed reactor [13]

Slurry bubble column, SBC

The interest for SBC reactors started in the 1950's and in the 1970's Sasol performed studies in their pilot plants comparing SBC and MTFB reactors. At that point they were found to have about the same conversion and selectivities and due to the lack of an efficient and cost-competitive catalyst separation system the development halted [13]. The difficulties associated with this separation is due to the fact that SBC reactors uses a fine catalyst powder instead of traditional pellets [9]. This makes it less straight forward to separate it form the liquid products, however it eliminates potential internal mass transfer problems, making it possible to achieve high activity and selectivity [9]. In 1990 however, such a filtration system was tested and proved successful, and the first commercial SBC unit was commissioned in 1993 [13].

Figure 4.11 shows the design and operational concept of the SBC reactor and as can be seen from the figure, the syngas enters in the bottom of the reactor and bubbles up trough the slurry bed[80]. This bed consist of produced wax and liquids from the Fischer-Tropsch process and finely dispersed catalyst particles. The lighter components and unreacted gas leaves at the top of the reactor, while the heavier components must be separated out from the slurry[80]. In order to control the temperature, water is passed through coils in the reactor. This water is consequently heated as the reaction proceeds and steam is produced[80].

The SBC reactor is well mixed and gives an essentially isothermal reactor[80]. In contrast to the MTBR the SBC therefore have virtually no temperature gradients and thereby higher conversion and utilization of the catalysts as a consequence of a higher average operating temperature[80]. The isothermal nature of the reactor also leads to easier control and hence reduced opertaional costs[80]. Another advantage of this type of reactor is the possibility of continuous catalyst replacement. This reduces downtime related to replacing catalyst which is a huge advantage[80].

However this reactor also has some significant drawbacks. Scale-up of this system is considered more difficult than for the MTFB reactor and difficulties associated with separation of solid catalyst from the liquid products has lead to a decrease in its commercialisation[39, 9]. As a consequence these reactors have less commercial experience than the MTFB recators[32].

Following from this outline it is not given which reactor is the best option for the LTFT process which is also reflected in both being used industrially

today (ref Table 3.1) and Table 4.2 summarizes the positive and negative attributes of the two reactors.

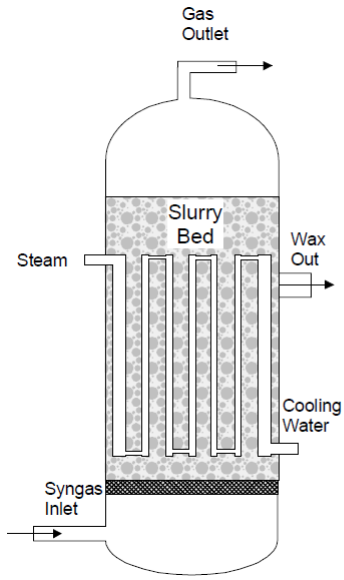

Figure 4.11 – Illustration of a slurry bubble column reactor [32]

Table 4.2 – Comparison of the MTFB and SBC reactor [13, 9, 80]

MTFB	**SBC**
+ easy scale up	+ isothermal
+ easy separating solid-liquid	+ low capital cost
+ less catalyst attrition	+ less catalyst use per tonne of product
+ if catalyst poisoned only a fraction affected	+ easy to replace catalyst
+ long commercial experience	- less commercial experience
- more catalyst per tonne of product	- if catalyst poisoned, all is affected
- high capital cost	- more catalyst attrition
- temperature gradients	- difficult with scale-up
- catalyst replacement costly	- difficulties in solid-liquid separation

4.3 Fischer-Tropsch Catalysts

For Fischer-Tropsch processes the metals in group VIII B are considered to be suitable as catalysts[9]. This include iron, cobalt, nickel and ruthenium. However the two most common metals are iron and cobalt as nickel produces to much methane and ruthenium is too expensive to be applied industrially

and [9, 13]. Using the price of scrap metal as relative basis, cobalt is 1000 times more expensive and ruthenium is 50000 times more expensive[13].

Although cobalt catalyst are more expensive they have a longer lifetime than iron catalyst with replacements about every 5th year and 6 months respectively[9]. This is an attribute that could be crucial if the reactor of choice has a difficult or time consuming catalyst replace technology.

Iron catalysts are considered to have water gas shift activity for the Fischer Tropsch reactions, while cobalt does not. This means that the WGS reaction, as shown in Equation 4.13 will go to the right. This is beneficial for feedstock rich in CO, as this type of feedstock normally produces a syngas with a low $\frac{H_2}{CO}$ ratio of approximately 1 [81]. Hence with the use of a catalyst with WGS activity more hydrogen will be produced at the expense of CO, increasing the $\frac{H_2}{CO}$ ratio. Consequently it is not favourable for natural gas feedstock as this have a high hydrogen content, normally produces syngas with a ratio of approximately 2 as shown in Figure 4.12, and hence does not need alteration for the Fischer Tropsch reactions[81].

$$\mathrm{CO} + \mathrm{H_2O} \leftrightarrow \mathrm{CO_2} + \mathrm{H_2} \tag{4.13}$$

The water produced in the Fischer-Tropsch reaction however inhibits the iron catalyst kinetically and hence the cobalt catalyst have a higher activity and is considered the preferred choice when high conversions per pass is required[9, 80]. For the LTFT process both Iron and Cobalt are applied industrially, however for the HTFT process only iron is applied as catalyst. This is due to an excess amount of methane produced at the high temperature process when cobalt is used as catalyst[13].

4.4 Anderson-Schulz-Flory Distribution, ASF

In the Fischer-Tropsch reactor, syngas is converted to long chained hydrocarbon molecules of various chain length. The generic formation reactions for parafins and olefins are shown in Equation 4.14 and 4.15 respectively[9].

$$n\mathrm{CO} + (2n+1)\mathrm{H_2} \rightarrow C_nH_{2n+2} + n\mathrm{H_2O} \tag{4.14}$$

$$nCO + 2n\mathrm{H_2} \rightarrow C_nH_{2n} + n\mathrm{H_2O} \tag{4.15}$$

The Fischer-Tropsch synthesis can be considered as a step wise polymerisation reaction where units of (-CH_2-) is added to the chain. The product distribution from this chain propagation can be modelled by the use of the

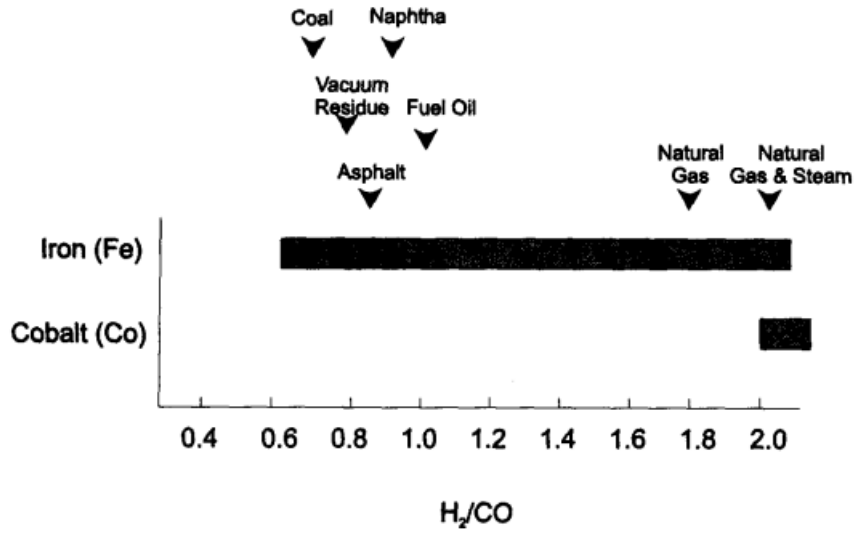

Figure 4.12 – Plot of the $\frac{H_2}{CO}$ ratio obtained with Iron (Fe) and Cobalt (Co) catalyst respectively as a function of type of feedstock [82]

Anderson-Schulz-Flory distribution model. This model gives the distribution of the product weight fractions as a function of carbon number, as displayed in Equation 4.16. Here, w_n is the weight fraction of C_n, is the chain growth probability factor and n indicates the given carbon number. The chain growth probability factor is given by the catalyst being used [9, 31].

$$w_n = n(1-\alpha)^2\alpha^{n-1} \tag{4.16}$$

Figure 4.13 shows the main features of the model schematically. Where α indicates the probability of another chain propagation step and consequently (1-α) indicates the probability for chain termination. For the LTFT process α values up to 0.95 or higher is common[80].

This model gives an ideal distribution scenario and when compared to experiments it has been found to underestimate methane, and overestimate for ethane and propane. The overestimation of ethane and propane is slightly lower than predicted when Fe catalyst is used and a lot less when Co or Ru catalyst are used[83, 9].

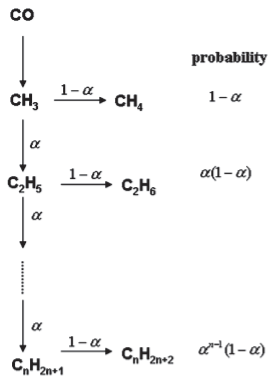

Figure 4.13 – Schematic display of the Anderson-Schulz-Flory chain propagation model [31]

4.5 Upgrading Unit

The third and last main section of a GTL plant is the upgrading unit and is the processing step that decides the composition of the final product pool. The main process is the cracking of the long chained hydrocarbons into desired products such as naphta, diesel and kerosene [10]. Besides hydrocracking this processing step also usually involves hydrotreating, hydroisomerization and separation[32].

The upgrading process is not further outlined as it is not modelled in the optimization and hence not part of the scope of this work.

Chapter 5

Choice of modelled process

The objective of this work is to investigate the potentials for optimization of a GTL plant and for this purpose such a plant was modelled and simulated in Unisim. The choices made for the base case is outlined in the following sections and is based on previous discussed theory and industrial examples.

5.1 Feed

The feed to the modelled process was chosen to be the same as used in a paper on GTL modelling by Panahi et al[31]. The composition and conditions for this feed is displayed in Table 5.1 and as can be seen from the table the feed is assumed to be sulphur free. This simplifies the modelling as a de-sulphurization unit is not needed.

In the report by Panahi et al. this feed was used to model a 17000 $\frac{bbl}{d}$ train, which is the same capacity as each of the two trains at the Oryx GTL plant [31]. Consequently it offers direct comparison potential with a state of the art commercially used train, which is beneficial for evaluation of the simulation results. The reactors used at the Oryx plant is of the SBC type, but as Shell has reported 9000 $\frac{bbl}{d}$ capacity for its SMDS reactors, this feed is suitable for modelling of both types by considering a train of two SMDS reactors for the MTFB type of reactor scenario[84]. The capacity is also in a suitable range application wise, being larger than the Bintulu capacity, representing the first generation large scale GTL plants, and smaller than Pearl GTL, being the world largest GTL plant.

Finally it was also considered an advantage to use this feed as it also provided comparison potential to another optimization attempt for the GTL process as given by Panahi et al.

Table 5.1 – Composition and inlet conditions for the feed chosen for modelling of the GTL plant

Conditions:		
	Molar Flow	8195 $\frac{kmol}{hr}$
	Temperature	40°C
	Pressure	3000 kPa
Composition:		
	Component	**Mole fraction[%]**
	CH_4	95.5
	C_2H_6	3
	C_3H_8	0.5
	C_4H_{10}	0.4
	N_2	0.6

5.2 Reforming

The reforming section was chosen to be the ATR reforming technology and in specific to be the process offered by Haldor Topsøe including the pre-reforming and reheating units. The benefits of this combined system was outlined in section 4.1 and is the system chosen for the Oryx GTL plant that came on line in 2007 [51]. A simplified illustration is shown in Figure 5.1. As can be seen from this figure the system normally also includes a desulphurization unit, however as the feed chosen is sulphur free, this unit operation was omitted from the modelling.

From the discussion in section 4.1 it was found that ATR was the reforming system providing the best $\frac{H_2}{CO}$ ratio for the Fischer Tropsch process with HEX and combined reforming as the two main alternative options. In relation to the ATR, HEX reforming is still in its development stage, includes two units making it more complex and operates in a metal dusting prone region. It was for these reasons not chosen for the modelling. Combined reforming also includes two units and in addition is considered more expensive than ATR alone and was therefore not chosen either.

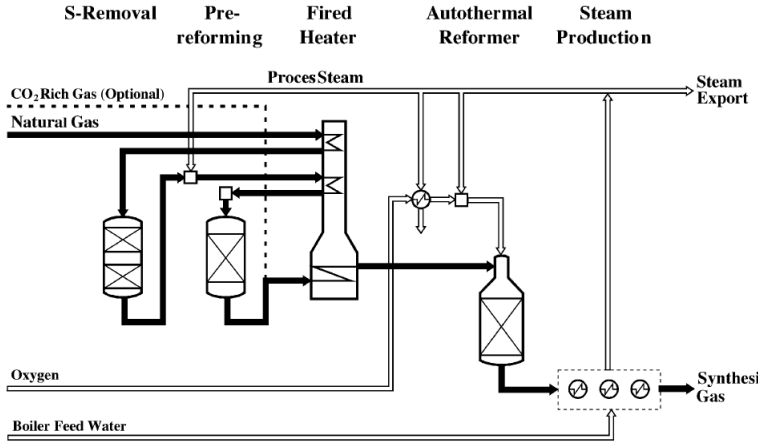

Figure 5.1 – Simplified schematic of ATR syngas as supplied by Haldor Topsøe [67]

In addition to be considered to have the most favourable $\frac{H_2}{CO}$ ratio, ATR reforming is considered by many to be the most economic route for producing syngas for GTL, as was presented in section 4.1. These features in combination with it being used for the state of the art Oryx GTL plant justifies this as the preferred choice for the modelling.

5.3 Reactor, catalyst and kinetics

The LTFT process was chosen for the simulation as it is the preferred choice for monetizing stranded gas and also the one applied in four of five GTL plants in operation today (refer to section 3.1.3 and Table 3.1) [80]. This process maximizes the wax and diesel production, which presently are the most commercially desired Fischer-Tropsch products and consequently making LTFT more relevant [80].

With the choice of LTFT process, the natural choice of catalyst was considered to be Cobalt as outlined in section 4.3. This will give the desired $\frac{H_2}{CO}$ ratio for the Fischer-Tropsch reactions and is also the catalyst most applied commercially together with the LTFT process (refer to section 3.1.3 and Table 3.1).

The MTFB reactor was further chosen for the simulation. This was mainly done due to it providing a better modelling option in Unisim than the SBC reactor, but also justified by it being the reactor of choice for both the Pearl and Bintulu GTL plants and due its long commercial experience.

There exist a range of theories and proposed mechanisms for the kinetics of the Fischer-Tropsch reactions and it is an entire research field of its own. The kinetics chosen for the modelling of the Fischer-Tropsch reactions in this work however was chosen to be the one provided by Iglesia.

Iglesia has proposed reaction rates for the consumption of CO and CH_4 for cobalt catalyst and these are valid in the following environment [31] :

Temperature : 473-483 K
Pressure : 100-3000 kPa
$\frac{H_2}{CO}$ ratio : $1 - 10$

The original rate expressions by Iglesia are in the units mol per second and gram of surface metal. These rate expressions were however converted to more common units of mol per second and cubic meter reactor by Rafiee by assuming a catalyst density of 2000 $\frac{kg}{m^3}$, 20 wt% cobalt and 10% exposed as surface atoms[53]. The converted reaction rates are as follows:

$$r_{\mathrm{CH_4}} = \frac{7.334 \times 10^{-10} P_{\mathrm{H_2}} P_{CO}^{0.05}}{1 + (3.3 \times 10^{-5} P_{CO}}) \tag{5.1}$$

$$r_{CO} = \frac{1.331 \times 10^{-9} P_{\mathrm{H_2}}^{0.6} P_{CO}^{0.65}}{1 + (3.3 \times 10^{-5} P_{CO}}) \tag{5.2}$$

Chapter 6

Modelling Procedure and Base Case

6.1 Modelling environment

The GTL plant was modelled steady-state in Unisim R400 from Honeywell.

In setting up the model the fluid package was chosen to be Peng-Robinson, as recommended in the Unisim Simulation Basis and Reference Guide: "*For oil, gas and petrochemical applications, the Peng-Robinson Equation of State is generally the recommended property package. The enhancements to this equation of state enable it to be accurate for a variety of systems over a wide range of conditions. It rigorously solves most single phase, two phase and three-phase systems with a high degree of efficiency and reliability.*"[85]

6.2 Implementation of the base case in Unisim

6.2.1 Components

All hydrocarbon components with four or more C-atoms was added as n-type hydrocarbons and $C_{21\rightarrow\infty}$ was modelled as C_{30} due to similarities in properties. The reactions were added in sets for the three main unit operations, Pre-reformer, ATR and FT-reactor respectively. These are further described in the following sections.

6.2.2 Fired Heater

As outlined in section 5.2, the reforming technology was chosen to be the one proposed by Haldor Topsøe, only omitting the desulphurization unit. In this system a fired heater is used for heating of natural gas feed, steam, oxygen and for reheating the pre-reformed gas before entering the reformer. In Unisim however, a fired heater can only be used for dynamic modelling mode and as this modelling was done steady-state the fired heater was modelled as individual heaters for preheating the natural gas and reheating. The oxygen and steam streams were for simplicity modelled to enter at desired temperatures for the base case scenario.

Consequently, for the pre-reformer, the natural gas was heated from the inlet temperature of 40 °C to 455 °C, as is in the common range for the inlet temperature of the pre-reformer as stated in section 4.1.1. and the steam stream was modelled to enter at 252 °C.

6.2.3 Pre-reformer

The pre-reforming reactions are considered to go to equilibrium and the pre-reformer was consequently modelled as an equilibrium reactor and the reactions as an equilibrium set. As the reactions are equilibrium reactions, only the stoichiometric coefficients are needed in Unisim. Table 6.1 shows the reactions modelled and their corresponding enthalpy of reaction.

Table 6.1 – Overview of the reactions modelled in the pre-reformer and their corresponding enthalpy of reaction [57]

Reaction	$\Delta_{rxn}H^{\circ}_{298}$ $[\frac{kJ}{mol}]$
$C_2H_6 + 2H_2O \leftrightarrow 5H_2 + 2CO$	350
$C_3H_8 + 3H_2O \leftrightarrow 7H_2 + 3CO$	500
$C_4H_{10} + 4H_2O \leftrightarrow 9H_2 + 4CO$	650
$CO + 3H_2 \leftrightarrow CH_4 + H_2O$	-210
$CO + H_2O \leftrightarrow CO_2 + H_2$	-41

A heater was installed after the pre-reformer to model the fired heater for re-heating of the pre-reformed gas. This stream is heated to 650 °C in Haldor Topsøes reforming design, but could be increased further to about

675 °C [67, 53]. However at this point there exist considerations for available piping material, but at the same time savings in oxygen is experienced[53]. For this work the temperature was chosen to be set at 675 °C.

6.2.4 ATR

In addition to the reheated natural gas, oxygen is needed for the partial oxidation in the ATR. For simplicity the oxygen was modelled as a pure oxygen stream entering at 200 °C without including the air separation unit in the model.

The reactions in the ATR is assumed to be in equilibrium due to the high outlet temperature and hence the ATR was modelled as an equilibrium reactor [53]. The reaction set was consequently also modelled as equilibrium reactions and Table 6.2 shows the equations modelled and their corresponding reaction enthalpy.

Table 6.2 – Overview of the reactions modelled in the ATR and their corresponding enthalpy of reaction [57]

Reaction	$\Delta_{rxn}H^{\circ}_{298}$ $[\frac{kJ}{mol}]$
$CH_4 + \frac{3}{2}O_2 \leftrightarrow CO + 2H_2O$	-520
$CH_4 + H_2O \leftrightarrow CO + 3H_2$	210
$CO + H_2O \leftrightarrow CO_2 + H_2$	-41

The reactions in the ATR are very exothermic and results in an increase in temperature for the produced syngas. An upper limit of 1030 °C was set to assure soot free operation [31]

As outlined in section 4.1.7, a waste heat boiler system is usually applied downstream of the ATR. For simplicity this system was modelled as a heat exchanger with water flowing on the shell side for this simulation, resulting in a cooled syngas at 38 °C. At this temperature the steam generated in the ATR is converted to water that can be separated out before the reactor, reducing the volume flow and hence reactor size [31]. However 38 °C is a too low temperature in on the reactor as the LTFT process is run at 200-240 °C and hence a heater was included in the model heating up the reactor inlet to 210 °C.

6.2.5 Fischer-Tropsch reactor

The reactor was modelled as a plug flow reactor as this being the flow pattern that mostly resembles a MTFB reactor and a starting volume of 1000 m^3 was chosen. The Fischer-Tropsch reaction set was defined as kinetic and includes the Fischer-Tropsch reaction and the methanation reaction. The stoichiometric coefficients for the FT-reactions are modelled based on the ASF-distribution and the kinetics is implemented by the use of Iglesias rate of reactions as outlined in section 4.4 and section 5.3 respectively.

For the Fischer Tropsch reaction only paraffins were considered in this work and the value of α was assumed to be 0.9. This gives a hydrogen usage ratio of 2.1 as given by Equation 6.1 [86]. All of the components with carbon number below 21 was modelled as individual units, while the components with carbon number from 21-30 was lumped in a component designated C_{21+}. The stoichiometric coefficients was calculated after Equation 6.2 and 6.3 as outlined in a paper by Hillestad and Appendix A shows the resulting values [86].

The modelled reactions are given in Table 6.3, but the Fischer-Tropsch reaction has been simplified due to space limitations and can be found fully expanded in Appendix A.

$$U = 3 - \alpha \tag{6.1}$$

$$r_{FT} = (1-\alpha)^2 \alpha^{(i-1)} \quad \text{for } C_i, i = 1, ...20 \tag{6.2}$$

$$r_{FT} = (1-\alpha)\alpha^{20} \quad \text{for} \quad C_{[21 \to \infty]} \tag{6.3}$$

As the reactions are modelled in kinetic mode, not only the stoichiometric coefficients are needed but also the rate expressions must be determined in Unisim and is written on the form outlined in Equation 6.4.

Table 6.3 – Overview of the reactions modelled in the Fischer-Tropsch reactor and their corresponding enthalpy of reaction [57].

Reaction	$\Delta_{rxn}H^{\circ}_{298}$ $[\frac{kJ}{mole}]$
$CO + 2.1H_2 \rightarrow \sum_{i=1}^{20}(\text{ASF coefficient})_i\ C_iH_{2i+2}$	
$+(\text{ASF coefficient})_{30}\ C_{30}H_{62} + H_2O$	-160
$CO + 3H_2 \leftrightarrow CH_4 + H_2O$	-210

$$rate = \frac{k \times f(basis)}{(1 + K_1 \times f_1(basis) + K_2 f_2(basis) + ..)^n}$$

$$\text{Where:} \quad k = A \exp\left(\frac{-E}{RT}\right) \times T^{\beta} \tag{6.4}$$

$$K_1 = A_1 \exp\left(\frac{-E_1}{RT}\right)$$

Rewriting the modified rate expressions by Iglesia from section 5.3 to the form needed in Unisim gives Equation 6.5 and 6.6 and it can be seen by comparison that

$$\begin{aligned} \text{k1} &= 7.334 \times 10^{-10} \\ \text{K1} &= 3.300 \times 10^{-5} \\ \text{k2} &= 1.331 \times 10^{-9} \end{aligned}$$

$$r_{CH_4} = \frac{k_1 P_{H_2} P_{CO}^{0.05}}{1 + K_1 P_{CO}} \tag{6.5}$$

$$r_{CO} = \frac{k_2 P_{H_2}^{0.6} P_{CO}^{0.65}}{1 + K_1 P_{CO}} \tag{6.6}$$

Only A,E,n and the various component exponents for the respective equations is required for Unisim and these were given by Rafiee to be as

Table 6.4 – Parameters used for kinetic rate expression in Unisim for modelling of the Fischer-TRopsch reactions [53]

Reaction	**A**	**-E**	**exponent** P_{H_2}	**exponent** P_{CO}		**n**
				numerator	denominator	
r_{CH_4}:						
k_1	$8.8 \cdot 10^{-6}$	37326	1	0.05	-	-
K_1	$1.096 \cdot 10^{-12}$	-68401.5	-	-	1	1
r_{CO}:						
k_2	$1.6 \cdot 10^{-5}$	37326	0.6	0.65	-	-
K_1	$1.096 \cdot 10^{-12}$	-68401.5	-	-	1	1

seen in Table 6.4 [53]

As stated in section 4.2 one of the most important aspects in a GTL plant is to control the reactor temperature. In Unisim there are two ways to simulate cooling of a PFR, direct cooling where the duty is specified, or formula cooling where the inlet temperature, heat transfer coefficient, heat capacity and molar flow of the cooling medium is specified. For both options the cooling can only be modelled as an energy stream and not a material stream. As a result the boiling water is only modelled as a duty. The latter of the two cooling options was found to perform better in keeping a constant temperature of the reactor and was consequently applied in the modelling. Water at 220 °C was chosen as cooling medium for the base case and a very large molar flow was applied to keep the cooling water at a constant temperature.

In a MTFB reactor, gas and liquid products are separated inside the reactor by gas leaving at the top and liquid products trickling down and exiting the bottom. When using a PFR in Unisim it is only possible with one exit stream and hence to achieve this in the model a separator is modelled separately after the reactor.

6.2.6 Products and recycle

The gaseous products are cooled by heat exchanging with water to 38 °C before entering the 3-way separator together with the liquid products. This is done to separate out water that left the reactor as steam. This will elim-

inate unnecessary recycling and water being sent to product upgrading.

In the 3-way separator more water is separated out, liquid products are sent to upgrading unit and the remaining gases is split in a purge and a recycle stream. For the base case this split fraction was set to 0.2 to purge and 0.8 in recycle. The recycle stream needs to be compressed before it is further split into two, one back to the Fischer-Tropsch reactor while the other is recycled back and mixed with fresh feed. The split ratio was set to be 0.768 and 0.232 respectively. With recycling, the flow sheet is looped and in Unisim this requires one or more recycle blocks for the iteration to be successful. Figure C.1 in Appendix C shows the base case as modelled in Unisim and shows the placement of this block.

6.3 Base case

The modelled base case process, as a result of the discussion in the previous sections and chapter 5 is shown in Figure 6.4 and the Unisim model is given in Figure C.1 in Appendix C while the woorkbook from Unisim is found in Appendix D.

The composition of the feed was given in Table 5.1 in section 5.1. The other input values are given in Table 6.5. They were chosen based on values given in an article on GTL optimization by Panahi et. al [31]. In addition to these input values a number of streams was set to a fixed value throughout the simulations. These are listed in Table 6.6.

Table 6.7 gives the conditions for the main streams together with an overview over the composition of the main components resulting from the base case simulation.

Table 6.5 – Base case input values for steam, oxygen and reactor volume

Tag	**T [°C]**	**Pressure[kPa]**	**Molar flow[$\frac{kmol}{h}$]**	**Volume[m^3]**
4	252	4045	5204	-
7	200	3000	5236	-
R-100	-	-	-	1000

Table 6.6 – Fixed process temperatures for the modelled process in °C.

Stream	**T [°C]**
3	455
6	675
13	38
15	210
18	38

6.4 Base case PFD

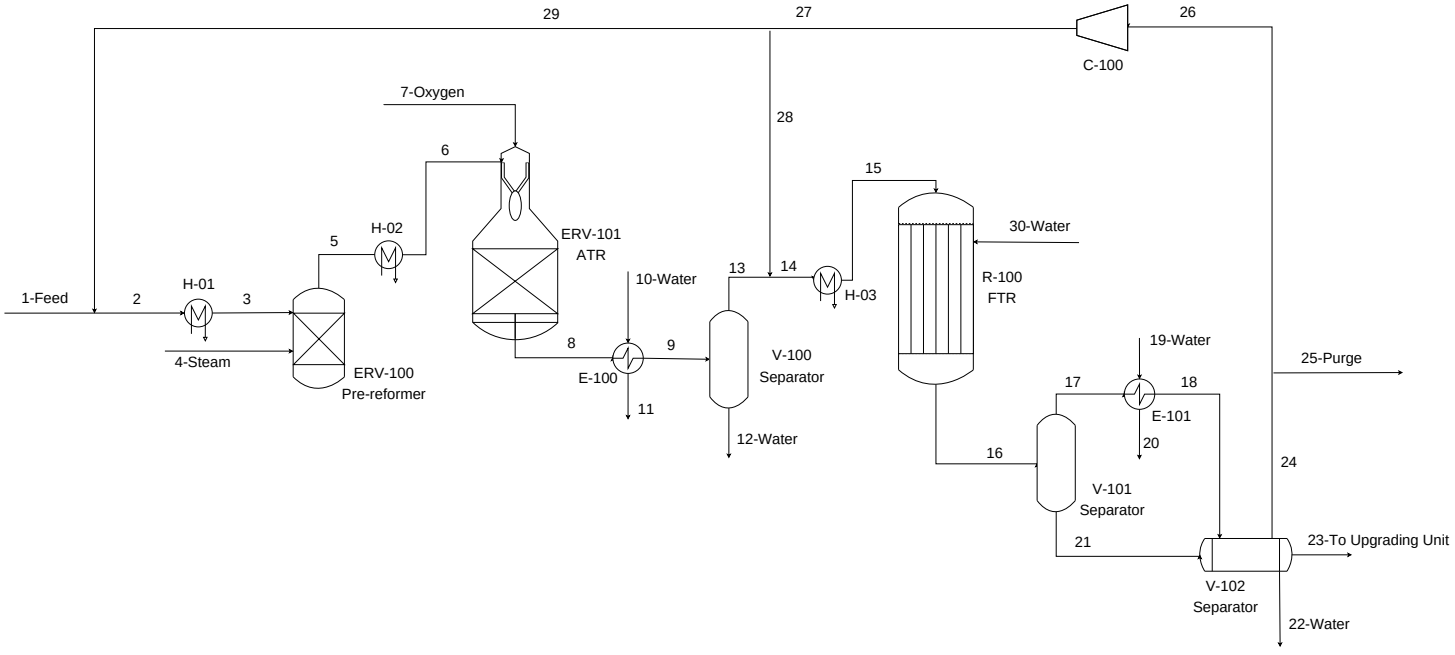

Figure 6.1 – Process flow diagram of the modelled base case in Unisim

Table 6.7 – Stream table with the most important features and composition for the modelled base case. The * indicates that the stream consists of some other components, but is mainly pure

Stream	**T [°C]**	**Pressure [kPa]**	**Molar flow** $[\frac{kmol}{h}]$								
			Total	Pure	CO	H_2	Light ends C_{1-2}	LPG C_{3-4}	Gasoline C_{5-11}	Diesel C_{12-20}	Wax C_{21+}
1	40	3000	8195	-	-	-	8072.07	73.76	-	-	-
2	58.64	3000	13330.98	-	1115.96	2292.46	8796.69	114.23	42.54	0.04	2.11E-09
4	252	4045	5659	H_2O	-	-	-	-	-	-	-
5	527.3	3000	18495.46	-	123.55	1745.12	9708.16	7.74E-04	42.54	0.04	2.11E-09
7	200	3000	4850	O_2	-	-	-	-	-	-	-
8	979.3	3000	35701.83	-	8521.95	18059.47	1104.99	7.74E-04	42.54	0.04	2.11E-09
13	38	3000	29692.02	-	8521.85	18059.30	1104.99	7.74E-04	42.54	0.04	2.11E-09
15	210	2000	46563.17	-	12183.53	25595.98	3476.09	133.81	185.18	0.17	9.08E-09
16	221.8	1940	34228.03	-	6015.95	12354.56	3908.84	223.78	385.27	112.55	71.07
17	221.8	1940	34130.80	-	6015.27	12353.48	3908.15	223.62	383.33	93.04	0.77
21	221.8	1940	97.23	-	0.68	1.07	0.69	0.16	1.94	19.51	70.31
22	46.60	1940	6186.70	H_2O*	-	-	-	-	-	-	-
23	46.60	1940	369.01	-	3.15	2.85	4.66	5.68	156.08	112.33	71.07
25	46.60	1940	5534.46	-	1202.55	2470.32	780.84	43.62	45.84	0.04	2.28E-09
26	46.60	1940	22137.85	-	4810.19	9881.28	3123.35	174.48	183.35	0.17	9.11E-09
28	95.48	3000	17001.87	-	3694.23	7588.83	2398.73	134.00	140.81	0.13	7.00E-09
29	95.48	3000	5135.98	-	1115.96	2292.46	724.62	40.48	42.54	0.04	2.11E-09

6.5 Base case evaluation

With the base case set up, an evaluation of the process was conducted to reveal if the process was running as expected and to reveal the potential optimization possibilities.

6.5.1 ASF distribution

As outlined in section 6.2.5 the model for the Fischer-Tropsch reaction is based on the ASF distribution in addition to the methanation reaction. For the ASF distribution a plot of the logarithm of the weight fraction dived by carbon number, against carbon number, is to yield a straight line with the logarithm of α as slope. This is given directly from the mathematical form of the equation and to make sure the reactions were modelled correctly, such a plot was constructed for the base case. The weight fractions were obtained from stream 16 of the Unisim base case and for this purpose the two recycle loops were opened so that the recycle would not affect the distribution. Also as the components $C_{21} - C_{30}$ are lumped into one component it was omitted from the plot as this would give a misrepresentation of component C_{30}. Figure 6.2 shows the plot for the base case and it can be seen that the components with 2-20 carbon atoms in the chain appears to follow a straight line. This is as expected from the ASF distribution and as the chain growth probability factor in these simulations is set to be constant at 0.9 the slope should theoretically be -0.04575. Taking out methane from the plot and adding a linear trend line, results in a straight line with an accuracy of 0.9997 and a slope of -0.0468. This is a deviation of 2.27% from the theoretical value and shows that the simulation predicts the right outcome of the Fischer-Tropsch reactions. This plot is given in Figure B.1 in Appendix B

For methane there is a large positive deviation from the line. This deviation was also expected as outlined in section 4.4. However the deviation is also emphasized due to the methanation reaction being modelled in addition for the Fischer-Tropsch reactor. This is confirmed by taking out the methanation reaction from the simulation and plot the same parameters. This is shown in Figure B.2 in Appendix B and the postive deviation for methane is now of a smaller magnitude than it was previously.

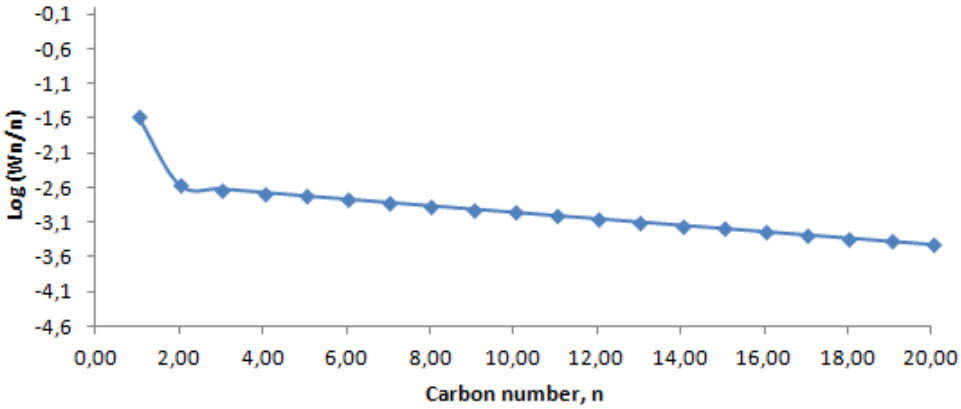

Figure 6.2 – The logarithmic of the weight fraction divided by carbon number plotted against carbon number (n), for components C1-C20 in the stream leaving the Fischer Tropsch reactor from the base case simulation.

6.5.2 Performance

AS the reaction fundament of the model was confirmed to be correct the performance of the base case could be evaluated and in Table 6.7 there are some significant features to take notice of.

First it can be seen from the molar flows of LPG and light ends from stream 2 and 5, that the higher hydrocarbons are almost completely converted to methane in the pre-reformer and that this unit seems to operate very well. However the temperature of stream 5 does not correspond with the endothermic reactions occuring in the reactor. Realizing the large amounts of CO and H_2 recycled back in stream 29 to the feed, and hence reformer, could explain this anomaly. If the two exothermic reactions in the pre-reformer, shift and methanation reaction, which uses these two components as feed have very large reaction extents the overall reaction could be exothermic instead of endothermic. From the reaction extents found in Unisim as shown in Table 6.8 this explanation is plausible.

Second, it is observed that the stream 8 has a $\frac{H_2}{CO}$ ratio at 2.119 which is close to the theoretical value of 2.1. However there is still methane left in the stream indicating, together with the syngas temperature of 979.3, that further potential for the production of syngas i present.

Table 6.8 – Reaction extents for the reactions in the pre-reformer for the simulated base case

Reaction	**Extent**
Pre-reforming of C_2H_6	51.28
Pre-reforming of C_3H_8	269.98
Pre-reforming of C_4H_10	622.95
Shift reaction	744.91
Methanation reaction	1181.45

Third it can be seen that there is still much H_2 and CO present in the stream leaving the reactor, indicating a low conversion in the reactor, which naturally is undesirable. This is confirmed by Unisim with conversions of 47.98 and 2.64% for the Fischer Tropsch reaction and methanation reaction respectively.

Moreover stream 23 shows that the stream going to the upgrading unit mostly consists of gasoline, diesel and wax and with relatively small amounts of both light ends, LPG, CO and H_2. This indicates an effective separation system after the reactor.

It can also be seen that the molar flow of stream 23 is small compared to the inflow of feed, which at first glance seems to indicate a poorly used feedstock. However in terms of liquid product, this correspond to 14310 $\frac{bbl}{d}$, which is about the capacity of the Bintulu GTL plant, and not too far from the estimated 17000 $\frac{bbl}{d}$ the feed was intended for. Consequently whether or not this is an indication of well or poorly utilized feedstock will have to be decided by also including other parameters.

For the recycle stream, small amounts of desired products are being recycled and the stream mainly consists of hydrogen, carbon monoxide and methane. However the recycle stream is three times the size of the inlet feed, which is not optimal.

From this evaluation it was experienced that parameters such as the $\frac{H_2}{CO}$ ratio, temperature of the syngas, reaction extents in the Fischer Tropsch reactor and the liquid volume of product gives important information of the performance of the process. It can also be concluded that the process

operates as expected, but is nevertheless not at an optimal stage and shows optimization potential in terms of conversion in the Fischer Tropsch reactor. The following sections will therefore consider these and additional indicators for process performance, the optimization variables present and the targets for the optimization.

Chapter 7

Optimization

7.1 Defining process optimization aims

For the optimization of a plant, there needs to be defined a set of targets outlining which parameters that is desired to improve and at what level this is accomplished. For this modelling, these targets were initially set to be carbon and thermal efficiency in addition to liquid volume of products produced in barrels per day.

7.1.1 Carbon efficiency, CE

Carbon efficiency is a measure of how well the carbon atoms in the feedstock is utilized in the production of products[8]. It is displayed mathematically in Equation 7.1 and typical CE values for a GTL plant is about 77% (ref. section 2.2.1) The calculation procedure for CE is outlined in Appendix E.

$$\text{Carbon efficiency, (CE)} = \frac{\text{Carbon molecules in the final product}}{\text{Carbon molecles in natural gas feed}} \times 100\% \tag{7.1}$$

7.1.2 Thermal efficiency, TE

Heating value and calorific value are two names for the same term and is a measure on the heat available when completely burning a fuel[87]. Gross calorific value is equivalent to higher heating value, (HHV) while net calorific value is equivalent to lower heating value. In gross calorific value the water

produced in combustion is in liquid state, hence the latent heat of water condensation is recovered. In net calorific value the water produced is in the gaseous state and the latent heat of water vapor is lost in the combustion[87].

Thermal efficiency is hence a measure of how well the total energy in the feedstock has been utilized in production of the desired products[8]. It is displayed mathematically in Equation 7.2 and typical values for GTL plants is about 60%(ref. section 2.2.1). The calculation procedure is outlined in Appendix F.

$$\text{Thermal efficiency, (TE)} = \frac{\text{LHV of liquid final products}}{\text{LHV of natural gas feed}} \times 100\% \quad (7.2)$$

7.1.3 Liquid volume of product

This was chosen as an optimization target as this is the most frequent used production measure in industry and hence offers direct comparison with existing plants.

7.2 Defining optimization variables

In order to be able to modify the output of the simulation a set of optimization variables or degrees of freedom must be identified. The following discussion outlines the variables used in this modelling and how they affect the process.

7.2.1 Reactor Volume

The size of the reactor is of great importance for the possible extent of reactions. If the reactor is too small, the reactions will be incomplete at the reactor outlet leading to unused reactants and low conversion to products. However the scenario of a too big reactor will not affect the optimization result, as the reactions will have gone to completion, but rather affect the economics as the reactor cost tend to increase with volume.

7.2.2 Molar flow of steam

The molar flow of steam added to the system affects the $\frac{H_2}{CO}$ ratio out of the reformer as more steam will increase the probability of converting all hydrocarbons with more than one carbon atom into methane, but it will also make the shift reaction go to the right, consuming CO and producing hydrogen (ref. section 4.1). Hence the ratio increases with the amount of

steam, and consequently altering the flow rate of steam can help obtaining the desired $\frac{H_2}{CO}$ ratio for the simulations. However steam is not the only process parameter that affects this ratio and it can not be controlled by steam alone.

7.2.3 Molar flow of oxygen

The flow of oxygen to the reformer determines to what extent the exothermic oxidation reactions in the reformer is carried out and hence it affects the temperature of the produced syngas. The more oxygen, the greater the reaction extent of the exothermic oxidation reaction and hence the greater the temperature. However as explained in section 6.2 an upper limit of 1030°C is applied to avoid soot formation.

7.2.4 Recycle fraction and splits

The degree of recycling affects the process in various ways. Recycling of light ends, CO and H_2 can increase both CE, TE and amount of liquid product, but also put a larger load on the system requiring larger equipment and compression.

How the recycle is divided between returning to the feed and to the Fischer-Tropsch reactor is also a degree of freedom for the simulation. As the fraction recycled back to the reactor does not pass through the pre-reformer or the reformer, the recycling of the light ends and LPG does not give an additional amount of Fischer-Tropsch products as only H_2 and Co is utilized as reactants in the Fischer Tropsch reactor. If the recycle stream contains much of these higher hydrocarbons it would be more beneficial to convert those to methane in the pre-reformer before it sent through the process cycle again. On the other hand it is no need for sending a large fraction back to the pre-reformer if the stream is mainly methane and hence the recycling split is highly dependent on the composition of the stream being recycled.

However recycling all directly back to the feed would lead to unnecessary circulation of H_2, CO and heavier hydrocarbons.

7.2.5 Purge fraction

Although there are several advantages with recycling it also leads to an unavoidable build up of inerts. Recycling these components does not offer

an additional output to the process and only increases the volume flow. Hence it is necessary to purge the system to reduce the inert flow. However it is not only the inerts that is lost in the purge, but also valuable products and components. Consequently there is a trade off between reducing the load and loss of valuable components.

7.2.6 Cooling temperature for FTR

The temperature of the boiling water surrounding the FTR is another degree of freedom in the optimization process. With a large enough flow of boiling water, the temperature of the stream leaving the reactor will have the same temperature as the cooling medium and hence this could affect the reactions depending on the magnitude of the temperature change. As the reactions are exothermic, an increase in the temperature of the boiling water should lead to a decrease in products as given by Le Châtelier's principle, and opposite for a temperature decrease.

7.2.7 Indicators

From the discussion in this and the previous chapter, the parameters outlined in Table 7.1 were found to serve as good indicators for the process performance and how the optimization variables have changed. Consequently these values will be recorded for the various optimization schemes and serve as comparison basis. The respective values for the base case is given in the last column of the table.

Table 7.1 – Process indicators and their optimization targets

Variable	**Target**	**Base case**
Reaction extent in FTR	-	47.98
		2.64
Reactor Volume	-	1000
$\frac{H_2}{CO}$	$\backsimeq$ 2.0-2.1	2.119
$\frac{H_2O}{NG}$	-	0.6906
$\frac{O_2}{NG}$	-	0.5918
Temperature syngas [°C]	$\leq$ 1030	979.3
Purge fraction	-	0.2
Recycle fraction to FTR	-	0.768
Recycle fraction to feed	-	0.232
CE [%]	$\geq$ 77	59.98
TE [%]	$\geq$ 60	47.86
Product flow $[\frac{bbl}{d}]$	$\geq$ 17000	14310

Chapter 8

Optimization Procedure

The optimization procedure for the model can be divided in three main parts. First the base case was analysed in terms of performance as outlined in section 6.3 and chapter Optimization. The second part comprises the attempt of optimizing the base case in terms of TE, CE and product flow to upgrading. This process was carried out with the use of case studies and optimizer in Unisim. However, finding the optimal configuration based on these measures does not incorporate process economics and hence may not be a realistic alternative. Consequently the third part of the optimization consists of the inclusion of process economics. This was found to be closely related to energy efficiency and heat integration of the process. A heat integration analysis was thus conducted before a cost per produced unit function was created and tried optimized, in order to see if it affected the previous optimization results. The following sections will address these last two parts of the optimization procedure.

8.1 Case studies

Based on the evaluation of the base case a range of case studies were executed to reveal the interrelations of the process and to locate optimum values.

8.1.1 Case 1 - FTR Volume

It was indicated in the base case evaluation that the reactions in the FTR did not proceed to the degree that was desired and that this likely was due to a too small reactor.

Figure 8.1 shows the molar flow of CO and H_2 respectively as a function of the reactor length for the base case. From the figure it can be observed that there is large amounts of reactants left at the reactor outlet. In addition their respective slopes indicates that this is not due to the reactions lacking a driving force and that a larger reactor would lead to greater consumption of the reactants and hence increased formation of product.

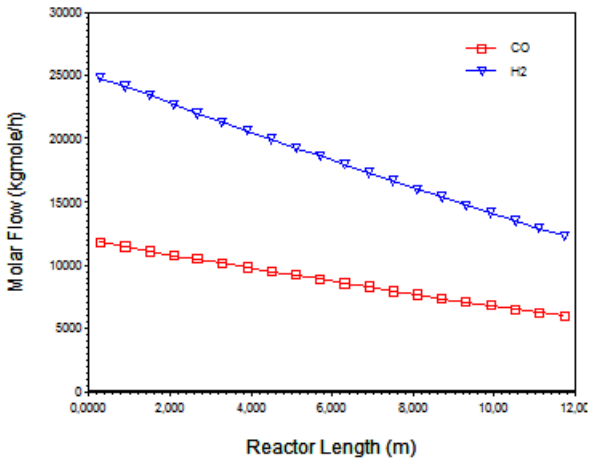

Figure 8.1 – Molar flow of hydrogen, (blue triangles) and carbon monoxide, (red squares) in $\frac{kmol}{h}$ as a function of reactor length, in meters, in the FTR for the base case.

This prompted a case study for the molar flow of CO and H_2 as a function of reactor volume to locate the volume that would give an optimal consumption of reactants and hence amount of product. The case study used reactor volumes between 400-2400 m^3 and the output is shown in Figure 8.2. Based on the case study an optimal reactor volume, based on the consumption of reactants, seems to be accomplished at about $1600m^3$. At this volume there is still a small mole flow left of both of reactants. This is done to try to maintain the $\frac{H_2}{CO}$ ratio at about 2 all the way through the

reactor as this is the desirable ratio for the Fischer Tropsch reaction. As seen from Figure 8.2, H_2 is used faster than CO and consequently there will be a point where the ratio will be below 2 and continue to decrease with increasing reactor volume. At this point, increasing the volume would not give more output, only a larger vessel.

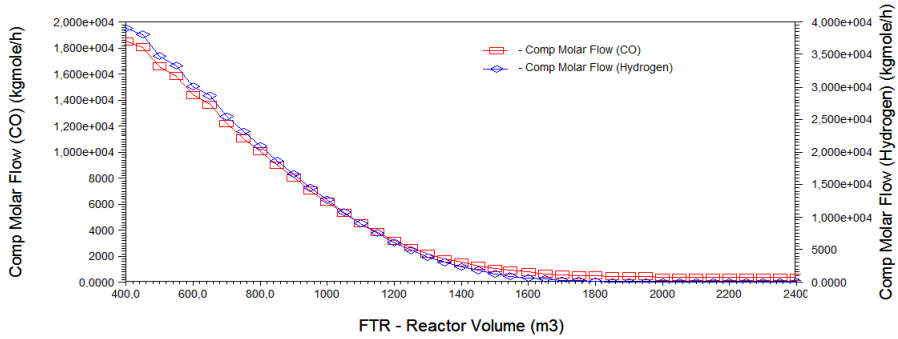

Figure 8.2 – Molar flow of hydrogen, (blue diamonds) and carbon monoxide, (red squares) ,in $[\frac{kmol}{h}]$, as a function of FTR volume, in m^3, for the base case.

1600 m^3 was consequently implemented as new value for the reactor volume,and the plot of molar flow of CO and H_2 as a function of reactor length can be assessed again. This is shown in Figure 8.3. As expected the components are close to completely consumed and the molar flows of hydrogen and carbon monoxide leaving the reactor are 716.63 and 780.48 $\frac{kmol}{h}$ respectively. This indicates that the reactor might be slightly oversized, but considering the early stage of the optimization the reactor volume was kept until further.

By examining the process further it can be seen from the parameters in Table 8.1 that with the increase in reactor volume the reaction extents also increased and the flow of products improved significantly. Already it produces more than the 17000 $\frac{bbl}{d}$ the feed was designed for. This improvement can also be seen through the increased carbon and thermal efficiency, now at typical values for a GTL plant, indicating that the feedstock is used more efficiently. Another interesting fact is the increased temperature of the syngas without changing the molar flow of oxygen. This indicates that the net exothermic reforming reactions now proceeds to a greater extent than for the base case. This is confirmed as the the steam reforming reaction in-

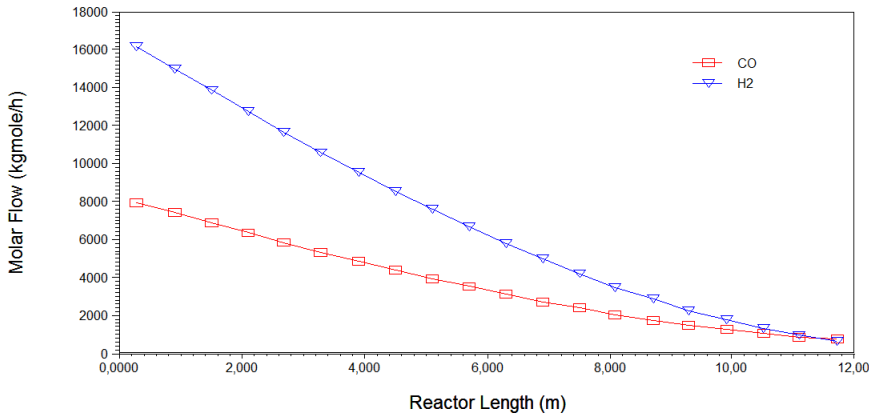

Figure 8.3 – Molar flow of hydrogen, (blue triangles) and carbon monoxide, (red squares) in $[\frac{kmol}{h}]$ as a function of reactor length for a reactor volume of 1600 m^3.

creased from 55.32 to 59.00% from the base case and the oxidation reaction increased from 33.31 to 35.81%.

8.1.2 Case 2 - Molar flow of oxygen

The exothermic oxidation reaction in the reformer converts methane to water and CO, and provides necessary heat for the steam methane reforming reaction. It is naturally desirable to convert as much methane as possible into syngas to increase the output of products and thus a large oxygen flow seems beneficial. However the increase in temperature accompanied by the increase in reaction extent for the oxidation reaction must comply with the upper temperature limit of 1030 °C, hence imposing an upper limit for molar flow of oxygen as well. Nevertheless, the produced water from the oxidation reaction might also push the shift reaction to the right consuming CO and produce H_2 and consequently alter the $\frac{H_2}{CO}$ ratio. This makes it difficult to predict how the addition of oxygen will affect the $\frac{H_2}{CO}$ ratio. A case study for the molar flow of oxygen and $\frac{H_2}{CO}$ ratio and one for the molar flow of oxygen and syngas temperature were hence conducted to find an optimal molar flow of oxygen and to highlight the correlation between the parameters.

The first of the two is shown in Figure 8.4 and shows an almost linear decrease in ratio with increasing oxygen. Based on this case study the molar

flow of oxygen should not exceed 5520 $\frac{kmol}{h}$ in order to keep the ratio above 2.

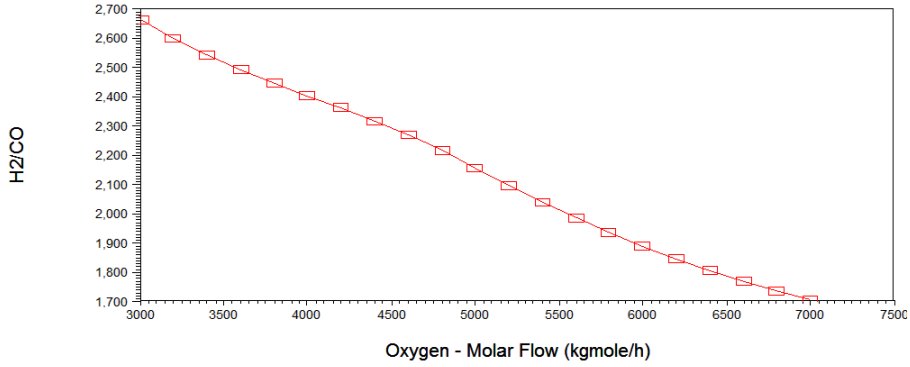

Figure 8.4 – $\frac{H_2}{CO}$ ratio in the syngas leaving the ATR as a function of molar flow of oxygen in the range 3000-7000 $\frac{kmol}{h}$, added to the ATR

The latter case study is shown in Figure 8.5 and indicates an increasing temperature with increasing oxygen flow as expected. To keep the temperature below 1030 °C the molar flow should be kept below 4880 $\frac{kmol}{h}$. Comparing to Figure 8.4 this would correspond to a $\frac{H_2}{CO}$ ratio of 2.193. The molar flow of oxygen was consequently adjusted to 4870 $\frac{kmol}{h}$ as this satisfied both constraints and from Table 8.1 it can be seen that it only resulted in a small increase in TE, CE, and product flow. It is also noted from Table 8.1 that the resulting $\frac{H_2}{CO}$ ratio was 2.090 and not 2.193 as indicated by the case studies. This is most likely caused by the iteration procedure of the flow sheet.

8.1.3 Case 3 - Molar flow of steam

The next variable to be optimized was steam and the increased $\frac{H_2}{CO}$ ratio with increasing molar flow rate of steam is confirmed as shown in Figure 8.6. From this figure it can be seen that in order to keep the ratio above 2, the molar flow of steam needs to exceed 4500 $\frac{kmol}{h}$.
Not only does the molar flow of steam affect the $\frac{H_2}{CO}$ ratio, but also the temperature leaving the ATR. Figure 8.7 shows this relationship and it can be seen that the temperature generally decreases with increased molar flow

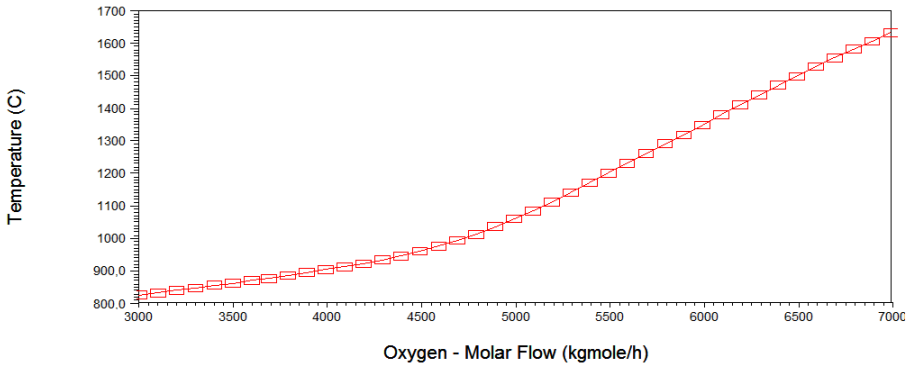

Figure 8.5 – Temperature [°C] of syngas as a function of molar flow of oxygen to the ATR in the range 3000-7000$[\frac{kmol}{h}]$

of steam. To maintain the temperature below 1030 °C the molar flow of steam should be above 5740 $\frac{kmol}{h}$. Comparing this value with the $\frac{H_2}{CO}$ ratio plot gives a ratio of approximately 2.1, which is above the minimum value of 2 and at the theoretical optimal value from the ASF distribution. The steam molar flow was consequently set to be 5740$\frac{kmol}{h}$. From Table 8.1 it can be seen that this lead to a further small increase in CE, TE and the molar flow of product.

Considering that both the molar flow of oxygen and steam affects the temperature, a case study was conducted with the temperature as a function of both of these. The result is shown in Figure 8.8 and indicates that the oxygen flow has a much greater effect on the temperature than steam.

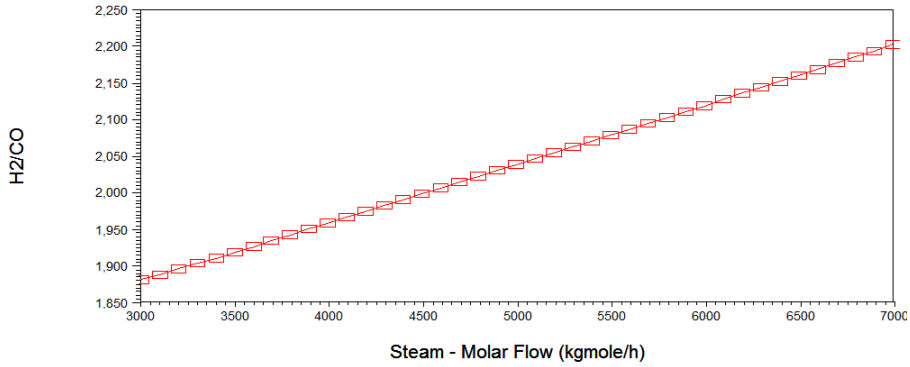

Figure 8.6 – $\frac{H_2}{CO}$ ratio plotted against molar flow of steam in the range 3000-7000 $\frac{kmol}{h}$

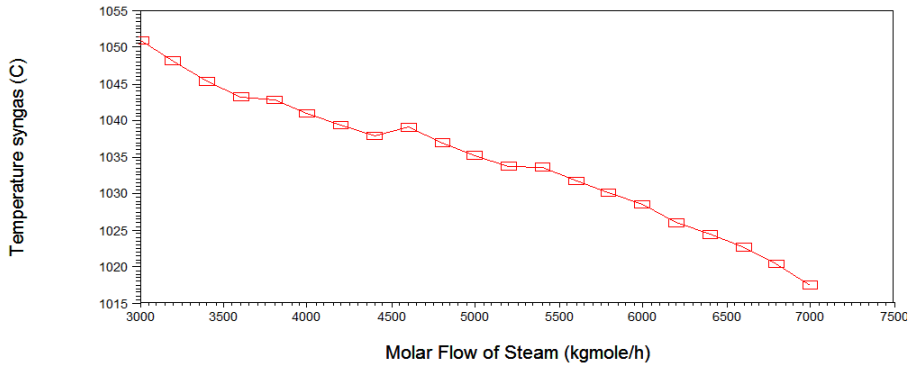

Figure 8.7 – Temperature [°C] of syngas leaving the ATR as a function of molar flow of steam in the range 3000-7500 $\frac{kmol}{h}$ added to the pre-reformer

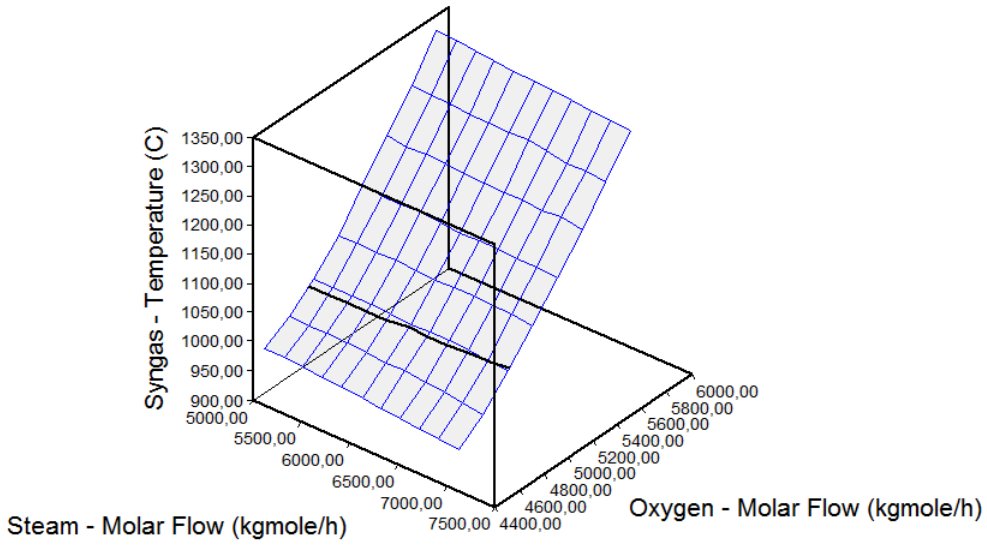

Figure 8.8 – Temperature [°C] of syngas leaving the ATR as a function molar flow of both oxygen and steam in $\frac{kmol}{h}$

8.1.4 Case 4 - Recycle fraction to FTR

So far the recycle split fraction between the FTR and feed has been kept constant at 0.765. It might however be more beneficial with another fraction depending on the composition of the recycled stream as discussed in Chapter 7.

Figure 8.9 shows the molar flow to upgrading unit as a function of the recycle ratio back to the Fischer-Tropsch reactor. The molar flow to upgrading unit increases with increased recycle as expected as the unconverted components from previous pass through the reactor i snow converted. However at a point the accumulation of higher hydrocarbons will make the recycle decrease the output instead. From the case study it can be seen that a recycle ratio of 0.85 would give the maximum product flow rate and was consequently applied in the simulation. However as can be seen from Table 8.1 this gave a syngas temperature of 1056 °C. This is above the constraint from a material aspect and hence this process is not an option. A case study investigating the effect of recycle ratio to FTR on temperature was consequently conducted to find the highest possible ratio. This is shown in Figure 8.10. The temperature increases linearly with increased recycle

which likely is attributed to increase in exothermic conversion of more feeds. From this figure it can be seen that in order to keep the temperature below 1030 °C, the highest recycle ratio possible is 0.768. This is the same value as used in the base case and previous case studies.

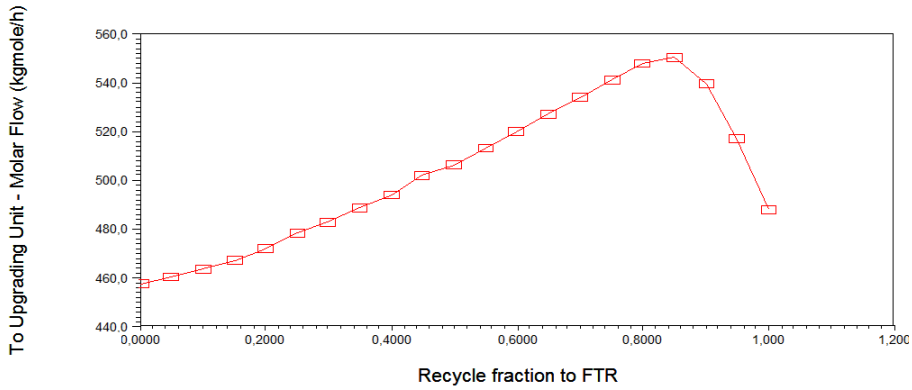

Figure 8.9 – Molar flow $[\frac{kmol}{h}]$ to upgrading unit as a function of recycle fraction back to the Fischer-Tropsch reactor

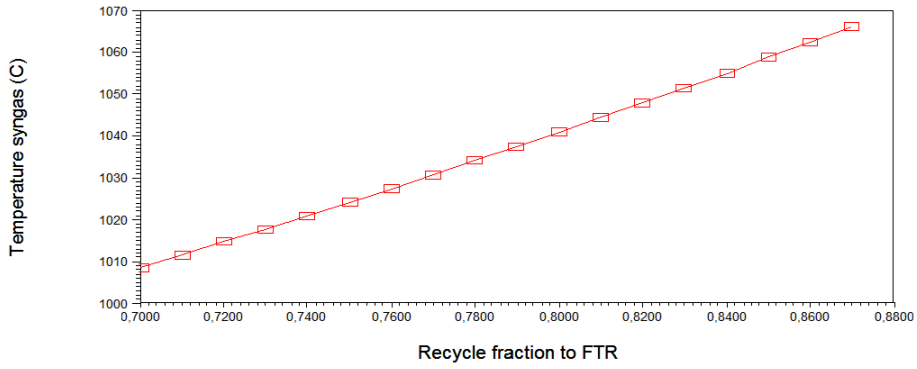

Figure 8.10 – Syngas temperature [°C] as a function of recycle fraction back to the Fischer-Tropsch reactor

8.1.5 Case 5 - $\frac{H_2}{CO}$ ratio of 2.15

Even though the case with a recycle ratio of 0.85 gave a too high temperature out of the ATR, it had a larger molar flow of products and a much higher $\frac{H_2}{CO}$ ratio than previous case studies and hence it was tried to achieve a ratio of approximately 2.15 while keeping the temperature below 1030, to see if this was the reason for the increased the output. This was tried achieved by altering the and from Case-3, it was found that a ratio of 2.15 was to be obtained, without exceeding 1030 °C, at approximately 6330 $\frac{kmol}{h}$. After some trial and error with values around this, a molar flow of steam at 6310 was found to give a good ratio. From Table 8.1 it can be seen that this increased ratio gave a improved CE, TE and molar flow to upgrading unit, but not an increase in volume of liquid product.

8.1.6 Case 6 - Steam and flow to upgrading

The increased flow to upgrading unit, as experienced from the previous case study, was desired to establish if could be further improved by further increasing the $\frac{H_2}{CO}$ ratio. As both ratio and molar flow to upgrading unit are dependent variables an independent variable was need to investigate this relationship. This variable was chosen to be steam as this is the main variable affecting the $\frac{H_2}{CO}$ ratio. Consequently a new case study was hence conducted outlining how the molar flow to upgrading and temperature behaved by varying the steam added. This is shown in Figure 8.11

It can be seen that the maximum molar flow to upgrading unit of 552 $\frac{kmol}{h}$ is achieved at a $\frac{H_2}{CO}$ ratio of 2.16 which corresponds to a molar flow rate of steam of 6500 $\frac{kmol}{h}$. Although it was determined at a previous stage that the flow of steam had a much smaller impact on temperature than oxygen a high temperature out of the ATR is still desired in relation to maximum conversion and hence the temperature was plotted against the molar flow to upgrading unit and steam. From the plot as shown in Figure 8.12 it can be seen that this molar flow of steam corresponds to a temperature of about 1023 °C.

As a consequence the steam molar flow was altered to 6500 $\frac{kmol}{h}$ and then the oxygen flow was adjusted by trial and error to achieve a temperature closer to 1030 °C. This was found to be at a oxygen flow rate of 4900 $\frac{kmol}{h}$. However adding oxygen to increase the temperature leads to a decrease in $\frac{H_2}{CO}$ ratio and the resulting ratio obtained in this simulation was 2.155. Both CE, TE flow to upgrading in terms of both molar flow and liquid volume was improved for this simulation as seen in Table 8.1. This could thus indicate

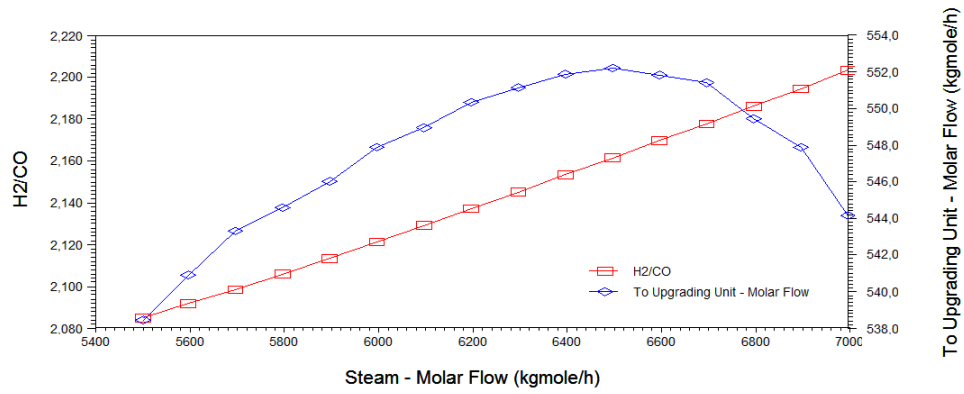

Figure 8.11 – Plot of $\frac{H_2}{CO}$ ratio and molar flow to upgrading unit $[\frac{kmol}{h}]$ as a function of molar flow of steam $[\frac{kmol}{h}]$.

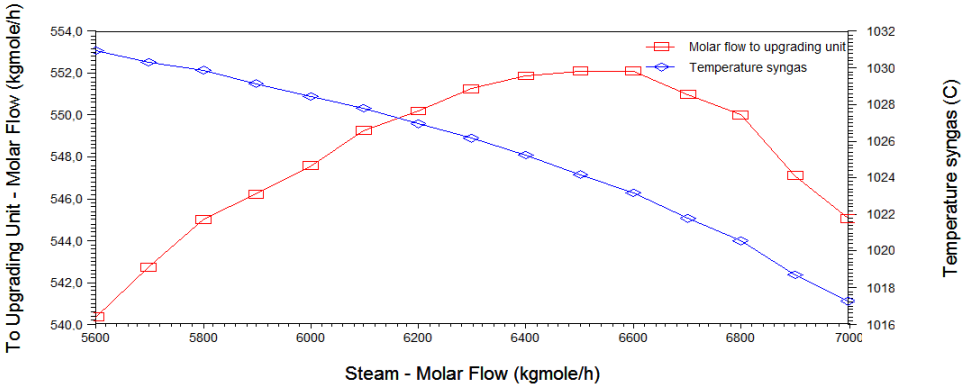

Figure 8.12 – Plot of molar flow to upgrading unit $[\frac{kmol}{h}]$ and temperature of syngas [°C] as a function of molar flow of steam $[\frac{kmol}{h}]$.

that a higher $\frac{H_2}{CO}$ ratio leads to improved production. However also the flow of steam, oxygen and the temperature of syngas increased from the previous case and due to the intertwined relationship of these variables it is difficult to point out the determining factor.

8.1.7 Case 7 - Multi variable

The previous section illustrates the intertwine relationship between oxygen, steam, syngas temperature and $\frac{H_2}{CO}$ ratio. As a tuning of one and one parameter seemed to be time consuming and inefficient, a multivariable case study was conducted. This was achieved by plotting molar flow of steam and oxygen against molar flow to product upgrading unit. The case study function in Unisim has a limitation of four variables per case study and three variables for the plot and hence the temperature was omitted from this first multi variable analysis. The case study analysis gave 7000 and 5000 $\frac{kmol}{h}$ in molar flow respectively for steam and oxygen as what would give the highest molar flow to upgrading of 558.7 $\frac{kmol}{h}$, and should give a $\frac{H_2}{CO}$ ratio of 2.147. Not unexpectedly, when considering Figure 8.8, the temperature obtained was 1058 °C, which is well over the target of 1030 °C.

By trial and error adjusting the flow of oxygen and steam a scenario was found to fulfil the criteria of temperature below 1030 °C with oxygen flow of 4900 $\frac{kmol}{h}$ and steam at 6700 $\frac{kmol}{h}$. The rest of the result variables from this scenario is shown in Table 8.1 and again an improvement in CE, TE and flow to upgrading unit was observed.

At this point it was decided to implement an adjust block to the simulation keeping the temperature of the syngas at 1030 °C by adjusting the molar flow of oxygen. By using the adjust block, the continuous manual tweaking and check ups on temperature was eliminated. The case study was then run again.

This time the optimum values were found to be 4954 $\frac{kmol}{h}$ and 6900 $\frac{kmol}{h}$ for oxygen and steam respectively. This should give an output of 557.5 $\frac{kmol}{h}$ and a $\frac{H_2}{CO}$ ratio of 2.159. However when these values were inserted in the simulation the adjust block automatically start and the actual values obtained was 4929 $\frac{kmol}{h}$ and 6900 $\frac{kmol}{h}$ in molar flows for oxygen and steam respectively with a $\frac{H_2}{CO}$ ratio of 2.177 and molar flow to upgrading of 553.7 $\frac{kmol}{h}$. As this value was lower than expected another try was done at inserting the values from the case study, this time only changing the oxygen flow to 4953 $\frac{kmol}{h}$ in case the value of 4954 was given by rounding up and making the adjust iterations search at "the wrong side of the optimum". Again the adjust block makes the flow sheet iterate and the actual values for the converged sheet was 4914 $\frac{kmol}{h}$, 6900 $\frac{kmol}{h}$, $\frac{H_2}{CO}$ ratio of 2.174 and an output of 557.1 $\frac{kmol}{h}$, which is much closer to the values from the case study. The rest of simulation parameters are given in Table 8.1 under Case

7 - adjust.

8.1.8 Case 8 - FTR volume revisited

From an article on steady state simulation and optimal operation of a GTL plant by Panahi et. al it was stated that a reactor volume over 2200 m^3 did not give any significant increase in the liquid production[57]. As the reactor volume applied in this simulation was at 1600 m^3 it was desired to see if an increase in volume would positively affect the production. The reactor volume was consequently increased to 1700 m^3 and resulted in a positive effect, hence another increase, this time to 2100 m^3 was carried out. The parameters for this last simulation is shown in Table 8.1.

As it was possible with further improvements for the reactor volume, by increasing it beyond the value previous found in an early case study, it was investigated if the same was the case for the molar flow of steam. Oxygen was not checked as this now is adjusted to keep syngas temperature at 1030 °C and hence not offers a degree of freedom any more. From the case study it was found that the maximum molar flow to upgrading unit, 566.8 $\frac{kmol}{h}$, was achieved by a molar flow of steam at 6200 $\frac{kmol}{h}$, which is much smaller than what was obtained from Case 7. This was then changed for the simulation and a molar flow to upgrading unit of 568.4 was obtained. This simulation is shown as Case 8 v2. in Table 8.1

This indicates that as other variables have changed through the range of case studies, the optimized value for steam found in the beginning, no longer was valid as many of the other parameters had changed.

8.1.9 Reflections on optimization procedure

Although case studies in Unisim is a very good tool to see how the different variables are connected, it has its disadvantages as an optimization tool. Case studies gives the effect of one, maximum three, parameters given all other are kept constant. This means that by first choosing an optimal value for one parameter based on a case study, where all other parameters are fixed, then choosing another, based on a separate case study, while keeping the parameter first optimized and all others, fixed, would most likely change the conditions for the optimal value the first parameter was optimized with respect to. As was experienced during the case studies conducted in this work. In principle one can continue this process for a long time, only getting local optimums. Hence another procedure was found to be necessary to be

able to find an overall optimum for the process.

I was also considered from a retrospective point that the adjust block most likely should have been added earlier on in the process for easier optimization.

Table 8.1 – Overview of the main process parameters, variables adjusted in the optimization and the optimization target variables for the various case studies conducted

	Case										
Parameter	Base Case	1	2	3	4	5	6	7	7-adjust	8	8 v2
FTR Volume $[m^3]$	1000	1600	1600	1600	1600	1600	1600	1600	1600	2100	2100
FTR conversions [%]											
FTR	47.98	86.09	84.44	85.78	90.83	90.53	91.11	90.77	91.81	93.51	93.31
Metahanation	2.64	4.78	4.59	4.75	5.69	5.56	5.74	5.66	5.96	6.51	5.77
Temperature syngas [°C]	979.3	1028	1030	1030	1056	1027	1029	1027	1030	1030	1030
Ratios											
$\frac{H_2}{CO}$	2.119	2.102	2.09	2.104	2.151	2.147	2.155	2.165	2.174	2.175	2.141
$\frac{H_2O}{NG}$	0.6906	0.6906	0.6906	0.7004	0.7004	0.77	0.7932	0.8176	0.8420	0.8420	0.7566
$\frac{O_2}{NG}$	0.5918	0.5918	0.5943	0.5943	0.5943	0.5943	0.5979	0.5979	0.5996	0.5992	0.5943
Purge fraction	0.20	0.20	0.20	0.20	0.20	0.20	0.2	0.2	0.2	0.2	0.2
Recycle to FTR	0.768	0.768	0.768	0.768	0.85	0.768	0.768	0.768	0.768	0.768	0.768
Recycle to feed	0.232	0.232	0.232	0.232	0.15	0.232	0.232	0.232	0.232	0.232	0.232
CE [%]	59.98	78.17	78.43	78.45	78.1	78.58	78.83	79.01	79.08	79.25	79.72
TE [%]	47.86	62.50	62.71	62.73	62.46	62.84	63.04	63.18	63.38	63.4	63.77
Product											
molar flow $[\frac{kmol}{hr}]$	369	541.4	542.5	543.0	550.7	550.8	553.1	554.7	557.1	564.8	568.4
in $\frac{std.bbl}{d}$	14310	18820	18890	18890	18830	18940	19000	19040	19060	19120	19240

8.2 Optimizer

Unisim contains a built-in optimization tool for steady state modelling able to account for multiple variables. Given the flow sheet has converged the optimizer can be applied to maximize or minimize a given objective function [88]. In addition to the objective function and optimization variables it can be added constraints for the optimizer.

Due to the struggle with optimization of the process manually and with the aid of case studies, the optimizer was applied to the simulation. The adjustable variables used in the optimizer is listed in Table 8.2 together with their starting upper and lower bounds. Two constraints were applied for all simulations. First the $\frac{H_2}{CO}$ ratio was set to be above 2 at all times and second the syngas temperature was set to be below 1031 °C.

Table 8.2 – List of the variables to be adjusted in the optimizer tool in Unisim along with the respective upper and lower bounds

Variable	**Range**	
	Minimum	Maximum
Reactor Volume [m^3]	500	2300
Molar flow oxygen [$\frac{kmol}{h}$]	3700	5500
Molar flow steam [$\frac{kmol}{h}$]	4500	7500
Recycle ratio to FTR	0.0	1.0
Purge split	0.0	1.0

8.2.1 Product flow

First the objective function was set to maximize the molar flow to the upgrading unit. In total 11 attempts were made at the optimizer for the optimization of product flow and Table 8.3 outlines results and values for the main process indicators. Table 8.4 outlines the main changes made with relations to previous try. For some of the cases the only change made relates to tolerance and iteration level or is simply a re-run and are omitted from Table 8.4. The complete list is however given in Table G.1 in Appendix G.

Table 8.3 – Overview of the main changes for the optimizer in Unisim when applied to flow to upgrading unit as objective function

Case	Change from previous/Note
Optimizer base case	Based on case 8v2 from the case study optimization
1	number of iterations set to 100, tolerance set to 0.001, boundaries for optimization variables changed, see Table 8.4
4	objective function changed to liquid volume flow at standard conditions
5	Number of iterations set to 200, tolerance set to $1 \cdot 10^{-5}$, maximum change per iteration set to 0.1, boundaries changes as shown in Table 8.4
6	Increased number of iterations and function evaluations to 500, lower bound reactor volume set to 1500
8	included temperature of boiling water to FTR in variables
9	Adjust not solved, however T=1030 °C
10	Adjust not solved, however T=1030 °C
11	Adjust solved

Table 8.4 – Overview of the optimization variables used by Optimizer in Unisim and their bounds applied for the respective simulations

Variable	Case 1 Range		Case 5 Range		Case 6 Range		Case 8	
	Min	Max	Min	Max	Min	Max	Min	Max
Reactor Volume [m^3]	1500	2300	1200	2300	1500	2300	1500	2300
Molar flow oxygen [$\frac{kmol}{h}$]	4400	5500	4400	6500	4400	6500	4400	6500
Molar flow steam [$\frac{kmol}{h}$]	5500	7500	5500	7000	5500	7000	5500	7000
Recycle ratio to FTR	0.3	0.9	0.3	0.9	0.3	0.9	0.3	0.9
Purge split	0.0	0.4	0.0	0.4	0.0	0.4	0.0	0.4
Boiling water to FTR [°C]	-	-	-		-	-	190	250

Table 8.5 – Results of the Optimizer applied to flow to upgrading unit in terms of the process performance indicators and optimization targets chosen for the simulations in this work

	Optimizer Case											
Parameter	Optimizer Base case	1	2	3	4	5	6	7	8	9	10	11
FTR Volume $[m^3]$	1911.959	1911.717	1911.717	1856.535	1911.703	1790.423	1892.3	1892.3	1893.433	1933.433	1933.546	1933.543
FTR conversions [%]												
FTR	85.96	87.23	88.4	89.47	86.95	91.15	91.23	91.86	85.96	86.68	85.75	84.22
Metahanation	4.29	4.46	4.63	4.79	4.44	5.22	5.30	5.46	4.36	4.45	4.30	4.10
Temperature [°C]												
Syngas	1030	1030	1030	1030	1030	1030	1030	1030	1030	1030	1030	1030
Boiling water	220	220	220	220	220	220	220	220	223	223	223.9	223.7
Molar flows $[\frac{kmol}{h}]$												
Steam	6030	6297	6297	6448	6293	6857	6594	6594	6478	6478	6600	6435
Oxygen	4958	4958	4963	4937	4971	4941	4910	4918	4954	4956	5005	5005
Ratios												
$\frac{H_2}{CO}$	2.021	2.049	2.056	2.082	2.041	2.122	2.129	2.136	2.062	2.066	2.037	2.014
$\frac{H_2O}{NG}$	0.7358	0.7684	0.7684	0.7689	0.7679	0.837	0.8046	0.8046	0.7904	0.7904	0.8053	0.7853
$\frac{O_2}{NG}$	0.605	0.605	0.6057	0.6024	0.6066	0.6029	0.5991	0.6001	0.6045	0.6047	0.6107	0.6107
Purge fraction	0.253	0.257	0.257	0.271	0.244	0.233	0.184	0.184	0.175	0.175	0.184	0.187
Recycle to FTR	0.552	0.563	0.563	0.560	0.580	0.655	0.761	0.761	0.727	0.727	0. 675	0.654
CE [%]	80.02	80.00	80.36	79.59	80.44	79.97	79.90	80.22	80.62	80.66	80.99	80.94
TE [%]	63.98	63.97	64.26	63.93	64.31	63.95	63.90	64.17	64.47	64.51	64.77	64.72
Product												
molar flow $[\frac{kmol}{h}]$	558.00	559.8	563.7	562.4	563.5	567.00	569.9	572.00	571.8	572.7	572.3	569.8
in $\frac{std.bbl}{d}$	19280	19280	19370	19270	19380	19280	19280	19360	19450	19460	19530	19510

8.2.2 Evaluation of Optimizer and product flow

From the optimization on molar flow it was observed that an increase in the molar flow not always led to an increase in the liquid volume flow when compared to previous cases. However the same was also experienced when the objective function was changed to liquid volume. It was further also observed for all objective functions that the best result in liquid volume never occurred at the same optimizer run as the best result in molar flow. This is most likely attributed to the fact that the molar flow only measures the total size of the stream and does not take into consideration variations in composition, while the liquid volume is dependent of the density and molar mass of the stream and consequently two identically molar flows can give two totally different volumes based on composition.

The relationship between molar flow and volume is given in Equation 8.3. From this relationship it can be seen that there are four interesting scenarios for the change in flow to the upgrading unit:

1) both molar flow and liquid volume increases
2) both molar flow and liquid volume decreases
3) molar flow increases and liquid volume decreases
4) molar flow decreases and liquid volume increases

For the first and second scenario it can be assumed that the compositions does not change much relative to each other, and rather indicates an improvement in the process or a decline respectively.

For the third and fourth scenario however, the differences lie in the composition. If the volume is increased while the molar flow is reduced compared to a previous optimization, it can be seen from Equation 8.3 that $\frac{\rho}{M_m}$ must have decreased as well to fulfil the equality. A decrease in this fraction is either attributed to a decrease in density, an increase in molar mass, a larger increase in molar mass than density or a larger decrease in density than molar mass. For the opposite case where the volume is decreased and the molar flow has increased the ratio of density to molar mass must have increased. This is attributed to a decrease in mass, increase in density, a larger increase an density than molar mass or a larger decrease in molar mass than density. However there will likely not be a change in one of the variable without a change in the other, leaving two explanations for each of the scenarios.

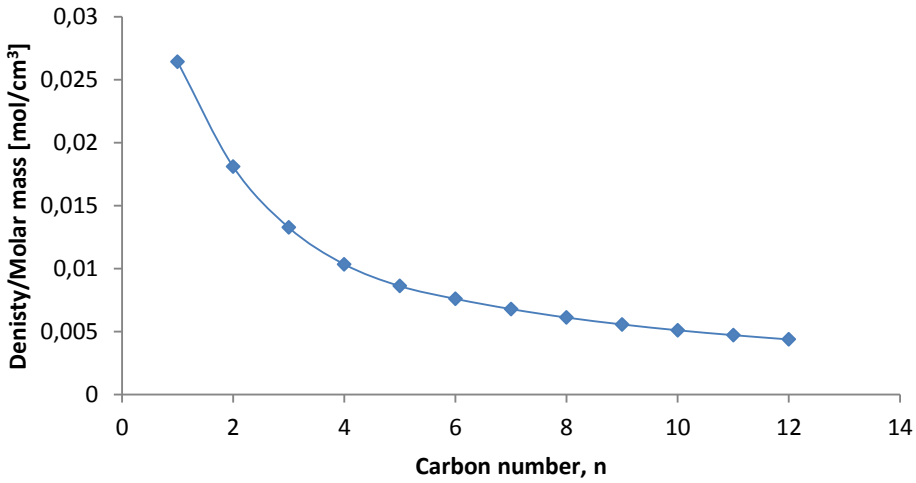

Figure 8.13 – Plot of the density to molar mass ratio $[\frac{mol}{cm^3}]$ as a function of carbon number for alkanes with 1-12 carbon atoms in the chain. Data obtained from SI Chemical Data [89]

Figure 8.13 shows the ratio of density to molar mass as a function of carbon number for the hydrocarbons with 1-12 carbon atoms in the chain (The data were obtained from SI Chemical Data 6th edition [89]). From this figure it can be seen that the ratio decreases with increasing carbon number. This implies that for scenario 3, where the fraction was decreasing, the stream consists of heavier components than previously, while for scenario 4, where the fraction was increasing, it indicates that the stream consists of lighter components.

$$n = \frac{m}{M_m} \tag{8.1}$$

$$\rho = \frac{m}{V} \tag{8.2}$$

$$n = \frac{\rho \times V}{M_m} \tag{8.3}$$

Hence it can be noted that the liquid volume is probably a more suitable optimization target than molar flow as an increase in this value while the molar flow has decreased is likely due to higher fraction of higher hydrocarbons while an increase in molar flow and decrease in liquid volume indicates the opposite. This does not mean that a high molar flow is undesirable, only that it must be seen together with the liquid volume flow and the scenario with increasing liquid volume flow is likely to be more optimal than increasing molar flow as it is more desirable with heavier hydrocarbons going to the upgrading unit.

From Table 8.5 it can be seen that Case 10 shows the best results in terms of CE, TE and liquid volume flow to upgrading unit and are highlighted in red. The highest molar flow is however found for case 9 and is highlighted in blue. It can also be seen that Case 11 has the second highest values for the three same parameters as Case 10. Comparing them to see if there are any trends indicating what will result in a high production ratio, they have the same oxygen to carbon ratio, almost same purge fractions and the two smallest $\frac{H_2}{CO}$ ratios, close to 2.0. The steam to carbon ratio is however not that similar and might thus not be the most important factor for liquid production.

First investigating the purge fraction, it can be seen that Case 6 and 7 have the same purge fraction as case 10 and gives only slighter smaller molar flow to upgrading, but have lower liquid volume to upgrading unit values. By further comparison it is also seen that Case 6 and 7 have a lower oxygen to carbon ratios, higher $\frac{H_2}{CO}$ ratios at about 2.13 than Case 10 and 11. Thus purge fraction alone is likely not the decisive factor. However Case 6 and 7 have about same steam to carbon ratio as Case 10 and as previously mentioned these three cases are most similar in terms of molar flow to upgrading unit and this could indicate that the steam added mostly affects the molar flow and not liquid flow to upgrading.

Next it can be seen that the base case has a low $\frac{H_2}{CO}$ ratio similar to Case 10 and 11, however it gives poorer optimization values indicating that neither $\frac{H_2}{CO}$ ratio alone dictates the optimum. Finally the oxygen to carbon ratio was found to be comparably smaller for all other cases, but came

closest for case 4. As for the base case however the optimization values are lower than for case 10 and 11 indicating that this probably is not the decisive factor either.

From this brief evaluation it appears as though there is not one factor alone dictating the optimum process, but rather a combination of factors is needed to yield a positive outcome.

8.2.3 CE optimization

The objective function was changed from maximizing product flow to maximizing the carbon efficiency. It was run four times and CE base case used Case 11 from the product flow optimization as basis. The change between each run is only related to numericals such as tolerance, maximum number of iterations etc. and is outlined in Table G.2 in Appendix G. Table 8.6 show the results from this optimizer.

8.2.4 Evaluation of Optimizer and CE

From Table 8.6 it can be seen that Case CE2 have the best CE,TE and liquid volume flow to upgrading unit and is highlighted in red. However as for when the optimizer was applied to the product flow the highest molar flow value to upgrading unit is found at a different case than the three other parameters. For this part Case CE3 was found to perform best for the molar flow and is highlighted in blue.

It can also be seen that the low $\frac{H_2}{CO}$ ratio as was observed to give good results from the product flow optimization is present at all four CE optimizations and that they all have comparable product flows as the Case 10 and 11 from the previous optimizer. The oxygen to carbon ratio is also at about 0.61 for the three last optimizations on CE, which was also observed for Case 10 and 11 from the product flow optimizer. Finally the purge ratio for CE2, CE3 and CE4 is equal and the same as for Case 11 and almost same as Case 10. These three cases have slightly higher liquid volumes than the base case for CE indicating that the combination of a low $\frac{H_2}{CO}$ ratio, oxygen to carbon ratio at about 0.61 and a purge ratio at about 0.187 is beneficial for the process.

Comparing the results from this optimization with the optimization on flow to upgrading unit shows an increase in all target variables applied to the simulation.

Table 8.6 – Results of the Optimizer applied to carbon efficiency in terms of the process performance indicators and optimization targets chosen for the simulations in this work

	Optimizer Case			
Parameter	CE base case	CE2	CE3	CE4
FTR Volume $[m^3]$	1933.523	1933.523	1933.33	1893.33
FTR conversions [%]				
FTR	85.93	82.17	85.19	85.06
Metahanation	4.3	3.86	4.23	4.21
Temperature syngas [°C]	1030	1030	1030	1030
Molar flows $[\frac{kmol}{h}]$				
Steam	6435	6435	6900	6600
Oxygen	4967	5027	5032	5021
Ratios				
$\frac{H_2}{CO}$	2.044	1.993	2.03	2.022
$\frac{H_2O}{NG}$	0.7853	0.7853	0.8419	0.8054
$\frac{O_2}{NG}$	0.6061	0.6134	0.6141	0.6126
Purge fraction	0.207	0.187	0.187	0.187
Recycle to FTR	0.654	0.654	0.654	0.654
CE [%]	80.7	81.24	81.05	81.06
TE [%]	64.53	64.96	64.81	64.81
Product				
molar flow $[\frac{kmol}{h}]$	568.5	570.3	572.6	571.4
in $\frac{std.bbl}{d}$	19450	19580	19540	19540

8.2.5 TE optimization

The objective function was changed from carbon efficiency to thermal efficiency to see if it changed the optimum. It was run eight times and new bounds as given in Table 8.8 and a higher penalty value to keep the $\frac{H_2}{CO}$ ratio above 2 was applied to the CE4 optimization to give a base case for TE optimization. Table 8.9 outlines results and values for the main process indicators while Table 8.7 outlines the main changes made with relations to previous try. For some of the cases the only change made relates to tolerance and iteration level or is simply a re-run and are omitted from Table 8.7. The complete list is however given in Table G.3 in Appendix G.

Table 8.7 – Overview of the main changes for the optimizer in Unisim when applied to TE as objective function

Case	Change from previous
TE base case	Based on CE4 but tolerance set to $1 \cdot 10^{-5}$ and maximum change per iteration set to 0.1 in addition to the new bounds as given in Table
TE2	lower bounds as given in Table 8.8, penalty for $\frac{H_2}{CO}$ ratio set to 1000
TE3	Penalty value increased to 10000, tolerance set to $1 \cdot 10^{-4}$, maximum change per iteration set to 0.2
TE4	new start value for steam
TE5	New bounds for steam as given by Table 8.8, maximum change per iteration set to 0.3
Bypass	Liquid from V-101 bypassed V-102 and sent straight to upgrade, new bounds as given in Table 8.8, penalty value back to 50, tolerance set to $1 \cdot 10^{-5}$, maximum change per iteration set to 0.1

Table 8.8 – Overview of the optimization variables used by Optimizer for TE in Unisim and their bounds applied for the respective simulations

Variable	TE base case		TE2		TE5		TE8	
	Range		Range		Range			
	Min	Max	Min	Max	Min	Max	Min	Max
Reactor Volume [m^3]	1500	2300	1500	2300	1500	2300	1100	2200
Molar flow oxygen [$\frac{kmol}{h}$]	4400	5700	3500	5700	3000	5700	3000	5700
Molar flow steam [$\frac{kmol}{h}$]	5500	9000	4500	9000	6500	11000	3000	9000
Recycle ratio to FTR	0.3	0.9	0.3	0.9	0.3	0.9	0.3	0.9
Purge split	0.0	0.4	0.0	0.4	0.0	0.4	0.0	0.4
Boiling water to FTR [°C]	190	250	190	250	190	250	190	250

Table 8.9 – Results of the Optimizer applied to TE in terms of the process performance indicators and optimization targets chosen for the simulations in this work

	Optimizer Case							
Parameter	TE base case	TE2	TE3	TE4	TE5	TE6	TE7	Bypass
FTR Volume $[m^3]$	1933.331	1933.331	1933.331	1933.331	1933.331	1933.331	1933.331	1933.36
FTR conversions [%]								
FTR	85.62	79.4	78.89	83.29	87.32	88.39	86.64	89.8
Metahanation	4.29	3.58	3.52	4.00	4.53	4.69	4.42	4.89
Temperature syngas [°C]	1030	1030	1030	1030	1030	1030	1030	1030
Molar flows $[\frac{kmol}{h}]$								
Steam	8300	7000	7000	8000	8750	8750	8750	8257
Oxygen	5137	5105	5110	5136	5154	5144	5176	5089
Ratios								
$\frac{H_2}{CO}$	2.03	1.944	1.937	2.002	2.052	2.063	2.03	2.086
$\frac{H_2O}{NG}$	1.013	0.8542	0.8542	0.9762	1.068	1.068	1.068	1.008
$\frac{O_2}{NG}$	0.6268	0.6229	0.6235	0.6267	0.6289	0.6277	0.6316	0.621
Purge fraction	0.173	0.173	0.173	0.173	0.173	0.173	0.173	0.190
Recycle to FTR	0.608	0.608	0.608	0.608	0.608	0.608	0.578	0.607
CE [%]	81.75	80.93	81.47	81.49	81.62	81.52	81.72	82.41
TE [%]	65.36	64.7	65.13	65.15	65.26	65.18	65.34	65.93
Product								
molar flow $[\frac{kmol}{h}]$	568.5	570.3	572.6	571.4	583.6	584.2	582.7	604.3
in $\frac{std.bbl}{d}$	19720	19500	19630	19650	19690	19670	19710	19940

8.2.6 Evaluation of Optimizer and TE

From Table 8.9 it can be seen that the best results in terms of CE,TE, molar flow and liquid flow to the upgrading unit, is obtained in the bypass case and is highlighted in green. As explained in Table 8.7, the liquid product from the FTR is now bypassing the 3-way separator. The liquid product from the FTR will have the same temperature as the reactor at about 223 °C while the gaseous product from the FTR is cooled to 38 °C before entering the 3-way separator. This is done to be able to separate out water and more efficiently separate the light ends for recycling. However with the liquid FTR product previously also passing through the 3-way separator the temperature increases significantly and hence the separation of both water and light ends becomes poorer as the water might evaporate and blend in with both flow to upgrading unit and recycling of light ends. There might also be some of the heavier hydrocarbons that have left the FTR with the gases and the entire point of cooling and passing it through the 3-way separator to recover them diminishes as the liquid product is also passed through this separator. It is therefore not surprising that this simulation appears to be in a class of its own in terms of performance. The Unisim workbook for this ismulation is given in Appendix D.

Taking out the bypass simulation from the set to evaluate the performance of the optimizer when applied to TE, it appears that the base case for the TE optimizer gives the best results for CE, TE and liquid flow to upgrading as highlighted in red. As also were the case for the CE and product flow optimizer, the best result in molar flow to upgrading does not belong to the same case as the three other optimization targets and is found for case TE6 as highlighted in blue.

From table 8.9 it can be seen that there is little change in the optimization variables from case to case and that all result in very good values for the optimization targets. Compared to the optimizers applied previously the obtained results are also better. Further, when comparing the simulations with the previous optimizers it can be seen that also here a low $\frac{H_2}{CO}$ rate close to 2.0 is present, the oxygen to carbon ratio is slightly higher and around 0.62-0.63 against previously 0.61, and the purge fraction previously about 0.187 is now at 0.173. However the steam to carbon ratio is much higher and is here above 1. As previously indicated this variable might affect the molar flow most and as the obtained results are very good, this is further emphasized.

8.2.7 Reflections on the use of optimizer

It was applied four main parameters to measure the success of this optimization procedure, flow to upgrading unit in molar flow and $\frac{std.bbl}{d}$, as well as carbon and thermal efficiency. The best result for each of these objective functions are given in Table 8.10.

During this part of the optimization the range of the adjustable variables was monitored to reveal any common denominators for success in optimization. Although there are no absolute guide lines to be drawn from this optimization procedure, it is observed that a $\frac{H_2}{CO}$ ratio of close to 2.0, a $\frac{O_2}{NG}$ ratio at about 0.61-0.63 and a purge ratio at 0.17-0.19 is present in many of the simulations providing the best results and could indicate a beneficial combination for the process.

From Table 8.10 The overall best result in terms of all four optimization targets were observed in for the optimization on TE with bypassing of the liquid product from the FTR in regards to the 3-way separator. This was also the last try at the optimizer and it should probably have been run a few more cases for this scenario to check for further optimization. However the positive results for this case is more attributed to the change of flow sheet structure and not the use of optimizer and it is hence not used for comparison of the optimization process. It is however acknowledged that this flow sheet structure is a much better option and should have been applied from the beginning.

When omitting the bypass simulation from the optimizer comparison the TE base case becomes the best case from the use of the Unisim Optimizer. When comparing the results to CE and TE benchmarks normally obtained for the GTL process of 77% and 60% respectively, it indicates a high degree of optimization of the process. However the simulations in this work does not take into account the upgrading unit and hence these values might have decreased some if that was to be included and this should be kept in mind. Nevertheless Rafiee also simulated a GTL plant with the exclusion of the upgrading unit, but with a CO_2 removal unit, and comparing efficiencies, the numbers for the work in this report is generally 10-15 percentage points higher than reported by Rafiee, which is strengthening the indication of a good optimization [53].

Another indicator for whether or not the optimization has been successful is the liquid volume of products to the upgrading unit. The feed

applied was designed for a 17000 $\frac{bbl}{d}$ train and from the optimization this is in the range 19700-19940 for the best cases. This further emphasizes the indication of a good optimization. However again it must be noted that the simulations in this work does not include the upgrading unit and that the separation and cracking processes usually applied there would likely decrease the final output some.

As also noted from the evaluation of the various optimizers, it can be seen that there is a continued increase in the values for the target variables for the optimizer simulations. The use of the optimizer was always applied with basis in the previous optimized flow sheet and the increased values experienced might be due to the optimization of a previous optimized flow sheet and not necessarily due to the choice of objective function or change of boundaries and should be kept in mind.

It can also seem like the optimizer does not search through the entire range given for the optimization variables as the rector volume for instance always ends up at about 1933 m^3. This might be due to a local minimum around this point and that the start condition given for the reactor volume is closest this solution. It was therefore tried a much lower starting value for the reactor volume of 600 m^3, but this did note change the optimized reactor volume away from 1933 m^3. This could indicate that the optimizer only execute a narrow search and should be kept in mind when considering the optimization results.

In terms of choice of objective function it was observed that the best result for CE, TE and liquid volume always belonged to the same simulation, but that this case never also had the highest value for molar flow to upgrading unit. It was also seen that an increase in either of these three first targets resulted in a increase in the other two as well. By considering the definition and calculation procedure for CE and TE as given in Section 7.1 and Appendix E and F it can be seen that both will increase with either increased flow of hydrocarbons or increased fraction of heavier hydrocarbons. As a increase in the liquid volume will be caused by both of these it becomes clear that they all go in the same direction when optimized with respect to liquid volume. This was also confirmed for instance by case 7 and 8 from Table 8.5. For the molar flow however it is only the size of the entire stream, which not necessarily is caused by an increase in hydrocarbons, that is measured and consequently does not need to be accompanied by an increase in TE, CE and liquid volume. Consequently as, CE, TE and liquid

volume follow each other optimization wise the choice between these three variables as objective function was found to be unimportant, but favoured over molar flow.

Table 8.10 – Summary of the best results for each of the Optimizer objective functions

Objective function	**Case name**	**CE** [%]	**TE** [%]	**Flow to upgrading** $[\frac{kmol}{h}]$	$\frac{std.bbl}{d}$
Flow to upgrading unit	10	80.99	64.77	572.3	19530
Carbon efficiency	CE2	81.24	64.96	570.3	19580
Thermal efficiency	TE base case	81.75	65.36	568.5	19720
	Bypass	82.41	65.93	604.3	19940

Chapter 9

Economics

In the previous chapter the process was optimized in regards to product flow, CE and TE. However this might not be the optimal process for production if the economics are also considered. As the production price of GTL compared to the price of crude oil is one of the arguments against applying this technology, the economics are of great importance. It was therefore decided to conduct a economic optimization and see if this affected the optimum.

When considering the plant economics it does not only consider the capital cost of the equipment, but also cost of raw material, utility costs, labour, maintenance, depreciation etc. However, in order to keep the complexity for the analysis at a reasonable level the economic considerations in this work have been limited to capital cost of equipment and operational costs. This is justified with the aim being to localize an optimum production rate of the process and this is mainly affected by the operational costs. The labour needed can also be a function of the plant size, but is not considered in this work due to simplicity. The operational costs considered in this work is utilities, raw material and catalysts.

In order to reduce the utility costs it is of great importance to have a good heat integration of the process, making the process as self-sufficient as possible. In order to achieve this a heat integration analysis was conducted to see if the heaters and coolers in the current flow sheet could be replaced by heat-exchangers.

9.1 Heat integration analysis

Pinch analysis is a technology that can be applied when there are multiple hot and cold streams leading to multiple possible heat exchanger networks in a process [90]. The pinch analysis is based on thermodynamic principles for maximum energy integration and gives a set of guidelines for achieving the most energetically favourable heat exchanger network configuration, minimizing the need for externally supplied utilities[90, 91]. A minimum temperature difference ΔT_{min}, must be chosen and this gives the location of the pinch point when plotting the temperature versus heat transferred for the system as the point where the hot and cold curves are closest to each other[91]. This pinch observed in such plots are also the origin for the name of this analysis[90].

When the pinch point has been located the pinch analysis guide lines dictates that heat supplied from external sources can only do so at temperatures above the pinch temperature and consequently cooling supplied by external sources can only do so below the pinch temperature[91].

A pinch analysis was consequently conducted for the simulated process with basis in the flow sheet with bypass incorporated. To perform a pinch analysis, the streams in need for heating or cooling needs to be identified from the process flow sheet. These streams are shown in Table 9.1. The interval temperatures were calculated as indicated by Equation 9.1 and the minimum temperature difference was set to be 10 °C in this analysis. The heat capacities, mass flows and temperatures were taken directly from the Unisim file and from these data the heat load for each of the streams were identified as shown in Table 9.1.

$$\begin{aligned} &\text{Hot streams: } T_{int} = T_{Act} - \frac{\Delta T_{min}}{2} \\ &\text{Cold streams: } T_{int} = T_{Act} + \frac{\Delta T_{min}}{2} \end{aligned} \tag{9.1}$$

Table 9.1 – Data for the hot and cold streams included in the heat integration analysis.

Stream	**Type**	**Actual temperature [°C]**		**Interval temperature [°C]**		**Heat Capacity** $[\frac{kJ}{kg,C}]$		**Average heat capacity** $[\frac{kJ}{kg,C}]$	**Mass flow** $[\frac{kg}{s}]$	**CP** $[\frac{kW}{C}]$	ΔT [°C]	**Heatload** [kW]
		Source	Target	Source	Target	Source	Target					
2	cold	48.46	455	53.46	460	1.957	2.858	2.408	61.50	148.09	406.53	60203.39
5	cold	380.11	675	396.15	680	2.456	2.879	2.668	99.82	266.28	293.85	78247.67
7	cold	20	200	25	205	0.966	0.983	0.974	45.27	44.11	180	7940.52
8	hot	1030	38	1025	33	2.578	2.871	2.724	145.08	395.26	992	-392095.10
14	cold	42.39	210	47.39	215	2.000	2.053	2.027	136.90	277.49	167.61	46510.50
17	hot	224.09	38	219.09	33	1.699	2.307	2.003	136.89	274.25	186.09	-51035.64
30	cold	20	224.09	25	229.09	4.132	5.128	4.630	200.48	928.04	204.09	189443.94

Following a problem table was constructed as shown in Table 9.2 and from this a cascade was constructed to locate the pinch point. This is shown in Table 9.3. A negative sign in the last column of the cascade table, indicates that the temperature gradient is in the wrong direction and hence the heat exchange is not possible from a thermodynamic standpoint [90]. As can be seen from Table 9.3, there is no negative sign, indicating that no pinch occurs. This indicates a threshold problem, as they do not include a process pinch point [87]. A threshold problem means it only requires a heating or cooling utility and not both [90, 87]. From the cascade in Table 9.3 it can be seen that this process only requires a cooling utility. This is also confirmed from the combined composite curves shown in Figure 9.1 where it can be seen that hot composite curve continues past the cold composite curve. The calculation of the composite curves is shown in Appendix H together with the hot and cold composite curves displayed in Figure H.1 and H.2 respectively.

Table 9.2 – Problem table for the heat integration analysis

Interval	**Interval Temperature [°C]**	$\Delta T_{interval}$	**Streams in interval**	$\sum CP_c - \sum CP_h$ $[\frac{kW}{C}]$	$\Delta H[kW]$	**Surplus or Deficit**
	1025					
1	680	345	8	-395.26	-136363.72	s
2	460	220	5,8	-128.98	-28374.98	s
3	386.15	73.85	2,5,8	19.11	1411.48	d
4	229.09	157.05	2,8	-247.17	-38819.04	s
5	219.09	10	2,8,30	681.07	6810.68	d
6	215	4.09	2,7,8,30	406.82	1663.92	d
7	205	10	2,8,14,17,30	684.30	6843.02	d
8	53.46	151.54	2,7,8,14,17,30	728.42	110381.33	d
9	47.39	6.08	7,8,14,17,30	580.33	3526.98	d
10	33	14.39	7,8,17,30	302.84	4356.81	d
11	25	8	7,30	972.35	7778.81	d

For threshold problems the normal heat exchanger network design rules to be applied in pinch analysis no longer applies, as there is no pinch and consequently no streams adjacent to the pinch. However the normal procedure for these type of problems is to start the design from the most constrained end [90, 87]. The most constrained end in this work was found to be at the no utility end, due to the high target temperature of some of the cold streams which could only be satisfied by certain stream matching.

As the normal guide lines for stream matching given by the pinch analysis no longer applies there exist numerous stream combinations for the heat integration. In order to limit the combinations possible, some decision crite-

Table 9.3 – Cascade of the heat integration analysis for location of pinch point

Interval	**Cascade**	
Temperature [°C]	**Heat load [kW]**	$\Delta H[kW]$
1025	0	
	-136363.72	
680		136363.72
	-28374.98	
460		164738.70
	1411.48	
386.15		163327.23
	-38819.04	
229.09		202146.27
	6810.68	
219.09		195335.59
	1663.92	
215		193671.66
	6843.02	
205		186828.64
	110381.33	
53.46		76447.31
	3526.98	
47.39		72920.34
	4356.81	
33		68563.53
	7778.81	
25		60784.73

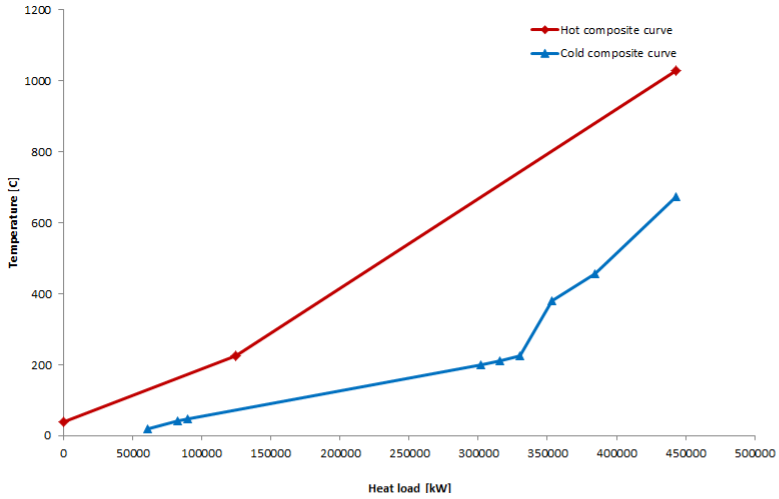

Figure 9.1 – Plot of the combined composite curves for the pinch analysis for the GTL model simulated in Unisim. Temperature in °C is the unit for the vertical axis, while heat load in kW is given on the horizontal axis.

ria was set. First the number of units was desired to be minimized. Second, if there still exists multiple choices, minimizing heat exchanger area would be the next criteria for network design. With this as basis the design was based on the following considerations:

1) The high target temperature of stream 5 and its relative high source temperature of 380.11 °C makes it only possible to match with stream 8 and was consequently chosen as teh first coupling.

2) Considering this match have been carried out, stream 8 still have much heat left. It is also clear from the target temperature of stream 2 that it also needs to be coupled with stream 8 to completely reach the target temperature, as the other possible hot stream starts at a temperature lower than this. However stream 17 could be used to partially heat up stream 2 from its source temperature to a maximum of $T_{source,17} - 10$ °C, which would be 213.8 °C. Consequently here there is two choices, first partially heat up stream 2 with stream 17, then heating the rest with stream 8 or let stream 8 transfer all of the needed heat.

3) Trying out the first of the two alternatives revealed that stream 17

would only have a temperature of 108 °C after transferring its maximum amount of heat to stream 2. As all of the streams left needs to be heated to 200 °C or above it means that stream 17 can not transfer the heat needed to any of these alone. With the design outlined so far the heat exchanger count is currently at three units. At this point there is three streams left to heat and if the rest of the heating is carried out by stream 8 and stream 17 is cooled by a cooler to its target temperature, another three heat exchangers will be needed. In addition there will still be heat left in stream 8, hence requiring a cooler. This gives a total minimum unit count of eight. If the coupling of stream 17 however continues, it will as mentioned not be able to completely heat one of the remaining streams alone. Hence stream 8 will also be used for heating up the same stream as was coupled to stream 17 and the unit count reaches five at this point. There will be two cold streams left to heat up at this point and in any case stream 8 must be cooled and the minimum total unit count reaches eight. If the heat in stream 17 is not completely transferred either at this point another cooler is needed and results in the total of nine units.

4) Choosing the other alternative of letting stream 8 heat up both stream 2 and 5 gives four theoretical new coupling alternatives for the rest of the streams as indicated in Table 9.4. All of the alternatives gives a minimum of seven units and hence was considered to be a better route than the first choice were all alternatives would give eight or more units. Hence these four alternatives were further investigated. They were first modelled in Excel to rule out any combinations that would give more than 7 units and then the remaining were to be tried out in Unisim where the respective heat exchanger areas also could be assessed.

5) There is also a range of combinations for the four different alternatives based on the order of the couplings. The high CP of stream 30 compared to stream 8 leads to a large reduction in the temperature of stream 8, when coupled together, hence reducing the potential for successful heat exchange with the rest of the streams. As there was not enough time to test all possible combinations based on order for the four alternatives, this coupling was consequently decided to be the last coupling for all alternatives. The order of coupling for stream 8 with stream 14 and 7 respectively was considered not to be of major importance as stream 7 only needs a small amount of heat and have

a very low CP hence not affecting the temperature or available heat in a great way.

Table 9.4 – List of the remaining possible stream combinations for the heat integration after stream 8 was decided first to be coupled to stream 5 and then 2.

Alternative 1	**Alternative 2**	**Alternative 3**	**Alternative 4**
8+14	17+30	17+7	17+14
8+7	8+14	8+14	8+7
8+30	8+7	8+30	8+30
Cool 8	8+30	Cool 8	Cool 8
Cool 17	Cool 8	Cool 17	Cool 17

Alternative 1

The first of the four alternatives to be investigated are the one where all streams are heated by stream 8 and stream 17 is not heat exchanged with any other stream, but brought to its target temperature by the use of a cooling utility. The network is displayed in Figure 9.2 and the respective heat transfers are outlined in Table 9.5. With this design a total of seven units are needed, with five heat exchangers and two coolers.

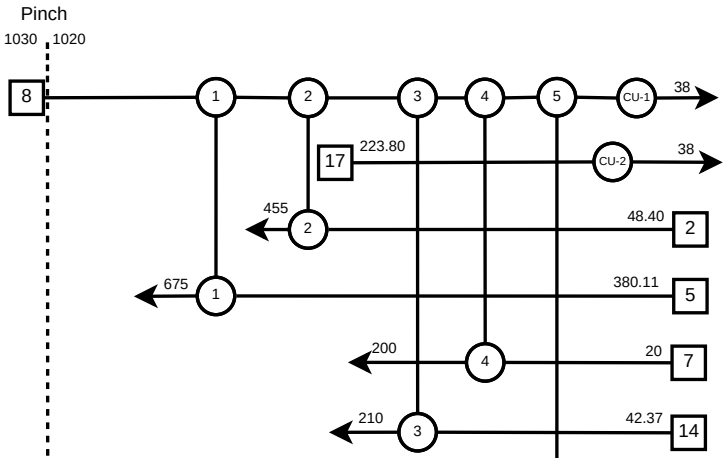

Figure 9.2 – Overview over the couplings in the heat exchanger network resulting from alternative 1

Table 9.5 – Overview of the heat transferred, the resulting new temperatures and the need for additional heating or cooling from each coupling in alternative 1

Coupling	**Maximum transferable heat [kW]**	**Maximum acceptable heat [kW]**	**Actually transferred [kW]**	**Excess [kW]**	**New T_H [°C]**	**New T_C [°C]**	**Target [°C]**	**Reached**	**Additional heat needed [kW]**
1	248974.43	78470.11	78470.11	170504.32	821.48	675	675	YES	-
2	301620.71	60191.61	60191.61	241429.10	669.20	455	455	YES	-
3	243812.81	46486.18	46486.18	197326.63	551.59	210	210	YES	-
4	203006.14	7940.52	7940.52	195065.62	531.50	200	200	YES	-
5	195065.62	189174.64	189174.64	5890.98	52.90	223.8	223.8	YES	-
Extra utilities	**Size[kW]**								
CU-1	5890.98								
CU-2	50919.84								

Alternative 2

Alternative 2 utilizes the possibility of stream 17 to transfer all its heat and hence reduce the number of coolers. Figure 9.3 shows the network layout and Table 9.6 shows the heat transferred in the different couplings. This design requires seven units in total, with six heat exchangers and one cooler.

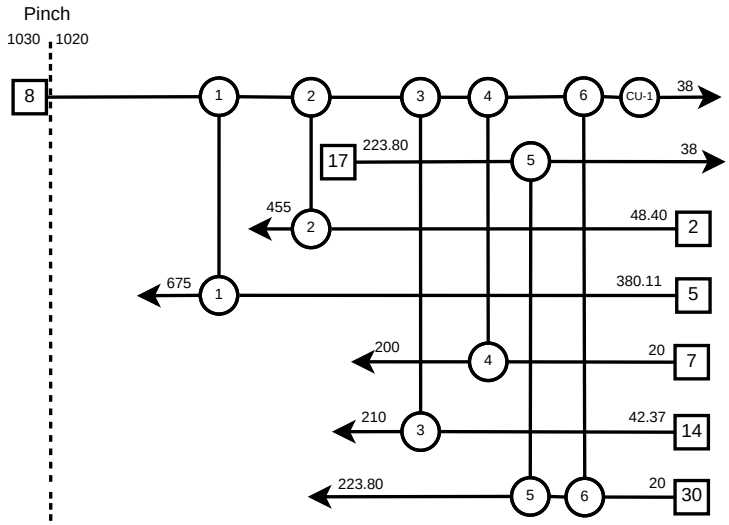

Figure 9.3 – Overview over the couplings in the heat exchanger network resulting from alternative 2

Table 9.6 – Overview of the heat transferred, the resulting new temperatures and the need for additional heating or cooling from each coupling in alternative 2

Coupling	**Maximum transferable heat [kW]**	**Maximum acceptable heat [kW]**	**Actually transferred [kW]**	**Excess [kW]**	**New T_H [°C]**	**New T_C [°C]**	**Target [°C]**	**Reached**	**Additional heat needed [kW]**
1	248974.43	78470.11	78470.11	170504.32	821.48	675	675	YES	-
2	301620.71	60191.61	60191.61	241429.10	669.20	455	455	YES	-
3	50919.84	179892.28	50919.84	0	38	74.86	210	NO	138254.80
4	243812.81	46486.18	46486.18	197326.63	551.59	210	210	YES	-
5	203006.14	7940.52	7940.52	195065.62	551.54	200	200	YES	-
6	202986.46	138254.80	138254.80	64731.66	402.60	223.80	223.80	YES	-
Extra utilities	**Size [kW]**								
CU-1	144113.74								

Alternative 3

In this design, stream 8 is heat exchanged with all streams except stream 7 which is heat exchanged with stream 17. This design exploits the potential of stream 17 to completely transfer the heat needed by stream 7. Figure 9.4 shows the network layout and Table 9.7 shows the respective heat transfers. This design also ends up needing seven units, where five are heat exchangers and two are coolers.

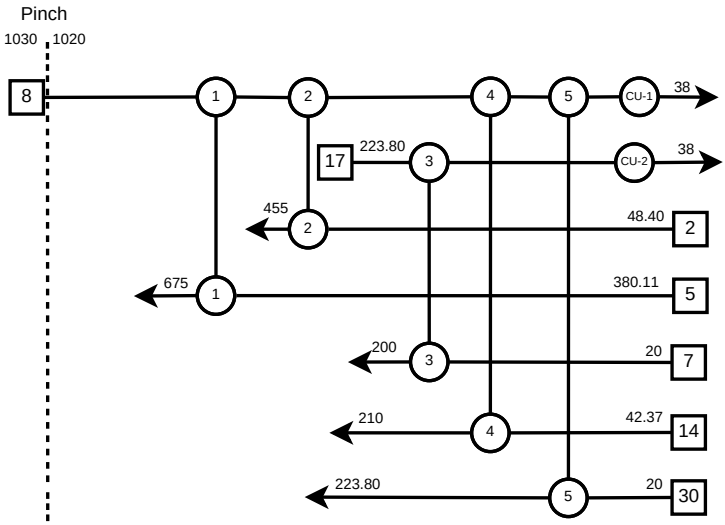

Figure 9.4 – Overview over the couplings in the heat exchanger network resulting from alternative 3

Table 9.7 – Overview of the heat transferred, the resulting new temperatures and the need for additional heating or cooling from each coupling in alternative 3

Coupling	**Maximum transferable heat [kW]**	**Maximum acceptable heat [kW]**	**Actually transferred [kW]**	**Excess [kW]**	**New T_H [°C]**	**New T_C [°C]**	**Target [°C]**	**Reached**	**Additional heat needed [kW]**
1	248974.43	78470.11	78470.11	170504.32	821.48	675	675	YES	-
2	301620.71	60191.61	60191.61	241429.10	669.20	455	455	YES	-
3	50919.84	7940.52	7940.52	42979.32	194.83	200	200	YES	-
4	243812.81	46486.18	46486.18	197326.63	551.59	210	210	YES	-
5	203006.14	189174.64	189174.64	13831.49	72.99	223.80	223.80	YES	-
Extra utilities	**Size [kW]**								
CU-1	13831.49								
CU-1	42979.32								

Alternative 4

This alternative uses the heat from stream 17 to heat up all of stream 14 while stream 8 is heat exchanged with the other four cold streams. The network layout is shown in Figure 9.5 and the respective heat transfers are shown in Table 9.8. Also this design requires seven units, five heat exchangers and two coolers.

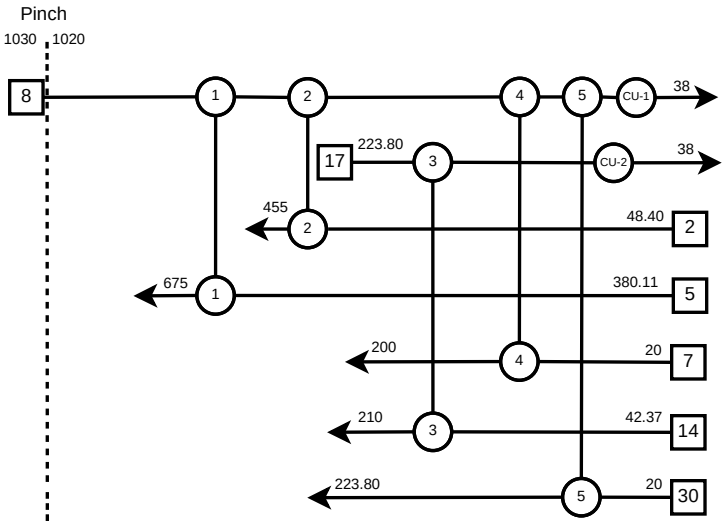

Figure 9.5 – Overview over the couplings in the heat exchanger network resulting from alternative 4

Table 9.8 – Overview of the heat transferred, the resulting new temperatures and the need for additional heating or cooling from each coupling in alternative 4

Coupling	**Maximum transferable heat [kW]**	**Maximum acceptable heat [kW]**	**Actually transferred [kW]**	**Excess [kW]**	**New T_H [°C]**	**New T_C [°C]**	**Target [°C]**	**Reached**	**Additional heat needed [kW]**
1	248974.43	78470.11	78470.11	170504.32	821.48	675	675	YES	-
2	301620.71	60191.61	60191.61	241429.10	669.20	455	455	YES	-
3	46981.99	46486.18	46486.18	495.81	54.18	210	210	YES	-
4	249492.32	7940.52	7940.52	241551.80	649.11	200	200	YES	-
5	241551.80	181974.64	181974.64	52377.16	170.51	223.8	223.8	YES	-
Extra utilities	**Size [kW]**								
CU-1	52377.16								
CU-2	4433.66								

9.1.1 Evaluation

All of the four network design alternatives explored resulted in the total need of seven units. Which one of the networks to be utilized must hence be decided based on the second criteria of heat exchanger and cooler area. This impacts the economics in a great deal, and the smallest area will give the lowest capital cost and hence be chosen for this work.

The actual implementation of the heat exchangers and obtaining the areas from Unisim was not straight forward.

First the boiling water used for cooling of the FTR reactor have so far been modelled as an energy stream and not material stream as this was not possible to connect to the PFR in the Unisim model. For the purpose of the heat integration an actual material stream was needed for connection to the heat exchangers and consequently a dummy material stream was constructed to model the cold water entering the process. The required amount of water was obtained by dividing the duty from the FTR by the heat of vaporization of water. The water was then pumped up to the saturation pressure corresponding to the temperature of the boiling water for the FTR and from here it was implemented in the various heat exchanger designs.

The second obstacle encountered in Unisim relates to obtaining the heat exchanger area. By default Unisim calculates the UA value and consequently changes the value for U to satisfy a built in default value for the heat exchanger area of 60.32 m^2. As a consequence, the calculation of U must be done manually in order to get the actual area of the heat exchanger. This procedure is outlined in Appendix I and was implemented in a spreadsheet for each exchanger so that the calculation changed with iterations in the flow sheet and optimization processes.

The procedure used to calculate the overall heat transfer coefficient does not take into account the potential phase transfer in the exchangers and is hence a uncertainty in the calculation. However the occurrence of a phase transition from gas to liquid should in theory give a higher value for the overall heat transfer compared to the gas-gas heat transfer and hence a smaller area. This is also the potential scenario for all the heat exchangers, except the one heating up the water for cooling of the FTR. Here liquid enters for heating and could potentially go through heat transfer to gas, however the boiling water is specified to remain in liquid phase and consequently this does not offer a problem. Hence the area estimates used in this work is potentially overestimated and consequently yield a worst case

estimate for the economics of the respective heat exchangers.

By implementing these spreadsheets for each heat exchanger and cooler in the four alternative proposed configurations, the total heat exchanger area was obtained and are given in Table 9.9.

Table 9.9 – Overview over the heat exchanger and cooler area [m^2]for the four alternative heat exchanger network design considered in this work

Heat exchanger	**Alternative 1** [m^2]	**Alternative 2** [m^2]	**Alternative 3** [m^2]	**Alternative 4** [m^2]
1	93.02	92.23	93.27	93.27
2	66.81	66.56	66.80	66.80
3	43.13	43.14	167.30	2650
4	14.43	14.37	43.05	10.76
5	623.80	4353	566.8	339.4
6	-	121.40	-	-
Sum [m^2]	**841.19**	**4690.70**	**937.22**	**2820.83**
CU-1	148.6	258.00	156.3	194.2
CU-2	238.5	-	155.2	189.2
Sum Cooler [m^2]	**387.10**	**258.00**	**311.5**	**383.4**
Total area [m^2]	**1228.29**	**4948.70**	**1248.72**	**3204.23**

From the table it can be seen that alternative 1 and 3 are the two that gives the smallest overall heat exchanger area. Considering the area of cooler 1 and 2 can be determined to a certain degree by the molar flow of water used on the shell side, the choice of network design was done on the basis of heat exchanger and not cooler area. However decreasing the molar flow of water would give an increased temperature of the water leaving the heat exchanger on the shell side, providing a possibility for steam generation which can have a positive effect on the economics consequently it exist a trade-off between small heat exchanger area and low temperature on shell side water or larger heat exchanger areas and the option of steam production. An important factor in this trade-off is off course whether or not the water is free of charge and easily available or scarce and expensive. Due to time limitations this trade-off was not considered in this work and the water flow was rather arbitrarily chosen with a low temperature increase in the shell side.

By this reasoning, alternative 1 offers the best solution and was used for the subsequent simulations in this work. It should however be noted that this heat integration results in temperatures for stream 8 in the temperature range for metal dusting and might be considered as a forbidden match industrially. Normal practice is as previously stated (ref. section 4.1.7) to use a WHB system or a water quench. However as the purpose of this analysis was to obtain a maximum heat integration for reduction in utilities the configuration was applied to the flow sheet.

9.2 Additional process integration

As already indicated, the economic performance of the process is closely related to efficient use of utilities and energy. It was therefore investigated if there were any further potential in addition to the heat exchanger network for process integration. For that purpose the concept of energy efficiency was introduced to locate the various energy sinks and sources.

9.2.1 Energy efficiency

The energy efficiency is a measure of the ratio of energy added and produced in the process. It is displayed mathematically in Equation 9.2

$$\text{Energy efficiency, (EE)} = \frac{\text{Energy produced}}{\text{Energy added}} \times 100\% \tag{9.2}$$

By considering the existing flow sheet, the energy added was identified as the LHV of the natural gas feed and energy needed for compressor and pump work. For the produced energy, both the energy actually produced by the flow sheet and the potentials for energy generation was considered. The only produced energy directly from the current flow sheet was identified to be the LHV of the syncrude products. However there also exist potential for extra energy generation through utilizing the purge stream as fuel for power generation and also the produced steam from cooling of the FTR reactor could be used to supply steam to the process or produce power. For the most realistic approach for the optimization of the flow sheet it was decided to include the steam and power production unit in the flow sheet, such that the required energy needed to be bought would change with the process iterations.

To make the calculation the simplest possible, compressor, pump and turbine work was treated as a net work term, as displayed in Equation

9.3. A positive sign indicates surplus work produced and a negative sign indicates that work produced is not enough to keep plant self sufficient and that additional work will have to be supplied from a power plant.

$$\text{Net work, } (W_{net}) = \sum (W_{turbines} - W_{compressors} - W_{pumps}) \tag{9.3}$$

However, there are two different energy forms present in the process, mechanical work and energy in the terms of heat of products and feed. In order to compare them there needed to be a common reference for the calculation, equivalent work or equivalent heat. It was found that the most suitable term was equivalent work, W_{eq}, which, as the term indicates, is the amount of work that could be achieved by utilizing the heat to generate work. This was accomplished by considering the feed of natural gas, products and purge as input in a natural gas combined cycle with an efficiency of 60% and the corresponding output work as the respective equivalent work terms. Consequently a more detailed version of Equation 9.2 is outlined in Equation 9.4 and 9.5 for surplus and deficit work respectively.

$$\text{Energy Efficiency} = \frac{\mathrm{W_{eq,purge}} + \mathrm{W_{eq,syncrude}} + \mathrm{W_{net}}}{\mathrm{W_{eq,feed}}} \tag{9.4}$$

$$\text{Energy Efficiency} = \frac{\mathrm{W_{eq,purge}} + \mathrm{W_{eq,syncrude}}}{\mathrm{W_{eq,feed}} + \mathrm{W_{net}}} \tag{9.5}$$

As the economic performance of the plant is closely related to the use of utilities and heat integration, the energy efficiency was added as an extra optimization target to the optimization.

9.2.2 Construction of a new flow sheet

For the purpose of the economic analysis, a new flow sheet was consequently constructed based on the chosen heat exchanger network design and the combined steam and electricity production unit. The construction of this flow sheet is described in the following paragraphs and the resulting process is shown in Figure 9.7 and was considered as a base case for evaluation of the economics. The main parameter values for this economic base case i given in Table 9.10 and he flow sheet as modelled in Unisim is shown in Figure C.2 in Appendix C while the Unisim workbook is given in Appendix D

For the steam and power generation it was assumed that the same molar flow of boiling water used for cooling of the FTR was completely converted

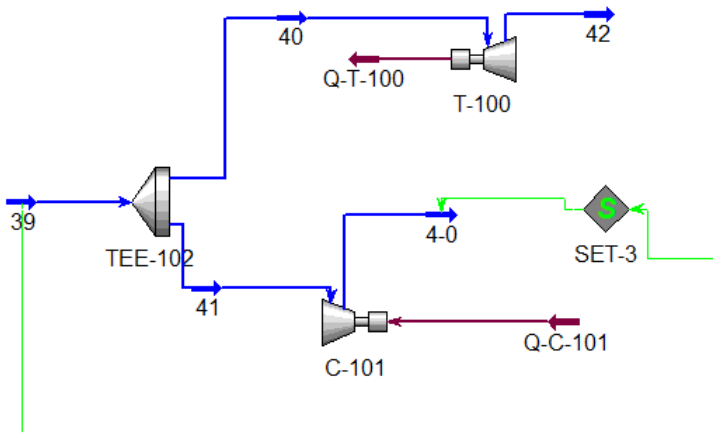

Figure 9.6 – The steam power production unit as modelled in Unisim.

to steam in the process. Depending on the stream size it can as mentioned be utilized for providing steam to the pre-reformer, electric power for mechanical equipment or potentially both. In this work it was decided that the first priority would be to be self-reliant with regards to providing the pre-reformer with steam, and if there were more steam available it would be used for electricity production.

The actual implementation of this system in Unisim was not straight forward. The steam stream resulting from the cooling of the FTR is not an actual stream in the flow sheet and hence a dummy material stream was constructed to model the steam from the reactor. The size of this stream was given by connecting a set block between the dummy stream modelling the cold utility water as explained for the implementation of the heat exchangers in Section 9.1.1 to the dummy steam stream. This is shown in Figure C.2 in Appendix C. The steam stream was then split between a turbine for power production and a compressor for steam production to the pre-reformer as shown in Figure 9.6. The size of the steam stream was given by connecting it to a set block for the inlet stream of steam to the pre-reformer and consequently this dictated the split fraction between steam and power generation.

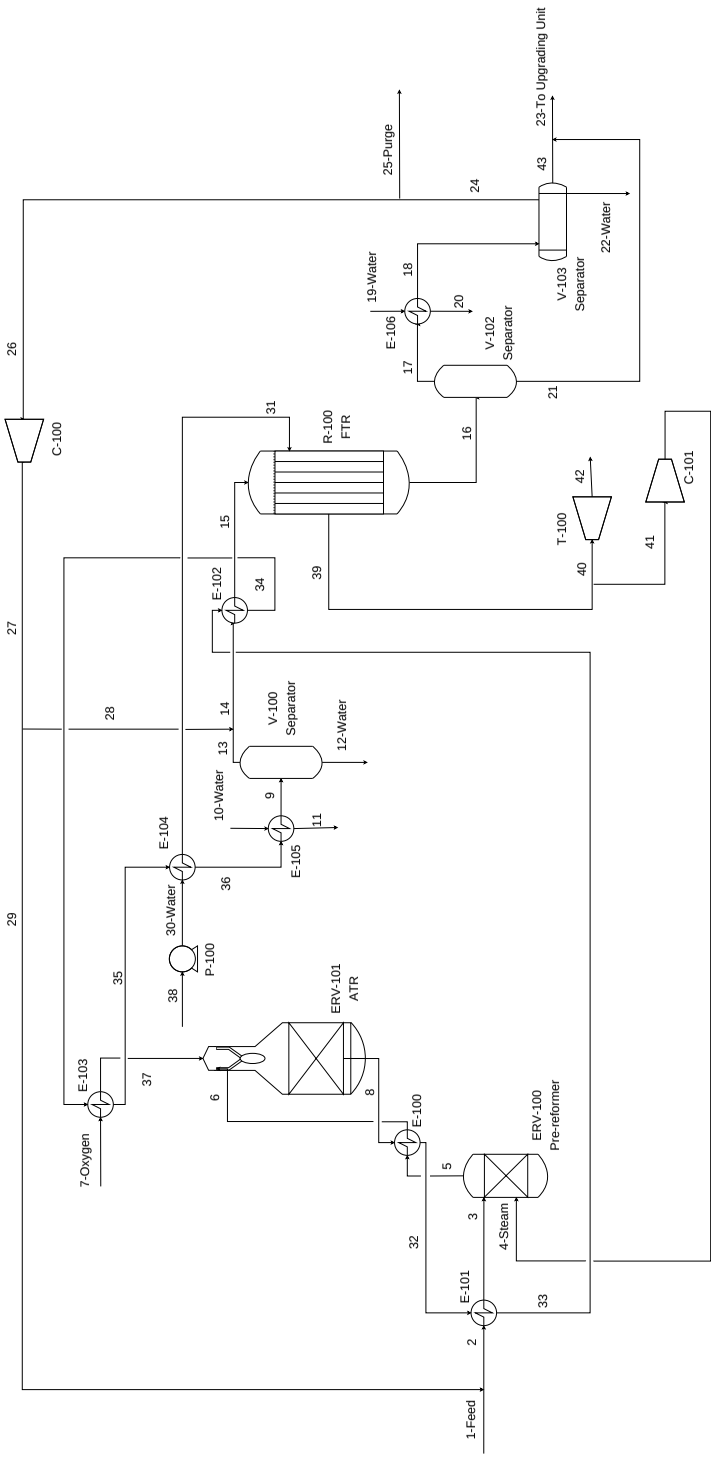

Figure 9.7 – Process flow diagram of the modelled base case in Unisim for economic simulation

Table 9.10 – Indicator table

Parameter	**Economic base case**
FTR Volume $[m^3]$	1860
FTR conversions [%]	
FTR	89.74
Metahanation	4.88
Temperature syngas [°C]	1029
Ratios	
$\frac{H_2}{CO}$	2.088
$\frac{H_2O}{NG}$	1.098
$\frac{O_2}{NG}$	0.6260
Purge fraction	0.190
Recycle to FTR	0.577
Recycle to feed	0.423
CE [%]	82.17
TE [%]	65.73
Product	
molar flow $[\frac{kmol}{hr}]$	131.7
in $\frac{std.bbl}{d}$	19870
Energy efficiency	71.30

9.3 Method for economic evaluation

9.3.1 Capital Cost

The economic evaluation of the capital costs for the simulated GTL plant, has been based on the module costing technique. This technique is generally accepted as the best for assessing the preliminary costs of new chemical plants and was introduced by Guthrie in the late 1960's and beginning of 1970's [92]. The main principle of the technique is to calculate the bare module cost, C_{BM}, for each equipment in the process and adding them all together to obtain an estimate for the fixed capital cost. The bare module cost includes all direct an indirect cost associated with the purchase of a given item and is calculated as presented in Equation 9.6.

$$C_{BM} = C_P^0 \times F_{BM} \tag{9.6}$$

C_P^0 is the purchased cost at the base conditions, which is defined as the most commonly applied material and operation at near ambient pressure, while F_{BM} is a cost factor to account for a different type of material, pressure and potential other factors to be included in the cost estimate [92].

The purchased equipment cost, C_P^0 is calculated by the use of the correlation given in Equation 9.7. This correlation has been developed based on data collected in a survey sent to several equipment manufacturers about costs of different process items. The survey was last conducted between May and September 2001.

$$log_{10}C_P^0 = K_1 + K_2 log_{10}(A) + K_3[log_{10}(A)]^2 \tag{9.7}$$

A is the capacity measure for the given process equipment, such as volume and heat exchanger area, while K_1, K_2, K_3 are item specific constants for parameter fitting of the equation. Table A.1 in Analysis, Synthesis, and Design of Chemical Processes, Fourth Edition, by Richard Turton et al. (from here referred to as Turton et. al) provides a list of various equipments and the corresponding K values, and was used in this work [92]

The cost factor, F_{BM}, is calculated as according to Equation 9.8 or found from Table A.6 and Figure A.19 in Turton et al. [92]. B_1 and B_2 are item specific constants equivalently to K_1, K_2 and K_3 in Equation 9.7 and is obtained from Table A.4 in Turton et. al[92]. F_M and F_P are correction factors accounting for a different material and pressure than the base conditions respectively.

$$F_{BM} = (B_1 + B_2 F_M F_P) \tag{9.8}$$

The pressure factor, F_P is calculated in two different ways depending on the type of equipment in question. For pressurized process vessels, Equation 9.9 is applied and is only valid as long as the vessel thickness is less than 0.0063 m. D represents the diameter of the vessel, while P represents the pressure.

For all other process equipment Equation 9.10 is applied. Here, C_1,C_2 and C_3 represents item specific constants and, as for pressurized vessels, P represents the pressure. Table A.2 in Turton et. al list the C-values applied

for Equation 9.10

$$F_{P,vessel} = \frac{\dfrac{(P+1)D}{2[850-0.6(P+1)]} + 0.00315}{0.0063} \quad \text{for } t_{vessel} > 0.0063m \tag{9.9}$$

$$log_{10}F_P = C_1 + C_2 log_{10}P + C_3(log_{10}P)^2 \tag{9.10}$$

The material factor, F_M, based on equipment type and material used is found schematically from tables A.3 and Figure A.18 in Turton et.al [92]

This technique for estimating capital cost of the various units has a lower and upper bound for where the correlation for each equipment is valid. In the case of cost estimation outside the range, two different approaches was considered. The first is based on a scale-up of the equipment and is shown in Equation 9.11. Subscript a and b refers to item a and b respectively, C represents the cost, A represents the capacity measure and n is the scaling factor.

$$C_a = C_b \times \left(\frac{A_a}{A_b}\right)^n \tag{9.11}$$

The other approach considered is rather simple and basically divides the capacity measure in a multiple of maximum capacity units as shown in Equation 9.12

$$\text{Cost}_i = \text{Cost}_{max} \times \frac{A_i}{A_{max}} \tag{9.12}$$

It proved difficult to obtain scale-up factors for all of the various equipment types utilized in the simulation and for some of the equipment the capacity exceeded the range in such a great way that multiple units would be more plausible than a scale-up. The latter of the two approaches was therefore chosen.

This approach is very simplified and renders calculations based on for instance 2.3 maximum units and this should be kept in mind. This does however most likely overestimate the cost that otherwise would economically benefit from a scale-up, resulting in a worst case scenario cost wise. If

the scale-up approach were to be used on all equipments the economic aspect would most likely be underestimated as it is more costly with multiple units than scale-up.

The cost data is calculated on a 2001 year basis, and should be corrected for inflation before they are used as estimates. This can be achieved by using the Chemical Engineering Plant Cost Index, CEPCI. This, in the same manner as the consumer price index, represents the cost of a "basket" of commonly applied items, only that these items are related to chemical engineering [92]. This gives the possibility of adjusting the data from 2001 and their price increase or decrease to today's representative value. Equation 9.13 illustrates how this is achieved.

$$\text{Cost in present year} = \text{Cost in 2001} \times \left(\frac{CEPCI_{\text{present year}}}{CEPCI_{2001}} \right) \quad (9.13)$$

9.4 Calculation of capital cost

9.4.1 Purchased equipment cost

The calculation of the purchased equipment cost, C_P^0, was not straight forward for all of the equipments used in the simulation, as not all of the units used in Unisim was listed for the the cost correlation and hence had to be modelled as other units or the capacity measure as needed for the correlation was not easily available from Unisim. Table 9.11 shows the various units of equipment utilized in the Unisim flowsheet and how they were modelled for the capital cost estimation.

ATR and pre-reformer

With both the pre-reformer and ATR modelled as Equilibrium reactors in Unisim, no volume is calculated for the vessel and hence had to be obtained differently. This was achieved by the use of gas hourly space velocity, GHSV, values. The GSHV values equals the volume of gas per hour at standard temperature and pressure, STP, divided by volume of the catalyst in the reactor in standard cubic feet per hour [93]. Table 17.1 Chemical Process Equipment - Selection and Design by Walas lists GHSV for many processes and was used to to obtain values for the pre-reforming and ATR [93]. The

Table 9.11 – Overview over what the different units in Unisim was modelled as to use the economical correlations in Analysis, Synthesis and Design of Chemical Processes by Richard Turton et al. [92]

Equipment in flowsheet	**Economically modelled as**	**Capacity measure**
Pre-reformer	Vertical pressure vessel	Volume $[m^3]$
ATR	Vertical pressure vessel	Volume $[m^3]$
FTR	U-tube heat exchanger	Area $[m^2]$
Heat exchanger	U-tube heat exchanger	Area $[m^2]$
Cooler (Heat exchanger)	U-tube heat exchanger	Area $[m^2]$
Separator	Vertical pressure vessel	Volume $[m^3]$
3-way separator	Horisontal pressure vessel	Volume $[m^3]$
Pump	Centrifugal pump	Power [kW]
Turbine	Radial gas/liquid expander	Power [kW]
Compressor	Centrifugal compressor	Power [kW]

process found to be most similar to the pre-reforming process was the production of hydrogen from steam and methane in the gaseous phase with the presence of a nickel catalyst and the corresponding GHSV value was 3000. For the ATR the reforming of naphta in a fixed bed reactor at about 490 °C was found to be the closest match. This corresponded to a GHSV value of 8000. By dividing the volumetric gas flow rate at standard conditions entering the reactor, with the GSHV value, the volume of catalyst is obtained as shown in Equation 9.14 [94]

$$V_{\text{catalyst}} = \frac{Q}{GHSV} \tag{9.14}$$

Then dividing the volume of the catalyst with the total percentage of the reactor filled with catalyst results in the total reactor volume. For both ATR and pre-reformer the catalyst was assumed to take up 45% of the overall volume.

FTR

The multi tubular fixed bed reactor was not listed as an equipment item in the cost correlation from Analysis, Synthesis, and Design of Chemical Processes, Fourth Edition by Richard Turton et.al and hence it was modelled as a heat exchanger in stead[92]. The heat exchanger cost calculations are based on heat exchanger area and consequently a corresponding parameter

for the FTR must be obtained. From Unisim the volume of the FTR can be obtained and by applying the relationship between volume and area as given in Equation 9.15 the area is also obtained. The tube diameter is also directly obtained from the simulation and consequently the calculation of the purchased equipment cost was possible.

$$A = V\left(\frac{4}{d}\right) \tag{9.15}$$

Separators and heat exchangers

The volume for the various separators used in the modelling was obtained with quick size in Unisim and the heat exchanger areas was obtained from the spreadsheets inserted to the simulation as outlined in Section 9.1.1 and Appendix I.

Power equipment

The power produced or required for the various turbines, pumps and compressors are directly given by Unisim and did not offer any obstacles for the calculation of the purchased cost.

9.4.2 Material factors

Based on Table 7.9 in Analysis, Synthesis, and Design of Chemical Processes, Fourth Edition by Richard Turton et. al [92] outlining the corrosion potential for various components and the corresponding material selection, and the components present in the simulation, it was decided that there were no need for a different material than the most common as included in the bare module cost. Hence the material factor was set equal to one in the equation for the cost factor, Equation 9.8, for all equipments.

9.4.3 Pressure factors

The calculation of pressure factors was carried out as described in Equation 9.9 and 9.10. The pressure used in the equations were chosen to be the maximum pressure experienced for the given unit operation regardless of it existing at the inlet or outlet, shell or tube side. The pressure factor was rather straight forward calculated for all equipments except the pressure vessels. For the separators, the quick size function made it possible to obtain the diameter directly from Unisim, but for the ATR and pre-reformer

the diameter had to be found by the use of heuristics and the volume of a cylinder. The heuristic applied is the ratio of length to diameter of the vessel, $\frac{L}{D}$. The volume of a cylinder is given by Equation 9.16. Rearrangement give the diameter as a function of the length as indicated in Equation 9.17. By using a ratio of length to diameter of 4 the unknown lenght can be recplaced by the diameter as shown in Equation 9.18 and the diameter is obtained from Equation 9.19 [94].

$$V = \pi r^2 L = \frac{\pi D^2 L}{4} \tag{9.16}$$

$$D = \sqrt{\frac{4V}{\pi L}} \tag{9.17}$$

$$D^2 = \frac{4V}{4D\pi} = \frac{V}{D\pi} \tag{9.18}$$

$$D = \sqrt[3]{\frac{V}{\pi}} \tag{9.19}$$

ASU plant

Even though the ASU plant is not included in the Unisim simulation of the GTL plant it is included in the economic evaluation of the plant as it is a considerable cost and dependent on the oxygen consumption, which is an optimization variable in the simulation. The oxygen supplied to the simulated GTL plant is assumed to be supplied by an ASU with the capacity of producing 325 ton of oxygen per day. The cost of such an unit is estimated to be 125 MNOK on a 2001 basis including the installation costs [95]. Using the average exchange rate for May between USD and NOK of 0.1726 this corresponds to 21.575 million USD [96].

9.4.4 Capital cost summary

With the procedure outlined in Section 9.3.1 and the assumptions for the various equipment as outlined, the capital cost for the economical base case scenario is shown in Table 9.12. This results in a total capital cost for the modelled plant at $1.823 \cdot 10^8$ USD calculated based on prices from 2001.

Table 9.12 – Overview of the parameters obtained to calculate the capital cost and the resulting value of the various equipment in the simulated process.

	Heat exchangers					**Coolers**		**Compressors**	
Parameter	**E-100**	**E-101**	**E-102**	**E-103**	**E-104**	**E-105**	**E-106**	**C-100**	**C-101**
Capacity measure				**Area [m^2]**				**Power[kW] consumption**	
C_P^0 [USD]	$2.888{\cdot}10^4$	$2.449{\cdot}10^4$	$2.027{\cdot}10^4$	$1.457{\cdot}10^4$	$1.074{\cdot}10^5$	$3.767{\cdot}10^4$	$5.117{\cdot}10^4$	$4.967{\cdot}10^5$	$5.562{\cdot}10^5$
F_P	1.119	1.119	1.119	1.119	1.119	1.119	1.065	-	-
F_M	1	1	1	1	1	1	1	1	1
F_{BM}	3.448	3.448	3.448	3.448	3.448	3.448	3.397	2.7	2.7
C_{BM} [USD]	$1.007{\cdot}10^5$	$8.542{\cdot}10^4$	$7.069{\cdot}10^4$	$5.083{\cdot}10^4$	$3.746{\cdot}10^4$	$1.314{\cdot}10^5$	$1.738{\cdot}10^5$	$1.341{\cdot}10^6$	$1.502{\cdot}10^6$

		Separators			**Reactors**			**Pumps**	**ASU**
Parameter	**Turbine**	**V-100**	**V-101**	**V-102**	**ERV-100**	**ERV-101**	**R-100**	**P-100**	
Capacity measure	**Produced Power [kW]**			**Volume** [m^3]			**Area [m^2]**	**Power [kW]**	
C_P^0 [USD]	$9.990{\cdot}10^6$	$1.298{\cdot}10^5$	$2.801{\cdot}10^5$	$5.397{\cdot}10^4$	$8.329{\cdot}10^4$	$2.717{\cdot}10^5$	$3.045{\cdot}10^7$	$6.099{\cdot}10^4$	-
F_P	-	12.28	10.86	6.937	10.36	15.37	1.068	1.399	-
F_M	1	1	1	1	1	1	1	1	-
F_{BM}	3.3	24.59	22.01	12.03	21.10	30.22	3.403	3.779	-
C_{BM} [USD]	$3.297{\cdot}10^7$	$3.438{\cdot}10^6$	$6.164{\cdot}10^6$	$6.375{\cdot}10^5$	$1.757{\cdot}10^6$	$8.211{\cdot}10^6$	$1.036{\cdot}10^8$	$2.305{\cdot}10^5$	$2.15{\cdot}10^7$

Adjusted to 2012 value

The CEPCI index for 2013 has naturally not yet been published as 2013 is not over and consequently the capital cost was adjusted to 2012 levels. The CEPCI value was 584.6 and 394 for year 2012 and 2001 respectively and implementation into Equation 9.13 results in a capital cost for the plant in 2012 values at $2.705 \cdot 10^8$ USD [92, 97].

Validity of procedure

There are a range of assumptions applied to this calculation. First of all it does not take into consideration the upgrading unit or the de-sulphurization process usually needed to remove sulfur from the feed. Both of these are part of the GTL plant structure, but as neither was modelled, the cost was not included either. This should consequently be kept in mind when evaluating the cost estimates. Second a range of assumptions was made for economical modelling of the equipment used in the simulations.

The ATR consist of a burner section a catalyst bed and a combustion zone. In the economic evaluation made in this work it is simulated as a vertical pressure vessel and is hence a major simplification. In addition it is normally constructed by as a brick lined vessel while it in this calculation has been treated as carbon steel, again another simplificatio n[98]. These were made on the basis of not managing to obtain a more detailed correlation for an ATR with respect to capacity measure, making it change upon iteration in the flow sheet and consequently this unit is likely to be very underestimated for the capital costs.

The calculation of capital cost of pre-reformer is likewise also simplified, but again due to time constraints and available cost correlations for such equipment, simplifications were inevitable. The design of an MTFB is almost equal to a heat exchanger and thus this unit might not be too simplified. However as the aim of the economic analysis is not an accurate economic costing of a GTL plant, but to derive an optimum operation rate the simplifications made were considered not to be too crucial.

The calculation of the heat exchangers also renders the economic evaluation with another uncertainty factor. However as explained for that calculation, the areas are rather over estimated than opposite and hence the economic evaluation does likely overestimate the cost.

The area of the coolers are dependent on the water flow used as cooling medium and is consequently also an uncertainty factor. The coolers used in this simulation uses a large water flow and hence results in small areas, which is reasonable where the cooling water is free of charge. As this already is assumed for the simulation, the cost estimate is also plausible. This is though subject to a trade off as previously mentioned in Section 9.1.1 and thus it is difficult to evaluate if the cost is over, under or reasonably estimated.

The size of the turbine needed for the economic base case results in 42.77 maximum turbines as a result of the applicable range for the correlation. However there exist industrial turbines in the size range needed and are among other produced by GE, but due to difficulties obtaining a quote for such a turbine the multiple unit method was used and hence probably overestimates the economic aspect further.

Comparison to other plants

For the economic base case scenario this equals a capital cost per daily barrel of 13613.48 USD. Estimates in literature for the same parameter ranges between 20000-30000 USD and for refineries the same literature value is 12000-14000 USD [99]. Even though a comparison between the literature values and the simulation is difficult as neither the upgrading or de-sulphurization unit is modelled for the cost, it does indicate a good economical potential.

9.5 Calculation of operational costs

The operational costs has been tried calculated based on as recent and stable price levels as possible. The respective procedures and assumptions are discussed in the following sections.

9.5.1 Raw natural gas

The natural gas is assumed bought from the Henry Hub terminal in Louisiana at spot price. Figure 9.8 shows the spot price from July 2011 to May 2013 while Table 9.9 shows the latest spot prices for May [100]. The average price for the dates given in Table 9.9 was used in the calculations and resulted in a price of 4.056 $\frac{USD}{MMBtu}$. Converted to cubic meters this yield 0.1432 $\frac{USD}{m^3}$ of natural gas.

Figure 9.8 – Plot of the spot prices for natural gas in $\frac{USD}{MMBtu}$ at the Henry Hub terminal in Louisiana for the period of July 2011 to May 2013[100]

Spot Prices | **Spot Prices Table** | NYMEX Prices | NGPL Prices

Spot Prices ($/MMBtu)	Thu, 16-May	Fri, 17-May	Mon, 20-May	Tue, 21-May	Wed, 22-May
Henry Hub	4.01	3.89	4.09	4.13	4.16
New York	4.13	3.96	4.35	4.45	4.32
Chicago	4.09	3.94	4.19	4.23	4.26
Cal. Comp. Avg,*	4.00	3.86	4.15	4.17	4.16
Futures ($/MMBtu)					
June Contract	3.932	4.055	4.090	4.192	4.186
July Contract	3.982	4.103	4.141	4.239	4.233

*Avg. of NGI's reported prices for: Malin, PG&E citygate, and Southern California Border Avg.

Source: NGI's Daily Gas Price Index

Figure 9.9 – Table of the spot prices of natural gas in $\frac{USD}{MMBtu}$ at the Henry Hub terminal in Louisiana for the 16th-17th, and 20th-22nd of May 2013 [100].

9.5.2 Oxygen

The oxygen used in the simulation is thought to be delivered from an ASU plant at 20 °C and 3000 kPa pressure. By modelling the oxygen supplied this way, the oxygen does not represent an operational cost in it self, as the operational cost is related to the power needed to produce the oxygen instead. The operational cost of oxygen is hence treated as a power requirement and will be further outlined in the section on steam and power.

9.5.3 Catalyst

Catalysts are needed in the pre-reformer, ATR and the Fischer-Tropsch reactor. Nickel is the preferred choice industrially for both the pre-reformer and the ATR as indicated in Chapter 4, and is hence also applied in this work. The cost and density of catalysts are difficult to obtain without making a large order from a vendor. However after conferring with a professional in the field the catalyst was assumed to be 20wt% nickel and with a density of $800\frac{g}{dm^3}$[101]. A rule of thumb estimate for the cost was also established to be 100 000 $\frac{NOK}{m^3}$ [101]. The average exchange rate for May between USD and NOK of 0.1726 as previously used for the ASU plant, gives the equivalent estimate of 17260 $\frac{USD}{m^3}$ for the nickel catalyst.

The Fischer-Tropsch reactor modelled uses a cobalt catalyst and cobalt being a more precious metal than nickel it is also more costly. It is assumed present in 20-30 wt%. The cost calculation for this catalyst is based on adding the price of cobalt to the rule of thumb price of 17260 $\frac{USD}{m^3}$ Using 25 wt% for Cobalt and the same density as for the nickel catalyst, the mass of Cobalt is calculated to be 200 $\frac{g}{dm^3}$. The price of cobalt at the London metal exchange was 28750 $\frac{USD}{\text{metric ton}}$ on the 28th of May and this gives a price of 0.02875 $\frac{USD}{g}$ and consequently the price of the cobalt catalyst becomes 23010 $\frac{USD}{m^3}$ [102].

Calculation of duration of catalyst

The catalyst thought to be used with the simulated process has a lifetime of about 2 and 4 years for the nickel and cobalt catalyst respectively. By assuming 350 operational days per year and 24 hours of operation per day the cost per hour of catalyst can be calculated and was found to be 200.6 $\frac{USD}{h}$ and 58.47 USD in the ATR and pre-reformer and 532.5 $\frac{USD}{h}$ for the FTR in the economic base case.

9.5.4 Steam and power

In the modelled process there are two compressors, a pump and the operation of the ASU that requires electric power and the only steam required is attributed to the operation of the ATR. The power needed to run the ASU is calculated based on the amount of oxygen needed and requires 0.8 kWh per kg of oxygen produced [103]. The utility cost of oxygen is consequently given as indicated in Equation 9.20.

$$\begin{aligned} \text{Cost of oxygen} \quad &= 0.8\ [\frac{kWh}{kg}] \times \dot{m}_{O_2}\ [\frac{kg}{h}] \times \text{electricity cost}\ [\frac{US\ cent}{kWh}] \\ &= \text{Cost in}\ [\frac{US\ cent}{h}] \end{aligned} \tag{9.20}$$

The power from pumps and compressors are taken directly from the Unisim simulation. These values are calculated with reference to a 75% adiabatic efficiency and hence does not need to be corrected for efficiency.

The price of electric power was chosen to be the average price, based on statistics from EIA, of steam delivered to the industrial sector in 2012 and was found to be 6.197 $\frac{US\ cent}{h}$ [104].

The economical base case produces steam and electric power as well. This results in it potentially being necessary to buy steam for the pre-reformer, and rather an option to sell electric power emerges if the steam stream is large enough. The power production was modelled by reducing the pressure of the steam from the cooling of the FTR to atmospheric pressure through a turbine. The turbine operates with a 75% adiabatic efficiency as the compressors and hence the power given by Unisim is considered the actual power produced. Consequently the electricity costs for the plant was calculated by subtracting the produced from the required amount.

9.5.5 Operational cost summary

For the economic base case described, the operational costs are outlined in Table 9.13. From this overview it is evident that the most important operational cost to minimize is related to the production of oxygen as it is over eight times larger than the second largest operational cost and contributes with 80% of the overall operational costs per hour.

Table 9.13 – Operational costs for the economic base case simulation

Variable	Cost $[\frac{USD}{h}]$
Catalyst	
Pre-reformer	58.47
ATR	200.6
FTR	573.2
Power	
C-100 C-101 T-100 P-100	304.9
ASU	8139
Natural gas	959.4
Water	- [a]
Steam	- [b]
Total	10235.57

[a] Assumed free of charge
[b] supplied internally

9.6 Income

9.6.1 Products

Although the plant modelled does not include the upgrading unit and hence an overview over the actual products produced, an estimate for revenue was desirable in order to be able to model the economic performance of the plant versus capacity. The product revenue was consequently calculated based on the composition of the stream going to upgrading and the revenue prices used are the same as applied in an article on GTL modelling for optimal operation by Panahi et. al and are given in Table 9.14 [31].

9.6.2 Electricity

In the case of produced power exceeding the internal processing needs the power was considered sold to the same price as it was assumed bought for.

Table 9.14 – The assumed selling price of the GTL products, LPG, Gasoline, Diesel and Wax given in $\frac{USD}{kg}$[31]

Components	**Price** $[\frac{USD}{kg}]$
LPG	0.90
Gasoline	0.73
Diesel	0.71
Wax	0.39

9.6.3 Total income

With the prices of products and electricity outlined above and the conditions for the economic base case the income is as shown in Table 9.15. The total income per hour corresponds to 75.99 $\frac{USD}{bbl}$.

Table 9.15 – Reveneue from the produced GTL products in the economic base case

Products	**Generated income** $[\frac{USD}{h}]$
LPG	1243
Gasoline	$1.974 \cdot 10^4$
Diesel	$2.263 \cdot 10^4$
Wax	$1.534 \cdot 10^4$
Electricty	3976
Total	$6.292 \cdot 10^4$

9.7 Cost per product

Both the capital cost and the operational cost are functions of the simulation variables and will change upon iteration. The main purpose of this was to construct a cost estimate as function of the production rate to see if this

alters the most optimal case from carbon and thermal perspective.

The operational cost are given as per hour of operation while the capital costs is a fixed number. To be able to calculate a cost per barrel produced, the total annual cost, TAC and the total yearly production must be calculated. Equation 9.21 shows how TAC is calculated. The ACCR is the annual capital charge ratio and is calculated as shown in Equation 9.22, where n is the plant lifetime and i is the interest rate [90].

$$\text{TAC} = \text{yearly operating costs} + \text{ACCR} \times \text{total capital cost} \tag{9.21}$$

$$\text{ACCR} = \frac{[i(1+i)^n]}{[(1+i)^n - 1]} \tag{9.22}$$

For this work the plant lifetime was chosen to be 20 years and the interest rate to be 10%, giving an ACCR value of 0.1175. The yearly utility costs were found by multiplying the number of operational hours with the operational cost per hour. Hence by simply multiplying the barrels produced per day with the number of operational days the yearly production is obtained and by dividing the obtained TAC value with the yearly production gives cost per barrel.

9.7.1 Implementation in Unisim

The cost per barrel was tried minimized with the optimizer in Unisim. With the economic base case flow sheet the optimizer would not converge and reported convergence error for the steam stream entering the pre-reformer and that produced from the steam from the FTR. This flow sheet is rather complicated as it tries to account for the economics of producing enough steam to the pre-reformer and rest to electricity production when the steam to pre-reformer changes with iteration. It is hence suspected that the numerical iteration process is too heavy for the program to handle. This procedure would possibly be better handled by implementation of Matlab and this is advisable to be considered for future work.

In an attempt to see if the optimizer would change on the basis of economics the loops connecting produced and needed steam was removed and the optimizer tried again. This process flow diagram of this flow sheet is shown in Figure 9.10 The direct consequences of this on the economic calculation are that the cost of a compressor and pump is not changed by

iteration. In addition the steam for the pre-reformer are no longer attached to the internal supply, but considering the steam was previously sufficiently supplied in the simulation a cost for this variable was not included and only assumed that the process would be self sufficient. With this simplified approach the optimizer did run properly and the results are shown in Table 9.16. However this simplification will affect the energy efficiency and this was consequently not recorded for these simulations.

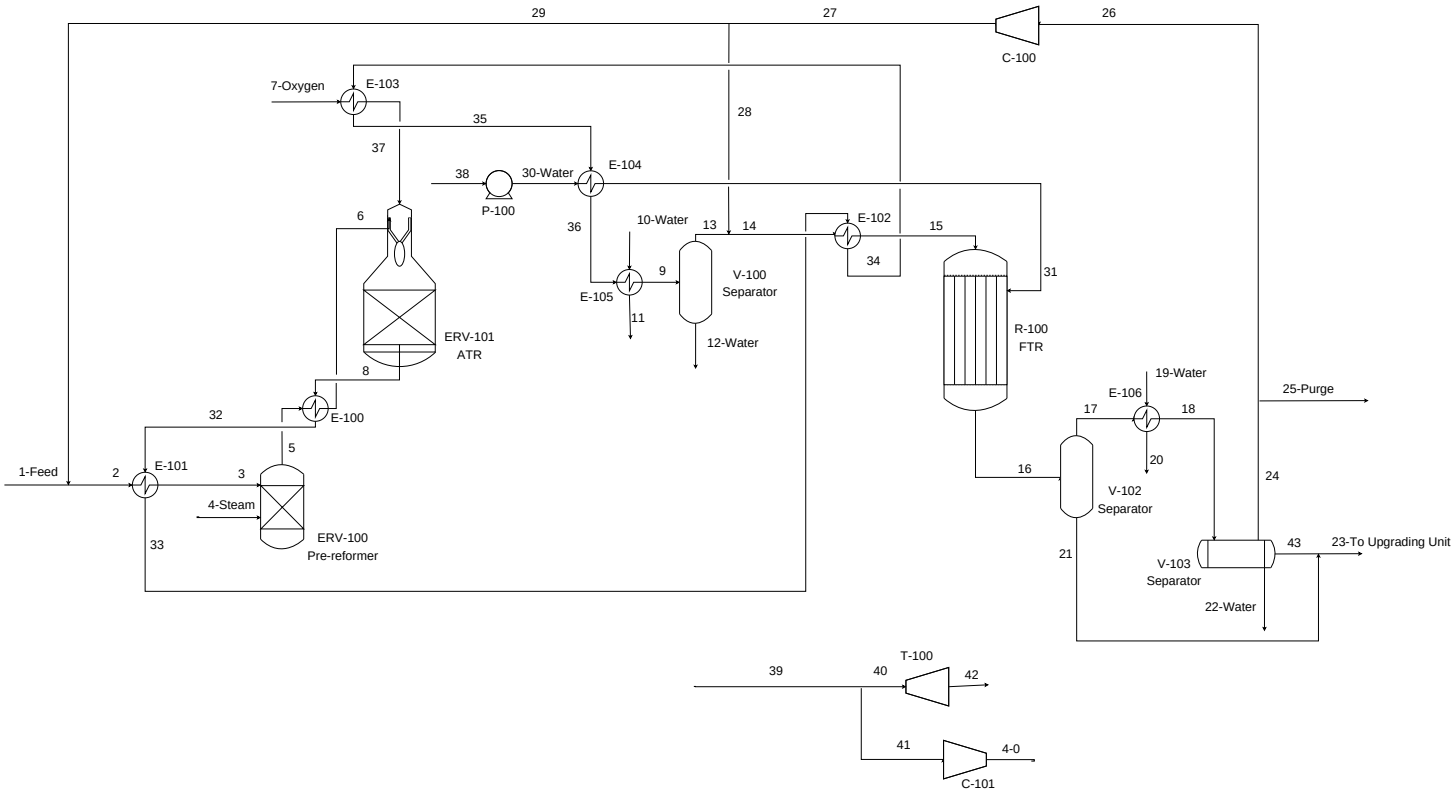

Figure 9.10 – Process flow diagram of the modelled base case in Unisim for economic simulation

9.7.2 Optimizer

The optimizer were tried run, first on the basis of the economic base case and then on the basis of this obtained optimization. Next a case study on reactor volume was carried out before a multi variable case study including reactor volume, steam, oxygen was conducted to get a more complete picture. The values obtained for the last case study was inserted directly and tried optimized. The resulting indicator values for all of the optimizer tries are listed in Table 9.16.

From Table 9.16 it can be seen that the inclusion of economics has changed the optimal reactor volume away from 1933m^3 as was experienced for the the optimization of CE, TE and flow to upgrading unit. Compared to these previous optimizations it is also noted that the $\frac{H_2}{CO}$ ratio is closer to 2.1, however the purge fraction, and oxygen to carbon ratio is in the range 0.61-0.63 as previously was found beneficial. It can also be seen that all of the target optimization variables still provide very good numbers, all though they are a bit smaller than what was experienced for the bypass scenario.

Table 9.16 – Indicator table

Parameter	Case **Economic base case**	**Optimized** $\frac{USD}{bbl}$	**Second optimizing** $\frac{USD}{bbl}$	**Multivariable economy**
FTR Volume $[m^3]$	1860	1740	1620	1199.71
FTR conversions [%]				
FTR	89.74	90.13	89.34	87.67
Metahanation	4.88	4.96	4.87	5.11
Temperature syngas [°C]	1029	1030	1031	1028
Ratios				
$\frac{H_2}{CO}$	2.088	2.091	2.088	2.137
$\frac{H_2O}{NG}$	1.098	1.098	1.098	0.7219
$\frac{O_2}{NG}$	0.6260	0.6252	0.6265	0.5915
Purge fraction	0.190	0.190	0.190	0.310
Recycle to FTR	0.577	0.577	0.577	0.633
Recycle to feed	0.423	0.423	0.423	0.367
CE [%]	82.17	82.31	82.09	77.25
TE [%]	65.73	65.84	65.66	61.77
Product				
molar flow $[\frac{kmol}{h}]$	131.7	131.9	131.5	123.3
in $\frac{std.bbl}{d}$	19870	19910	19850	18620
Production cost $[\frac{USD}{bbl}]$	16.93	16.67	16.53	16.10
Energy efficiency	71.30	-	-	-

9.7.3 Case study reactor volume

From the economic base case it can be seen that the reactor is the equipment in the process with the largest capital cost attached to it, influencing the cost per produced barrel and a case study was consequently carried out for this relationship. The results are shown in Figure 9.11 and indicates that the reactor volume should be between 1400-1800 m^3 in order to minimize production costs.

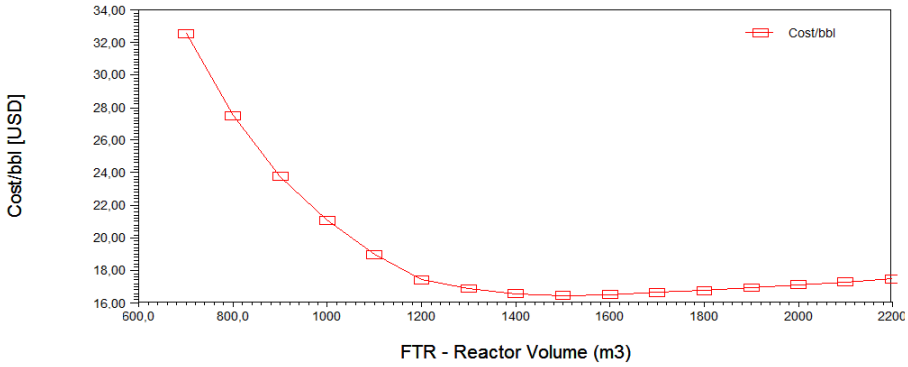

Figure 9.11 – Case study of the productin cost in USD per barrel as function of reactor volume

9.7.4 Case study multi variable

A case study for the production cost as function of oxygen, steam, and reactor volume was run to get a more complete picture of the behaviour of production costs and the results are given in Appendix J. Due to the time consuming process of this case study only a small range were chosen for each parameter as shown in Table 9.17. The optimum values was implemented in the simulation and optimized directly with the optimizer tool. The corresponding indicator values are shown in Table 9.16 and the Unisim workbook is found in Appendix D. And as can be seen the actual production cost was a bit higher than what was predicted by the case study, however this is likely due to the numerical iteration procedure.

Table 9.17 – Case study parameters for the multi variable economic evaluation

	Range		
Parameter	**Minimum**	**Maximum**	**Optimum**
Reactor volume	1200	1800	1200
Oxygen	4000	6000	5247
Steam	7000	9000	7300
Production cost	-	-	16.04

9.7.5 Evaluation

The cost per barrel for the economic base case was found to be 16.93 $\frac{USD}{bbl}$ and the corresponding income was 75.99 $\frac{USD}{bbl}$. This gives a revenue of 59 $\frac{USD}{bbl}$. With the use of optimizer the lowest production cost obtained was 16.10 USD /barrel, the total income was 76.39 $\frac{USD}{bbl}$ and the revenue was hence found to be 60.29 $\frac{USD}{bbl}$. The main observation from the inclusion of the economics is the change in reactor volume and efficiencies towards the bench scale numbers. The optimum process from a feedstock and production point of view does thus not provide the most economic process. Even though the economic simulation in this work is based on a range of assumptions and simplifications it does combined with today's oil price of 98.9 $\frac{USD}{bbl}$ appears to have a good economic potential.

Chapter 10

Conclusion

The parameter study conducted through the use of case studies was found to give good insight into parameter connectivity, but to be a poor optimization tool in regards to the continuously changing basis for selection of optimal values with every case study conducted.

The use of Optimizer in Unisim indicated that the choice of objective function between CE, TE and liquid flow to upgrading was irrelevant as optimization of one also optimized the two others. The molar flow to upgrading however did not display maximum values for the same simulations as the three other variables and was found to be a poorer choice of objective function. The differences was found to likely be due to liquid volume taking composition and not only size of flow into consideration. A continued increase in CE, TE and liquid flow to upgrading was observed with the use of Optimizer, however the best result was achieved with a change in flow sheet structure, bypassing the liquid product from the FTR in regards to the 3-way separator. This resulted in a CE of 82.41%, TE of 65.93% and a liquid production of 19940 $\frac{bbl}{d}$ of syncrude. These are very good results comparing to the conventional efficiencies for GTL of 77% and 60% respectively and considering the feed was deigned for a production of 17000 $\frac{bbl}{d}$. Two notes for the use of Optimizer should be mentioned. First, the continued increase experienced might be a result of optimizing an already optimized flow sheet, and second, the lack of variation in adjustable variables indicate that only a narrow search is conducted within the given range. Consequently the Optimizer is probably neither an optimal optimization tool for this process.

The results obtained from the Optimizer are not investigated enough in depth to be able to give direct recommendations for the optimal operation range, however it the simulations with best results all have $\frac{H_2}{CO}$ ratio close to 2.0, $\frac{O_2}{NG}$ ratio of 0.61-0.63 and a purge ratio of 0.17-0.19.

The inclusion of economics changed the operational optimum to a syncrude production of 18620 $\frac{bbl}{d}$ and efficiencies of 77.25% and 61.77% respectively. This resulted in a cost per barrel of 16.10 USD and a revenue of 60.29 USD per barrel. However as neither a de-sulphurization or upgrading unit is modelled it is difficult to compare the economic performance to existing processes. The current oil price of 98.9 USD per barrel nevertheless indicate a good economic environment for GTL.

Chapter 11

Future work

For future work it is suggested to apply Matlab in combination with Unisim to conduct the actual optimization. With the process model in Unisim and then calling Matlab for iteration and convergence of the flow sheet would most likely give a more powerful iteration tool and potential for more extensive search regions.

A more detailed and realistic economic calculation with inclusion of desulphurization and upgrading unit is also advised to assess the economic performance of the process.

Abbreviations

Abbreviation	Meaning
ACCR	Annual Capital Charge Ratio
ASF	Anderson-Schulz-Flory
ATR	Auto Thermal Reformer
BCM	Billion Cubic Meters
BTL	Biomass to Liquid
CE	Carbon Efficiency
CFB	Circulating Fluidized Bed
CIS	Commonwealth of Independent States
CNG	Compressed Natural Gas
CPP	Clean Petroleum Product
CTL	Coal to Liquid
EE	Energy Efficiency
FFB	Fixed Fluidized Bed
FT	Fischer Tropsch
FTR	Fischer Tropsch Reactor
GHSV	Gas Hourly Space Velocity
GTL	Gas to Liquid
GTW	Gas to Wire
GTS	Gas to Solid
HEX	Heat Exchange Reforming
HHV	Higher Heating Value
HTFT	High Temperature Fischer Tropsch
IEA	International Energy Agency
LNG	Liquefied Natural Gas

LPG	Light Petroleum Gas
LTFT	Low Temperature Fischer Tropsch
LHV	Lower Heating Value
NA	Not Available
NG	Natural Gas
NGH	Natural Gas Hydrates
NOK	Norwegian Kroner
MNOK	Million Norwegian Kroner
MTFB	Multi Tubular Fixed Bed
MMBtu	Million British Thermal Units
OPEC	Organization of the Petroleum Exporting Countries
PFD	Plug Flow Diagram
PFR	Plug Flow Reactor
POX	Partial Oxidation
SA	South Africa
SAS	Sasol Advanced Synthol
SMDS	Shell Middle Distillate Synthesis
SMR	Steam Methane Reforming
STP	Standard Temperature and Pressure
TAC	Total Annualized Costs
TE	Thermal Efficiency
UN	United Nations
USD	US dollars
WHB	Waste Heat Boiler
WGS	Water Gas Shift

Symbollist

Symbol	Meaning	Units
A	Area	m^2
A	Capacity measure	
A	Pre exponential factor in Arrhenius' equation	
A_i	Capacity item i	
A_{max}	Maximum Capacity	
A_t	Tube cross sectional area	mm^2
A_s	Hypothetical tube cross flow area on shell side	mm^2
α	Chain growth probability factor	
°C	Degree Celsius	
B_1, B_2	Item specific constants for calculation of cost factor	
C_1, C_2, C_3	Item specific constants for calculation of Pressure factor	
C_i	Cost item i	USD
C_{BM}	Bare module cost	USD
C_i	Alkane with i carbon atoms in the chain	
C_n	Alkane with n carbon atoms in the chain	
C_p	Heat capacity	$\frac{kJ}{kg,C}$
CP	$C_p \times m$	$\frac{kW}{C}$
C_p^0	Purchased equipment cost	USD

Symbol	Meaning	Units
CP_c	CP for cold stream	$\frac{kW}{C}$
CP_h	CP for hot stream	$\frac{kW}{C}$
CU-1	Cooling utility 1	kW
CU-2	Cooling utility 2	kW
$C_{21\rightarrow\infty}$	molecules with 21 and more carbon atoms in the chain	
d	diameter	mm
d_o	outer diameter	mm
d_i	inner diameter	mm
de	equivalent diameter	mm
D	Diameter	m^2
D_s	Shell side inside diameter	mm
F_{BM}	Cost factor	
F_P	Pressure factor	
$F_{\text{P,vessel}}$	Pressure factor for pressure vessels	
G_s	Shell side mass velocity	$\frac{kg}{s,m^2}$
Δ H	Enthalpy change	$\frac{kJ}{mol}$
$\Delta_f H^\circ_{298}$	Enthalpy of formation	$\frac{kJ}{mol}$
h	hour	
h_i	inside heat transfer coefficient	$\frac{W}{m^2,C}$
h_s	shell side heat transfer coefficient	$\frac{W}{m^2,C}$
j_h	Heat-transfer factor	
K_1, K_2, K_3	Item specific constants for calculation of purchased equipment cost	
k_f	fluid thermal conductivity	$\frac{W}{m^2,C}$
L	Length	meter
l_B	baffle spacing	mm
m	mass	gram
$\dot{m}_{O_2}$	mass flow oxygen	$\frac{kg}{h}$
M_m	Molar mass	$\frac{g}{mol}$
n	counting variable for variables such as number of carbon atoms	
NO_x	Nitrous oxides	
Nu	Nusselt number	
ρ	density	$\frac{g}{dm^3}$
π	Pi	
P	Pressure	kPa
P_{CO}	Partial pressure of CO	kPa
P_{H_2}	Partial pressure of H_2	kPa
Pr	Prandtl number	
p_t	tube pitch	mm

Symbol	Meaning	Units
Q	Volumetric gas flow	$\frac{m^3}{h}$
Re	Reynolds number	
r_{CH_4}	reaction rate for consumption of methane	
r_{CH_4}	reaction rate for consumption of CO	
r_{FT}	Stoichiometric coefficients for Fischer Tropsch reaction	
St	Stanton number	
t_{vessel}	vessel thickness	mm
T	Temperature	°C
T_{act}	Actual temperature	°C
T_C	Temperature cold stream	°C
T_H	Temperature hot stream	°C
T_{int}	Temperature of interval	°C
T_{min}	Minimum temperature approach	°C
$\Delta T_{interval}$	Temperature difference in interval	°C
ΔT_{min}	Minimum temperature difference	°C
$\frac{USD}{bbl}$	US dollars per barrel	
U	Usage ratio of hydrogen	
U	Overall heat transfer coefficient	$\frac{W}{m^2,C}$
μ	fluid viscosity	$\frac{Ns}{m^2}$
μ_w	fluid viscosity at the wall	$\frac{Ns}{m^2}$
u_s	linear velocity	$\frac{m}{s}$
V	volume	m^3
$V_{catalyst}$	volume of catalyst	m^3
vol%	Volume percentage	
w_n	weigth fraction of C_n	
$W_{compressors}$	Compressor work	kW
W_{eq}	Equivalent work	kW
W_{net}	Net work	kW
W_{pump}	Pump work	kW
$W_{turbines}$	Turbine work	kW
$W_{eq,purge}$	Equivalent work	kW
$W_{eq,feed}$	Equivalent work	kW
$W_{eq,syncrude}$	Equivalent work	kW
W_s	Fluid flow rate on shell side	$\frac{kg}{s}$

Appendix A

Modelling of Fischer-Tropsch reaction in Unisim

The Fischer-Tropsch synthesis was modelled as given by the ASF distribution. Only paraffins were considered in this work and, α was assumed to be 0.9. All of the components below carbon number 21 was modelled as individual units, while the components with carbon number from 21-30 was lumped in a component designated C_{21+}. The stoichiometric coefficients was calculated after Equation A.1 and A.2 as was outlined in a paper on ASF modelling by Hillestad [86].

$$r_{FT} = (1-\alpha)^2 \alpha^{(i-1)} \quad \text{for } C_i, i = 1, ...N \tag{A.1}$$

$$r_{FT} = (1-\alpha)\alpha^{20} \quad \text{for} \quad C_{[N+1,\infty]} \tag{A.2}$$

Table A.1 shows the calculated stoichiometric coefficients used in the Unisim simulations. The lumped component C_{21+} is modelled as $C_{30}H_{62}$ due to similar properties.

With the coefficients from TableA.1 the full Fischer-Tropsch reaction can be written as displayed in EquationA.3

Table A.1 – Stoichiometric coefficients used to model the Fischer-Tropsch synthesis in Unisim as calculated by Equation A.1 and A.2 [86]. The molar mass for each component was found in the component library of the simulation in Unisim.

Component	**Mole weight**$[\frac{g}{mole}]$	**Stoichiometric coefficient**
CO	28.011	-1.000
H_2	2.016	-2.100
H_2O	18.015	1.000
CH_4	16.043	0.010
C_2H_6	30.070	0.009
C_3H_8	44.097	0.008
C_4H_{10}	58.124	0.007
C_5H_{12}	72.151	0.007
C_6H_{14}	86.178	0.006
C_7H_{16}	100,205	0.005
C_8H_{18}	114,232	0.005
C_9H_{20}	128.259	0.004
$C_{10}H_{22}$	142.285	0.004
$C_{11}H_{24}$	156.313	0.003
$C_{12}H_{26}$	170.339	0.003
$C_{13}H_{28}$	184,367	0.003
$C_{14}H_{30}$	198.380	0.003
$C_{15}H_{32}$	212.410	0.002
$C_{16}H_{34}$	226.429	0.002
$C_{17}H_{36}$	240.457	0.002
$C_{18}H_{38}$	254.479	0.002
$C_{19}H_{40}$	268.510	0.002
$C_{20}H_{42}$	282.540	0.001
$C_{30}H_{62}$	422.799	0.012

$$\begin{aligned} CO + UH_2 \rightarrow\ & 0.01CH_4 + 0.009C_2H_6 + 0.008C_3H_8 + 0.007C_4H_{10} \\ & + 0.007C_5H_{12} + 0.006C_6H_{14} + 0.005C_7H_{16} + 0.005C_8H_{18} \\ & + 0.004C_9H_{20} + 0.004C_{10}H_{22} + 0.003C_{11}H_{24} + 0.003C_{12}H_{26} \\ & + 0.003C_{13}H_{28} + 0.003C_{14}H_{30} + 0.002C_{15}H_{32} + 0.002C_{16}H_{34} \\ & + 0.002C_{17}H_{36} + 0.002C_{18}H_{38} + 0.002C_{19}H_{40} + 0.001C_{20}H_{42} \\ & + 0.012C_{30}H_{62} + H_2O \end{aligned} \tag{A.3}$$

Appendix B

ASF distribution for base case

The plot of the the logarithmic of the weight fraction divided by carbon number, W_n, plotted against carbon number, n, for components C2-C20 with methanation reaction present in the FTR and for components C1-C20 without methanation reaction present in the FTR is shown in Figure B.1 and B.2 respectively.

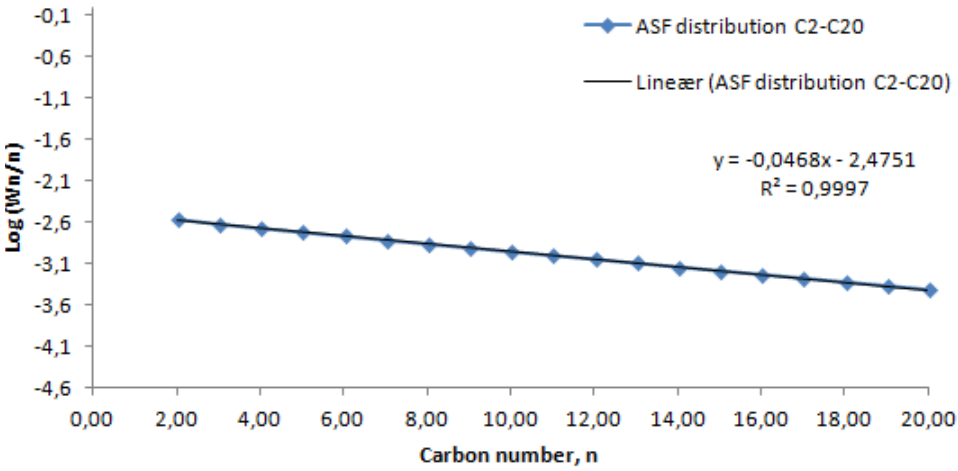

Figure B.1 – The logarithmic of the weight fraction divided by carbon number plotted against carbon number (n), for components C2-C20 in the stream leaving the Fischer Tropsch reactor from the base case simulation together with an added linear trend line.

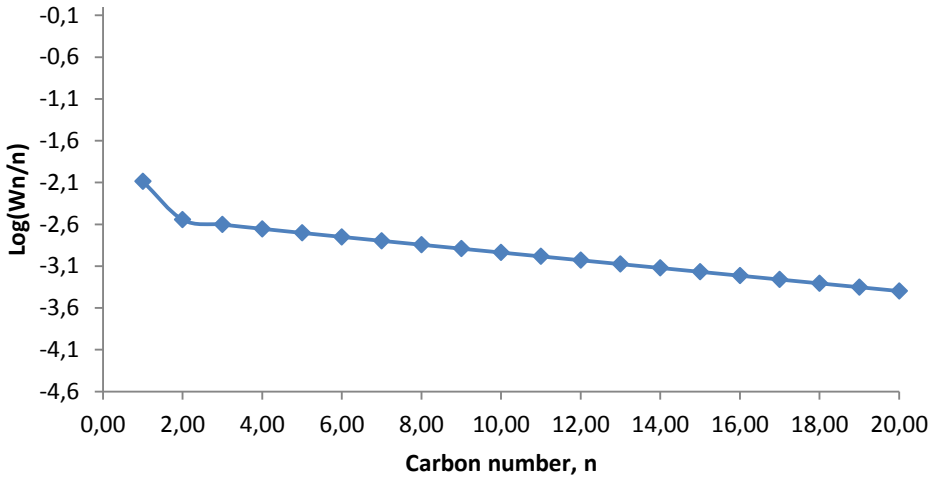

Figure B.2 – The logarithmic of the weight fraction divided by carbon number plotted against carbon number (n), for components C1-C20 in the stream leaving the Fischer Tropsch reactor from the base case simulation when the methanation reaction is neglected

Appendix C

Unisim Flow Sheets

This appendix shows the flow sheet in Unisim for the base case, economic base case where heat and energy integration is included and finally the simplified flow sheet for the economics in order to run optimizer. These are outlined in Figure C.1, Figure C.2 and Figure C.3 respectively.

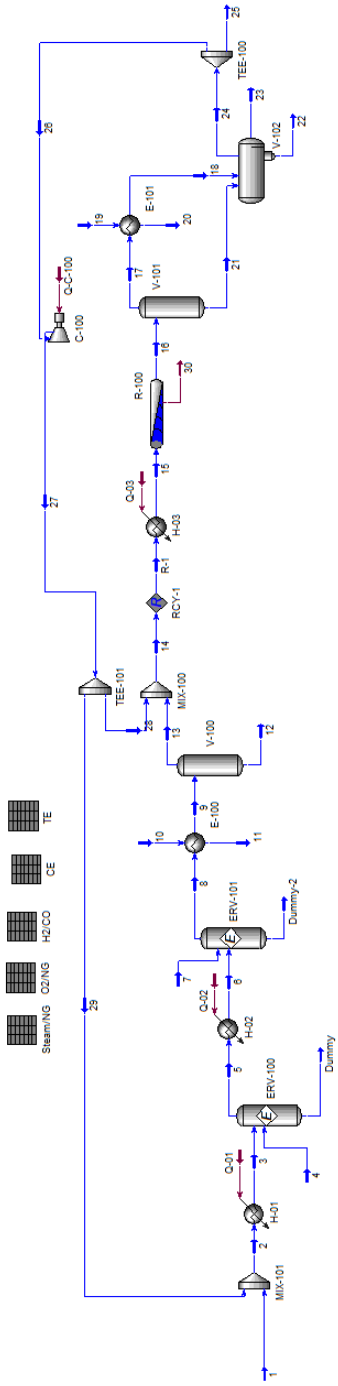

Figure C.1 – Flow sheet of the simulated base case in Unisim.

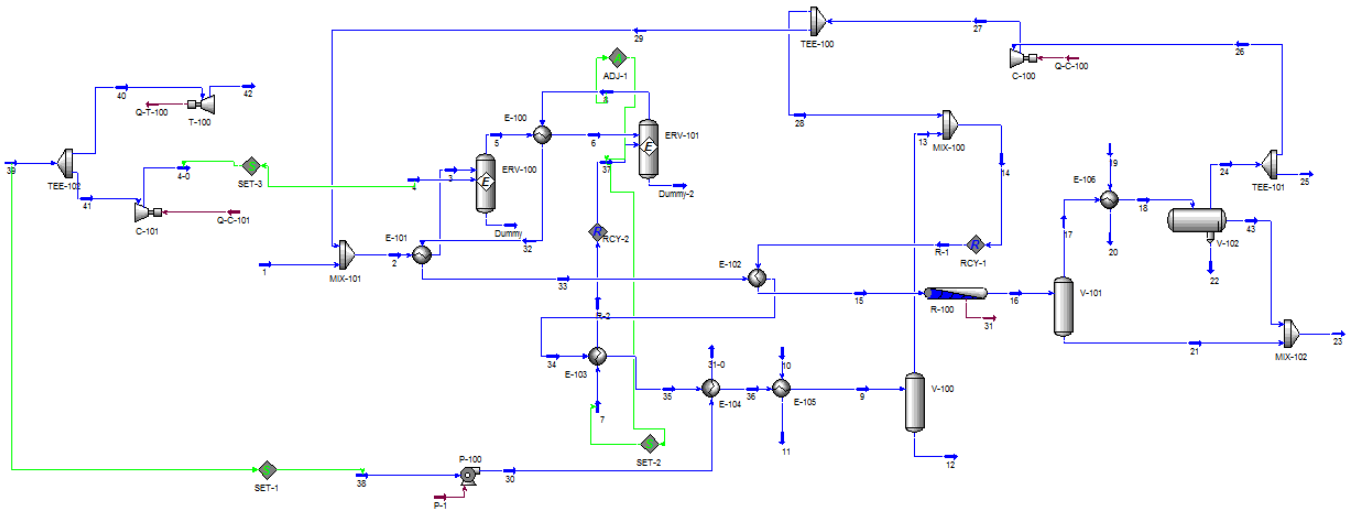

Figure C.2 – Flow sheet of the economic base case as simulated in Unisim.

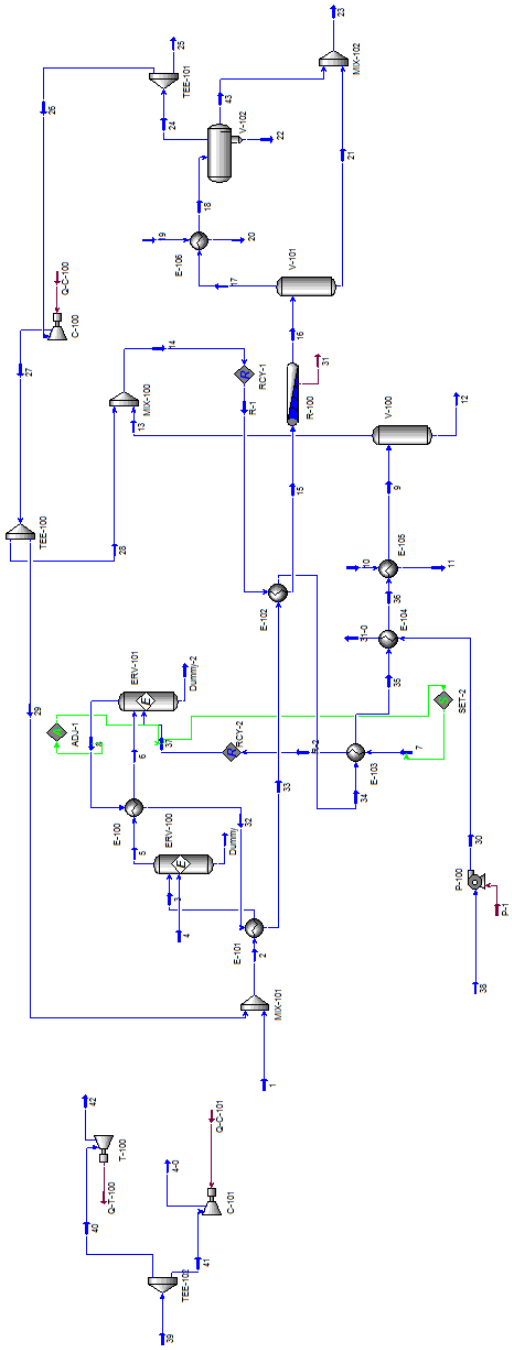

Figure C.3 – Flow sheet of the modified economic simulation applied to be able to run optimizer in Unisim

Appendix D

Woorkbooks

This appendix gives the workbook for four of the main simulation made in Unisim. The first two pages is for the base case, the three next is for the simulation with bypass, the following four are for the economic base case, where heat and energy integration was included, and the final three are for the simplified flow sheet optimized for economics.

Honeywell

Company Name Not Available
Calgary, Alberta
CANADA

Case Name:	C:\Users\...\Ny mappe\Base case.usc
Unit Set:	SI
Date/Time:	Monday Jun 10 2013, 7:15:26

Workbook: Case (Main)

STATUS

OK

Streams

Fluid Pkg: All

Name		1	3	4	5	Dummy
Vapour Fraction		1.0000 *	1.0000	1.0000	1.0000	0.0000
Temperature	(C)	40.00 *	455.0 *	252.0 *	527.3	527.3
Pressure	(kPa)	3000 *	3000 *	4045 *	3000	3000
Molar Flow	(kgmole/h)	8195 *	1.333e+004	5659 *	1.850e+004	0.0000
Mass Flow	(kg/h)	1.380e+005	2.304e+005	1.020e+005	3.324e+005	0.0000
Std Ideal Liq Vol Flow	(m3/h)	448.7	649.8	102.2	762.1	0.0000
Heat Flow	(kJ/h)	-6.153e+008	-8.919e+008	-1.335e+009	-2.227e+009	0.0000
Molar Enthalpy	(kJ/kgmole)	-7.508e+004	-6.691e+004	-2.359e+005	-1.204e+005	-1.204e+005

Name		7	6	8	10	11
Vapour Fraction		1.0000	1.0000	1.0000	0.0000 *	1.0000 *
Temperature	(C)	200.0 *	675.0 *	979.3	20.00 *	252.0 *
Pressure	(kPa)	3000 *	3000 *	3000	2.289	4045
Molar Flow	(kgmole/h)	4850 *	1.850e+004	3.570e+004	2.781e+004	2.781e+004
Mass Flow	(kg/h)	1.552e+005	3.324e+005	4.876e+005	5.010e+005	5.010e+005
Std Ideal Liq Vol Flow	(m3/h)	136.4	762.1	1093	502.0	502.0
Heat Flow	(kJ/h)	2.500e+007	-2.077e+009	-2.052e+009	-7.970e+009	-6.560e+009
Molar Enthalpy	(kJ/kgmole)	5154	-1.123e+005	-5.747e+004	-2.866e+005	-2.359e+005

Name		9	13	12	15	16
Vapour Fraction		0.8317	1.0000	0.0000	1.0000	0.9972
Temperature	(C)	38.00 *	38.00	38.00	210.0 *	221.8
Pressure	(kPa)	3000	3000	3000	2000 *	1940
Molar Flow	(kgmole/h)	3.570e+004	2.969e+004	6010	4.656e+004	3.423e+004
Mass Flow	(kg/h)	4.876e+005	3.792e+005	1.084e+005	6.829e+005	6.829e+005
Std Ideal Liq Vol Flow	(m3/h)	1093	984.6	108.6	1645	1291
Heat Flow	(kJ/h)	-3.462e+009	-1.747e+009	-1.714e+009	-3.224e+009	-4.230e+009
Molar Enthalpy	(kJ/kgmole)	-9.696e+004	-5.885e+004	-2.852e+005	-6.923e+004	-1.236e+005

Name		24	23	22	19	18
Vapour Fraction		1.0000	0.0000	0.0000	0.0000 *	0.8085
Temperature	(C)	46.60	46.60	46.60	25.00 *	38.00 *
Pressure	(kPa)	1940	1940	1940	3.110	2000 *
Molar Flow	(kgmole/h)	2.767e+004	369.0	6187	1.041e+004	3.413e+004
Mass Flow	(kg/h)	4.978e+005	7.350e+004	1.116e+005	1.876e+005	6.481e+005
Std Ideal Liq Vol Flow	(m3/h)	1084	95.80	111.9	188.0	1248
Heat Flow	(kJ/h)	-2.837e+009	-1.485e+008	-1.761e+009	-2.980e+009	-4.696e+009
Molar Enthalpy	(kJ/kgmole)	-1.025e+005	-4.024e+005	-2.846e+005	-2.862e+005	-1.376e+005

Name		20	26	25	17	21
Vapour Fraction		1.0000 *	1.0000	1.0000	1.0000	0.0000
Temperature	(C)	200.0 *	46.60	46.60	221.8	221.8
Pressure	(kPa)	1544	1940	1940	1940	1940
Molar Flow	(kgmole/h)	1.041e+004	2.214e+004	5534	3.413e+004	97.23
Mass Flow	(kg/h)	1.876e+005	3.983e+005	9.957e+004	6.481e+005	3.487e+004
Std Ideal Liq Vol Flow	(m3/h)	188.0	867.0	216.8	1248	43.27
Heat Flow	(kJ/h)	-2.464e+009	-2.270e+009	-5.674e+008	-4.180e+009	-5.002e+007
Molar Enthalpy	(kJ/kgmole)	-2.366e+005	-1.025e+005	-1.025e+005	-1.225e+005	-5.144e+005

Name		27	29	28	14	R-1
Vapour Fraction		1.0000	1.0000	1.0000	1.0000	1.0000
Temperature	(C)	95.48	95.48	95.48	60.53	60.47 *
Pressure	(kPa)	3000 *	3000	3000	3000	3000 *
Molar Flow	(kgmole/h)	2.214e+004	5136	1.700e+004	4.669e+004	4.656e+004 *
Mass Flow	(kg/h)	3.983e+005	9.240e+004	3.059e+005	6.851e+005	6.829e+005
Std Ideal Liq Vol Flow	(m3/h)	867.0	201.1	665.9	1650	1645
Heat Flow	(kJ/h)	-2.234e+009	-5.182e+008	-1.715e+009	-3.463e+009	-3.450e+009
Molar Enthalpy	(kJ/kgmole)	-1.009e+005	-1.009e+005	-1.009e+005	-7.416e+004	-7.410e+004

Workbook: Case (Main) (continued)

Streams (continued)

Fluid Pkg: All

Name		2	Q-01	Q-02	Q-03	30
Vapour Fraction		1.0000	---	---	---	---
Temperature	(C)	58.64	---	---	---	---
Pressure	(kPa)	3000	---	---	---	---
Molar Flow	(kgmole/h)	1.333e+004	---	---	---	---
Mass Flow	(kg/h)	2.304e+005	---	---	---	---
Std Ideal Liq Vol Flow	(m3/h)	649.8	---	---	---	---
Heat Flow	(kJ/h)	-1.133e+009	2.415e+008	1.503e+008	2.268e+008	1.006e+009
Molar Enthalpy	(kJ/kgmole)	-8.503e+004	---	---	---	---

Name		Q-C-100
Vapour Fraction		---
Temperature	(C)	---
Pressure	(kPa)	---
Molar Flow	(kgmole/h)	---
Mass Flow	(kg/h)	---
Std Ideal Liq Vol Flow	(m3/h)	---
Heat Flow	(kJ/h)	3.591e+007
Molar Enthalpy	(kJ/kgmole)	---

Unit Ops

Operation Name	Operation Type	Feeds	Products	Ignored	Calc Level
H-01	Heater	2 Q-01	3	No	500.0 *
H-02	Heater	5 Q-02	6	No	500.0 *
H-03	Heater	R-1 Q-03	15	No	500.0 *
ERV-100	Equilibrium Reactor	3 4	Dummy 5	No	500.0 *
ERV-101	Equilibrium Reactor	7 6	Dummy-2 8	No	500.0 *
E-100	Heat Exchanger	8 10	9 11	No	500.0 *
E-101	Heat Exchanger	17 19	18 20	No	500.0 *
V-100	Separator	9	12 13	No	500.0 *
V-101	Separator	16	21 17	No	500.0 *
R-100	Plug Flow Reactor	15	16 30	No	500.0 *
H2/CO	Spreadsheet			No	500.0 *
Steam/NG	Spreadsheet			No	500.0 *
O2/NG	Spreadsheet			No	500.0 *
TE	Spreadsheet			No	500.0 *
CE	Spreadsheet			No	500.0 *
V-102	3 Phase Separator	21 18	24 23 22	No	500.0 *
TEE-100	Tee	24	26 25	No	500.0 *
TEE-101	Tee	27	29 28	No	500.0 *
C-100	Compressor	26 Q-C-100	27	No	500.0 *
MIX-100	Mixer	13 28	14	No	500.0 *
MIX-101	Mixer	1 29	2	No	500.0 *
RCY-1	Recycle	14	R-1	No	3500 *

Workbook: Case (Main)

STATUS

OK

Streams

Fluid Pkg: All

Name		1	3	4	5	Dummy
Vapour Fraction		1.0000 *	1.0000	1.0000	1.0000	0.0000
Temperature	(C)	40.00 *	455.0 *	252.0 *	379.4	379.4
Pressure	(kPa)	3000 *	3000 *	4045 *	3000	3000
Molar Flow	(kgmole/h)	8195 *	1.037e+004	8257 *	1.909e+004	0.0000
Mass Flow	(kg/h)	1.380e+005	2.171e+005	1.488e+005	3.658e+005	0.0000
Std Ideal Liq Vol Flow	(m3/h)	448.7	565.4	149.1	737.8	0.0000
Heat Flow	(kJ/h)	-6.153e+008	-9.928e+008	-1.948e+009	-2.941e+009	0.0000
Molar Enthalpy	(kJ/kgmole)	-7.508e+004	-9.578e+004	-2.359e+005	-1.541e+005	-1.541e+005

Name		7	6	8	10	11
Vapour Fraction		1.0000	1.0000	1.0000	0.0000 *	1.0000 *
Temperature	(C)	200.0 *	675.0 *	1030	20.00 *	252.0 *
Pressure	(kPa)	3000 *	3000 *	3000	2.289	4045
Molar Flow	(kgmole/h)	5089 *	1.909e+004	3.672e+004	3.181e+004	3.181e+004
Mass Flow	(kg/h)	1.629e+005	3.658e+005	5.287e+005	5.730e+005	5.730e+005
Std Ideal Liq Vol Flow	(m3/h)	143.2	737.8	1084	574.2	574.2
Heat Flow	(kJ/h)	2.623e+007	-2.646e+009	-2.620e+009	-9.116e+009	-7.504e+009
Molar Enthalpy	(kJ/kgmole)	5154	-1.387e+005	-7.135e+004	-2.866e+005	-2.359e+005

Name		9	13	12	15	16
Vapour Fraction		0.7709	1.0000	0.0000	1.0000	0.9894
Temperature	(C)	38.00 *	38.00	38.00	210.0 *	223.8
Pressure	(kPa)	3000	3000	3000	2000 *	1940
Molar Flow	(kgmole/h)	3.672e+004	2.831e+004	8414	3.174e+004	1.559e+004
Mass Flow	(kg/h)	5.287e+005	3.770e+005	1.517e+005	4.997e+005	4.997e+005
Std Ideal Liq Vol Flow	(m3/h)	1084	932.2	152.1	1115	651.4
Heat Flow	(kJ/h)	-4.233e+009	-1.833e+009	-2.400e+009	-2.575e+009	-3.906e+009
Molar Enthalpy	(kJ/kgmole)	-1.153e+005	-6.474e+004	-2.852e+005	-8.114e+004	-2.506e+005

Name		24	43	22	19	18
Vapour Fraction		1.0000	0.0000	0.0000	0.0000 *	0.4423
Temperature	(C)	38.00	38.00	38.00	25.00 *	38.00 *
Pressure	(kPa)	2000	2000	2000	3.110	2000 *
Molar Flow	(kgmole/h)	6822	439.1	8162	9996	1.542e+004
Mass Flow	(kg/h)	2.485e+005	5.064e+004	1.479e+005	1.801e+005	4.471e+005
Std Ideal Liq Vol Flow	(m3/h)	367.0	70.21	148.5	180.4	585.7
Heat Flow	(kJ/h)	-1.867e+009	-1.260e+008	-2.331e+009	-2.861e+009	-4.324e+009
Molar Enthalpy	(kJ/kgmole)	-2.737e+005	-2.870e+005	-2.856e+005	-2.862e+005	-2.804e+005

Name		20	26	25	17	21
Vapour Fraction		1.0000 *	1.0000	1.0000	1.0000	0.0000
Temperature	(C)	200.0 *	38.00	38.00	223.8	223.8
Pressure	(kPa)	1544	2000	2000	1940	1940
Molar Flow	(kgmole/h)	9996	5528	1294	1.542e+004	165.3
Mass Flow	(kg/h)	1.801e+005	2.014e+005	4.716e+004	4.471e+005	5.262e+004
Std Ideal Liq Vol Flow	(m3/h)	180.4	297.4	69.63	585.7	65.61
Heat Flow	(kJ/h)	-2.365e+009	-1.513e+009	-3.542e+008	-3.829e+009	-7.778e+007
Molar Enthalpy	(kJ/kgmole)	-2.366e+005	-2.737e+005	-2.737e+005	-2.482e+005	-4.707e+005

Name		27	29	28	14	R-1
Vapour Fraction		1.0000	1.0000	1.0000	1.0000	1.0000
Temperature	(C)	74.76	74.76	74.76	42.20	42.20 *
Pressure	(kPa)	3000 *	3000	3000	3000	3000 *
Molar Flow	(kgmole/h)	5528	2170	3358	3.167e+004	3.174e+004 *
Mass Flow	(kg/h)	2.014e+005	7.906e+004	1.223e+005	4.993e+005	4.997e+005
Std Ideal Liq Vol Flow	(m3/h)	297.4	116.7	180.6	1113	1115
Heat Flow	(kJ/h)	-1.505e+009	-5.910e+008	-9.144e+008	-2.747e+009	-2.747e+009
Molar Enthalpy	(kJ/kgmole)	-2.723e+005	-2.723e+005	-2.723e+005	-8.675e+004	-8.654e+004

Workbook: Case (Main) (continued)

Streams (continued)

Fluid Pkg: All

Name		2	23	Q-H-01	Q-H-02	Q-H-03
Vapour Fraction		1.0000	0.0886	---	---	---
Temperature	(C)	47.38	138.9	---	---	---
Pressure	(kPa)	3000	1940	---	---	---
Molar Flow	(kgmole/h)	1.037e+004	604.3	---	---	---
Mass Flow	(kg/h)	2.171e+005	1.033e+005	---	---	---
Std Ideal Liq Vol Flow	(m3/h)	565.4	135.8	---	---	---
Heat Flow	(kJ/h)	-1.206e+009	-2.038e+008	2.135e+008	2.944e+008	1.716e+008
Molar Enthalpy	(kJ/kgmole)	-1.164e+005	-3.372e+005	---	---	---

Name		31	Q-C-100
Vapour Fraction		---	---
Temperature	(C)	---	---
Pressure	(kPa)	---	---
Molar Flow	(kgmole/h)	---	---
Mass Flow	(kg/h)	---	---
Std Ideal Liq Vol Flow	(m3/h)	---	---
Heat Flow	(kJ/h)	1.331e+009	7.448e+006
Molar Enthalpy	(kJ/kgmole)	---	---

Unit Ops

Operation Name	Operation Type	Feeds	Products	Ignored	Calc Level
H-01	Heater	2 Q-H-01	3	No	500.0 *
H-02	Heater	5 Q-H-02	6	No	500.0 *
H-03	Heater	R-1 Q-H-03	15	No	500.0 *
ERV-100	Equilibrium Reactor	3 4	Dummy 5	No	500.0 *
ERV-101	Equilibrium Reactor	7 6	Dummy-2 8	No	500.0 *
E-100	Heat Exchanger	8 10	9 11	No	500.0 *
E-101	Heat Exchanger	17 19	18 20	No	500.0 *
Sep-1	Separator	9	12 13	No	500.0 *
Sep-2	Separator	16	21 17	No	500.0 *
R-100	Plug Flow Reactor	15	16 31	No	500.0 *
H2/CO ratio	Spreadsheet			No	500.0 *
Steam/NG	Spreadsheet			No	500.0 *
Oxygen/NG	Spreadsheet			No	500.0 *
OptimizerSpreadsheet	Spreadsheet			No	500.0 *
CE	Spreadsheet			No	500.0 *
TE	Spreadsheet			No	500.0 *
V-102	3 Phase Separator	18	24 43 22	No	500.0 *
SPLIT-1	Tee	24	26 25	No	500.0 *
TEE-100	Tee	27	29 28	No	500.0 *
C-100	Compressor	26 Q-C-100	27	No	500.0 *
MIX-100	Mixer	13 28	14	No	500.0 *
MIX-101	Mixer	1 29	2	No	500.0 *

Workbook: Case (Main) (continued)

Unit Ops (continued)

Operation Name	Operation Type	Feeds	Products	Ignored	Calc Level
MIX-102	Mixer	21 43	23	No	500.0 *
RCY-1	Recycle	14	R-1	No	3500 *
ADJ-1	Adjust			No	3500 *

Workbook: Case (Main)

STATUS

OK

Streams

Fluid Pkg: All

Name		1	4	5	Dummy	37
Vapour Fraction		1.0000 *	1.0000	1.0000	0.0000	1.0000
Temperature	(C)	40.00 *	255.6 *	381.7	381.7	200.0 *
Pressure	(kPa)	3000 *	3000 *	3000	3000	3000 *
Molar Flow	(kgmole/h)	8195 *	9000 *	2.003e+004	0.0000	5130 *
Mass Flow	(kg/h)	1.380e+005	1.621e+005	3.874e+005	0.0000	1.642e+005
Std Ideal Liq Vol Flow	(m3/h)	448.7	162.5	761.8	0.0000	144.3
Heat Flow	(kJ/h)	-6.153e+008	-2.117e+009	-3.174e+009	0.0000	2.644e+007
Molar Enthalpy	(kJ/kgmole)	-7.508e+004	-2.352e+005	-1.585e+005	-1.585e+005	5154

Name		6	8	13	12	15
Vapour Fraction		1.0000	1.0000	1.0000	0.0000	1.0000
Temperature	(C)	675.0 *	1029	38.00	38.00	210.0 *
Pressure	(kPa)	3000	3000	3000	3000	2000 *
Molar Flow	(kgmole/h)	2.003e+004	3.771e+004	2.854e+004	9175	3.176e+004
Mass Flow	(kg/h)	3.874e+005	5.516e+005	3.861e+005	1.655e+005	5.055e+005
Std Ideal Liq Vol Flow	(m3/h)	761.8	1109	943.2	165.9	1116
Heat Flow	(kJ/h)	-2.870e+009	-2.843e+009	-1.911e+009	-2.617e+009	-2.639e+009
Molar Enthalpy	(kJ/kgmole)	-1.433e+005	-7.540e+004	-6.697e+004	-2.852e+005	-8.308e+004

Name		16	24	43	22	18
Vapour Fraction		0.9895	1.0000	0.0000	0.0000	0.4447
Temperature	(C)	223.8	38.00	38.00	38.00	38.00 *
Pressure	(kPa)	1940	1940	1940	1940	1940
Molar Flow	(kgmole/h)	1.563e+004	6876	434.7	8153	1.546e+004
Mass Flow	(kg/h)	5.055e+005	2.548e+005	5.044e+004	1.478e+005	4.530e+005
Std Ideal Liq Vol Flow	(m3/h)	653.0	369.3	69.84	148.4	587.5
Heat Flow	(kJ/h)	-3.969e+009	-1.932e+009	-1.255e+008	-2.329e+009	-4.386e+009
Molar Enthalpy	(kJ/kgmole)	-2.539e+005	-2.810e+005	-2.887e+005	-2.856e+005	-2.837e+005

Name		26	25	17	21	27
Vapour Fraction		1.0000	1.0000	1.0000	0.0000	1.0000
Temperature	(C)	38.00	38.00	223.8	223.8	77.61
Pressure	(kPa)	1940	1940	1940	1940	3000 *
Molar Flow	(kgmole/h)	5572	1305	1.546e+004	164.9	5572
Mass Flow	(kg/h)	2.064e+005	4.834e+004	4.530e+005	5.253e+004	2.064e+005
Std Ideal Liq Vol Flow	(m3/h)	299.2	70.07	587.5	65.49	299.2
Heat Flow	(kJ/h)	-1.566e+009	-3.666e+008	-3.891e+009	-7.767e+007	-1.557e+009
Molar Enthalpy	(kJ/kgmole)	-2.810e+005	-2.810e+005	-2.516e+005	-4.711e+005	-2.795e+005

Name		29	28	14	R-1	2
Vapour Fraction		1.0000	1.0000	1.0000	1.0000	1.0000
Temperature	(C)	77.61	77.61	42.42	42.44 *	48.53
Pressure	(kPa)	3000	3000	3000	3000 *	3000
Molar Flow	(kgmole/h)	2355	3217	3.175e+004	3.176e+004 *	1.055e+004
Mass Flow	(kg/h)	8.723e+004	1.192e+005	5.053e+005	5.055e+005	2.253e+005
Std Ideal Liq Vol Flow	(m3/h)	126.5	172.8	1116	1116	575.1
Heat Flow	(kJ/h)	-6.582e+008	-8.993e+008	-2.810e+009	-2.810e+009	-1.273e+009
Molar Enthalpy	(kJ/kgmole)	-2.795e+005	-2.795e+005	-8.851e+004	-8.848e+004	-1.207e+005

Name		23	32	33	3	34
Vapour Fraction		0.0849	1.0000	1.0000	1.0000	1.0000
Temperature	(C)	139.1	811.8	651.9	455.0 *	521.8
Pressure	(kPa)	1940	3000	3000	3000	3000
Molar Flow	(kgmole/h)	599.6	3.771e+004	3.771e+004	1.055e+004	3.771e+004
Mass Flow	(kg/h)	1.030e+005	5.516e+005	5.516e+005	2.253e+005	5.516e+005
Std Ideal Liq Vol Flow	(m3/h)	135.3	1109	1109	575.1	1109
Heat Flow	(kJ/h)	-2.032e+008	-3.147e+009	-3.364e+009	-1.057e+009	-3.536e+009
Molar Enthalpy	(kJ/kgmole)	-3.388e+005	-8.346e+004	-8.920e+004	-1.002e+005	-9.375e+004

Workbook: Case (Main) (continued)

Streams (continued)

Fluid Pkg: All

Name		4-0	41	40	42	7
Vapour Fraction		1.0000	1.0000	1.0000	0.8956	1.0000
Temperature	(C)	257.0	223.0	223.0	99.59	20.00 *
Pressure	(kPa)	3000 *	2429	2429	100.0 *	3000 *
Molar Flow	(kgmole/h)	9000 *	9000	3.112e+004	3.112e+004	5130
Mass Flow	(kg/h)	1.621e+005	1.621e+005	5.607e+005	5.607e+005	1.642e+005
Std Ideal Liq Vol Flow	(m3/h)	162.5	162.5	561.8	561.8	144.3
Heat Flow	(kJ/h)	-2.116e+009	-2.126e+009	-7.352e+009	-7.583e+009	-2.215e+006
Molar Enthalpy	(kJ/kgmole)	-2.352e+005	-2.362e+005	-2.362e+005	-2.436e+005	-431.8

Name		R-2	35	10	9	19
Vapour Fraction		1.0000	1.0000	0.0000	0.7567	0.0000
Temperature	(C)	200.0 *	499.8	20.00 *	38.00 *	20.00 *
Pressure	(kPa)	3000	3000	101.3 *	3000	101.3 *
Molar Flow	(kgmole/h)	5130	3.771e+004	1.000e+007 *	3.771e+004	1.000e+007 *
Mass Flow	(kg/h)	1.642e+005	5.516e+005	1.802e+008	5.516e+005	1.802e+008
Std Ideal Liq Vol Flow	(m3/h)	144.3	1109	1.805e+005	1109	1.805e+005
Heat Flow	(kJ/h)	2.644e+007	-3.564e+009	-2.866e+012	-4.528e+009	-2.866e+012
Molar Enthalpy	(kJ/kgmole)	5154	-9.451e+004	-2.866e+005	-1.201e+005	-2.866e+005

Name		20	11	38	30	39
Vapour Fraction		0.0000	0.0000	0.0000	0.0000 *	1.0000 *
Temperature	(C)	20.64	20.38	20.00 *	20.20	223.0 *
Pressure	(kPa)	101.3	101.3	101.3 *	2466 *	2429
Molar Flow	(kgmole/h)	1.000e+007	1.000e+007	4.012e+004	4.012e+004	4.012e+004
Mass Flow	(kg/h)	1.802e+008	1.802e+008	7.228e+005	7.228e+005	7.228e+005
Std Ideal Liq Vol Flow	(m3/h)	1.805e+005	1.805e+005	724.3	724.3	724.3
Heat Flow	(kJ/h)	-2.866e+012	-2.866e+012	-1.150e+010	-1.150e+010	-9.478e+009
Molar Enthalpy	(kJ/kgmole)	-2.866e+005	-2.866e+005	-2.866e+005	-2.866e+005	-2.362e+005

Name		36	31-0	31	Q-C-100	Q-C-101
Vapour Fraction		0.8545	0.0000 *	---	---	---
Temperature	(C)	135.2	223.8 *	---	---	---
Pressure	(kPa)	3000	2466	---	---	---
Molar Flow	(kgmole/h)	3.771e+004	4.012e+004	---	---	---
Mass Flow	(kg/h)	5.516e+005	7.228e+005	---	---	---
Std Ideal Liq Vol Flow	(m3/h)	1109	724.3	---	---	---
Heat Flow	(kJ/h)	-4.232e+009	-1.083e+010	1.330e+009	8.104e+006	9.609e+006
Molar Enthalpy	(kJ/kgmole)	-1.122e+005	-2.699e+005	---	---	---

Name		Q-T-100	P-1
Vapour Fraction		---	---
Temperature	(C)	---	---
Pressure	(kPa)	---	---
Molar Flow	(kgmole/h)	---	---
Mass Flow	(kg/h)	---	---
Std Ideal Liq Vol Flow	(m3/h)	---	---
Heat Flow	(kJ/h)	2.309e+008	2.254e+006
Molar Enthalpy	(kJ/kgmole)	---	---

Unit Ops

Operation Name	Operation Type	Feeds	Products	Ignored	Calc Level
ERV-100	Equilibrium Reactor	4 3	Dummy 5	No	500.0 *
ERV-101	Equilibrium Reactor	37 6	Dummy-2 8	No	500.0 *
E-100	Heat Exchanger	5 8	6 32	No	500.0 *
E-102	Heat Exchanger	R-1 33	15 34	No	500.0 *
E-101	Heat Exchanger	2 32	3 33	No	500.0 *
E-103	Heat Exchanger	7 34	R-2 35	No	500.0 *

Workbook: Case (Main) (continued)

Unit Ops (continued)

Operation Name	Operation Type	Feeds	Products	Ignored	Calc Level
E-105	Heat Exchanger	36 10	9 11	No	500.0 *
E-106	Heat Exchanger	17 19	18 20	No	500.0 *
E-104	Heat Exchanger	30 35	31-0 36	No	500.0 *
V-100	Separator	9	12 13	No	500.0 *
V-101	Separator	16	21 17	No	500.0 *
R-100	Plug Flow Reactor	15	16 31	No	500.0 *
H2/CO ratio	Spreadsheet			No	500.0 *
Steam/NG	Spreadsheet			No	500.0 *
Oxygen/NG	Spreadsheet			No	500.0 *
OptimizerSpreadsheet	Spreadsheet			No	500.0 *
CE	Spreadsheet			No	500.0 *
TE	Spreadsheet			No	500.0 *
Area - E-102	Spreadsheet			No	500.0 *
Area - E-103	Spreadsheet			No	500.0 *
HX-area	Spreadsheet			No	500.0 *
Economics	Spreadsheet			No	500.0 *
Area - E-101	Spreadsheet			No	500.0 *
Area - E-100	Spreadsheet			No	500.0 *
Area - E-106	Spreadsheet			No	500.0 *
Volume Pre-reformer	Spreadsheet			No	500.0 *
Volume ATR	Spreadsheet			No	500.0 *
Energy efficiency	Spreadsheet			No	500.0 *
Area - E-105	Spreadsheet			No	500.0 *
Area - E-104	Spreadsheet			No	500.0 *
Waterflow	Spreadsheet			No	500.0 *
SPRDSHT-1	Spreadsheet			No	500.0 *
V-102	3 Phase Separator	18	24 43 22	No	500.0 *
TEE-101	Tee	24	26 25	No	500.0 *
TEE-100	Tee	27	29 28	No	500.0 *
TEE-102	Tee	39	41 40	No	500.0 *
C-100	Compressor	26 Q-C-100	27	No	500.0 *
C-101	Compressor	41 Q-C-101	4-0	No	500.0 *
MIX-100	Mixer	13 28	14	No	500.0 *
MIX-101	Mixer	1 29	2	No	500.0 *
MIX-102	Mixer	43 21	23	No	500.0 *
RCY-1	Recycle	14	R-1	No	3500 *
RCY-2	Recycle	R-2	37	No	3500 *
ADJ-1	Adjust			No	3500 *
T-100	Expander	40	42 Q-T-100	No	500.0 *
SET-2	Set			No	500.0 *
SET-1	Set			No	500.0 *
SET-3	Set			No	500.0 *

Workbook: Case (Main) (continued)

Unit Ops (continued)

Operation Name	Operation Type	Feeds	Products	Ignored	Calc Level
P-100	Pump	38 P-1	30	No	500.0 *

Workbook: Case (Main)

STATUS

OK

Streams

Fluid Pkg: All

Name		1	4	5	7	6
Vapour Fraction		1.0000 *	1.0000	1.0000	1.0000	1.0000
Temperature	(C)	40.00 *	255.6 *	406.9	200.0 *	675.0 *
Pressure	(kPa)	3000 *	3000 *	3000	3000 *	3000
Molar Flow	(kgmole/h)	8195 *	5916 *	1.611e+004	4847 *	1.611e+004
Mass Flow	(kg/h)	1.380e+005	1.066e+005	2.914e+005	1.551e+005	2.914e+005
Std Ideal Liq Vol Flow	(m3/h)	448.7	106.8	655.7	136.3	655.7
Heat Flow	(kJ/h)	-6.153e+008	-1.392e+009	-2.129e+009	2.498e+007	-1.895e+009
Molar Enthalpy	(kJ/kgmole)	-7.508e+004	-2.352e+005	-1.322e+005	5154	-1.177e+005

Name		8	13	12	15	16
Vapour Fraction		1.0000	1.0000	0.0000	1.0000	0.9895
Temperature	(C)	1028	38.00	38.00	210.0 *	224.9
Pressure	(kPa)	3000	3000	3000	2000 *	1940
Molar Flow	(kgmole/h)	3.322e+004	2.728e+004	5933	3.009e+004	1.476e+004
Mass Flow	(kg/h)	4.465e+005	3.396e+005	1.070e+005	4.204e+005	4.204e+005
Std Ideal Liq Vol Flow	(m3/h)	994.8	887.6	107.2	1027	587.3
Heat Flow	(kJ/h)	-1.870e+009	-1.543e+009	-1.692e+009	-1.943e+009	-3.207e+009
Molar Enthalpy	(kJ/kgmole)	-5.631e+004	-5.656e+004	-2.852e+005	-6.459e+004	-2.173e+005

Name		24	43	22	18	26
Vapour Fraction		1.0000	0.0000	0.0000	0.4444	1.0000
Temperature	(C)	38.00	38.00	38.00	38.00 *	38.00
Pressure	(kPa)	1940	1940	1940	1940	1940
Molar Flow	(kgmole/h)	6490	381.1	7735	1.461e+004	4480
Mass Flow	(kg/h)	1.848e+005	4.610e+004	1.399e+005	3.708e+005	1.276e+005
Std Ideal Liq Vol Flow	(m3/h)	321.2	63.94	140.4	525.5	221.7
Heat Flow	(kJ/h)	-1.285e+009	-1.078e+008	-2.208e+009	-3.601e+009	-8.871e+008
Molar Enthalpy	(kJ/kgmole)	-1.980e+005	-2.829e+005	-2.855e+005	-2.465e+005	-1.980e+005

Name		25	17	21	27	29
Vapour Fraction		1.0000	1.0000	0.0000	1.0000	1.0000
Temperature	(C)	38.00	224.9	224.9	79.41	79.41
Pressure	(kPa)	1940	1940	1940	3000 *	3000
Molar Flow	(kgmole/h)	2010	1.461e+004	154.8	4480	1643
Mass Flow	(kg/h)	5.724e+004	3.708e+005	4.961e+004	1.276e+005	4.679e+004
Std Ideal Liq Vol Flow	(m3/h)	99.47	525.5	61.86	221.7	81.31
Heat Flow	(kJ/h)	-3.980e+008	-3.134e+009	-7.272e+007	-8.804e+008	-3.229e+008
Molar Enthalpy	(kJ/kgmole)	-1.980e+005	-2.146e+005	-4.697e+005	-1.965e+005	-1.965e+005

Name		28	14	R-1	2	23
Vapour Fraction		1.0000	1.0000	1.0000	1.0000	0.0490
Temperature	(C)	79.41	42.55	42.53 *	46.55	141.6
Pressure	(kPa)	3000	3000	3000 *	3000	1940
Molar Flow	(kgmole/h)	2837	3.012e+004	3.009e+004 *	9838	536.0
Mass Flow	(kg/h)	8.080e+004	4.203e+005	4.204e+005	1.848e+005	9.571e+004
Std Ideal Liq Vol Flow	(m3/h)	140.4	1028	1027	530.0	125.8
Heat Flow	(kJ/h)	-5.575e+008	-2.101e+009	-2.102e+009	-9.381e+008	-1.805e+008
Molar Enthalpy	(kJ/kgmole)	-1.965e+005	-6.974e+004	-6.986e+004	-9.536e+004	-3.369e+005

Name		32	33	3	34	4-0
Vapour Fraction		1.0000	1.0000	1.0000	1.0000	1.0000
Temperature	(C)	833.8	662.0	455.0 *	522.1	257.0
Pressure	(kPa)	3000	3000	3000	3000	3000 *
Molar Flow	(kgmole/h)	3.322e+004	3.322e+004	9838	3.322e+004	9000 *
Mass Flow	(kg/h)	4.465e+005	4.465e+005	1.848e+005	4.465e+005	1.621e+005
Std Ideal Liq Vol Flow	(m3/h)	994.8	994.8	530.0	994.8	162.5
Heat Flow	(kJ/h)	-2.104e+009	-2.305e+009	-7.374e+008	-2.464e+009	-2.116e+009
Molar Enthalpy	(kJ/kgmole)	-6.334e+004	-6.938e+004	-7.495e+004	-7.416e+004	-2.352e+005

Workbook: Case (Main) (continued)

Streams (continued)

Fluid Pkg: All

Name	41	40	42	ASU	R-2
Vapour Fraction	1.0000	1.0000	0.8956	1.0000	1.0000
Temperature (C)	223.0	223.0	99.59	20.00 *	200.0 *
Pressure (kPa)	2429	2429	100.0 *	3000 *	3000
Molar Flow (kgmole/h)	9000	3.112e+004	3.112e+004	4847	4847
Mass Flow (kg/h)	1.621e+005	5.607e+005	5.607e+005	1.551e+005	1.551e+005
Std Ideal Liq Vol Flow (m3/h)	162.5	561.8	561.8	136.3	136.3
Heat Flow (kJ/h)	-2.126e+009	-7.352e+009	-7.583e+009	-2.093e+006	2.498e+007
Molar Enthalpy (kJ/kgmole)	-2.362e+005	-2.362e+005	-2.436e+005	-431.8	5154

Name	35	10	9	19	20
Vapour Fraction	1.0000	0.0000	0.8214	0.0000	0.0000
Temperature (C)	497.9	20.00 *	38.00 *	20.00 *	20.60
Pressure (kPa)	3000	101.3 *	3000	101.3 *	101.3
Molar Flow (kgmole/h)	3.322e+004	1.000e+007 *	3.322e+004	1.000e+007 *	1.000e+007
Mass Flow (kg/h)	4.465e+005	1.802e+008	4.465e+005	1.802e+008	1.802e+008
Std Ideal Liq Vol Flow (m3/h)	994.8	1.805e+005	994.8	1.805e+005	1.805e+005
Heat Flow (kJ/h)	-2.491e+009	-2.866e+012	-3.235e+009	-2.866e+012	-2.866e+012
Molar Enthalpy (kJ/kgmole)	-7.498e+004	-2.866e+005	-9.740e+004	-2.866e+005	-2.866e+005

Name	11	38	30	39	36
Vapour Fraction	0.0000	0.0000	0.0000 *	1.0000 *	0.8479
Temperature (C)	20.14	20.00 *	20.20	223.0 *	96.41
Pressure (kPa)	101.3	101.3 *	2466 *	2429	3000
Molar Flow (kgmole/h)	1.000e+007	3.813e+004	3.813e+004	4.012e+004 *	3.322e+004
Mass Flow (kg/h)	1.802e+008	6.868e+005	6.868e+005	7.228e+005	4.465e+005
Std Ideal Liq Vol Flow (m3/h)	1.805e+005	688.2	688.2	724.3	994.8
Heat Flow (kJ/h)	-2.866e+012	-1.093e+010	-1.093e+010	-9.478e+009	-3.125e+009
Molar Enthalpy (kJ/kgmole)	-2.866e+005	-2.866e+005	-2.866e+005	-2.362e+005	-9.407e+004

Name	31-0	31	Q-C-100	Q-C-101	Q-T-100
Vapour Fraction	0.0000 *	---	---	---	---
Temperature (C)	223.8 *	---	---	---	---
Pressure (kPa)	2466	---	---	---	---
Molar Flow (kgmole/h)	3.813e+004	---	---	---	---
Mass Flow (kg/h)	6.868e+005	---	---	---	---
Std Ideal Liq Vol Flow (m3/h)	688.2	---	---	---	---
Heat Flow (kJ/h)	-1.029e+010	1.264e+009	6.758e+006	9.609e+006	2.309e+008
Molar Enthalpy (kJ/kgmole)	-2.699e+005	---	---	---	---

Name	P1
Vapour Fraction	---
Temperature (C)	---
Pressure (kPa)	---
Molar Flow (kgmole/h)	---
Mass Flow (kg/h)	---
Std Ideal Liq Vol Flow (m3/h)	---
Heat Flow (kJ/h)	2.142e+006
Molar Enthalpy (kJ/kgmole)	---

Unit Ops

Operation Name	Operation Type	Feeds	Products	Ignored	Calc Level
ERV-100	Equilibrium Reactor	4 3	Dummy 5	No	500.0 *
ERV-101	Equilibrium Reactor	7 6	Dummy-2 8	No	500.0 *
E-100	Heat Exchanger	5 8	6 32	No	500.0 *
E-102	Heat Exchanger	R-1 33	15 34	No	500.0 *
E-101	Heat Exchanger	2 32	3 33	No	500.0 *
E-103	Heat Exchanger	ASU 34	R-2 35	No	500.0 *

Workbook: Case (Main) (continued)

Unit Ops (continued)

Operation Name	Operation Type	Feeds	Products	Ignored	Calc Level
E-105	Heat Exchanger	36 10	9 11	No	500.0 *
E-106	Heat Exchanger	17 19	18 20	No	500.0 *
E-104	Heat Exchanger	30 35	31-0 36	No	500.0 *
V-100	Separator	9	12 13	No	500.0 *
V-101	Separator	16	21 17	No	500.0 *
R-100	Plug Flow Reactor	15	16 31	No	500.0 *
H2/CO ratio	Spreadsheet			No	500.0 *
Steam/NG	Spreadsheet			No	500.0 *
Oxygen/NG	Spreadsheet			No	500.0 *
OptimizerSpreadsheet	Spreadsheet			No	500.0 *
CE	Spreadsheet			No	500.0 *
TE	Spreadsheet			No	500.0 *
Area - E-102	Spreadsheet			No	500.0 *
Area - E-103	Spreadsheet			No	500.0 *
HX-area	Spreadsheet			No	500.0 *
Economics	Spreadsheet			No	500.0 *
Area - E-101	Spreadsheet			No	500.0 *
Area - E-100	Spreadsheet			No	500.0 *
Area - E-106	Spreadsheet			No	500.0 *
Volume Pre-reformer	Spreadsheet			No	500.0 *
Volume ATR	Spreadsheet			No	500.0 *
Energy efficiency	Spreadsheet			No	500.0 *
Area - E-105	Spreadsheet			No	500.0 *
Area - E-104	Spreadsheet			No	500.0 *
Waterflow	Spreadsheet			No	500.0 *
SPRDSHT-1	Spreadsheet			No	500.0 *
V-102	3 Phase Separator	18	24 43 22	No	500.0 *
TEE-100	Tee	24	26 25	No	500.0 *
TEE-101	Tee	27	29 28	No	500.0 *
TEE-102	Tee	39	41 40	No	500.0 *
C-100	Compressor	26 Q-C-100	27	No	500.0 *
C-101	Compressor	41 Q-C-101	4-0	No	500.0 *
MIX-100	Mixer	13 28	14	No	500.0 *
MIX-101	Mixer	1 29	2	No	500.0 *
MIX-102	Mixer	43 21	23	No	500.0 *
RCY-1	Recycle	14	R-1	No	3500 *
RCY-2	Recycle	R-2	7	No	3500 *
ADJ-1	Adjust			No	3500 *
T-100	Expander	40	42 Q-T-100	No	500.0 *
SET-2	Set			No	500.0 *
P-100	Pump	38 P1	30	No	500.0 *

Appendix E

Calculation of Carbon Efficiency

As outlined in Section 7.1 the Carbon efficiency is calculated from equation E.1 below.

$$\text{Carbon efficiency, (CE)} = \frac{\text{Carbon molecules in the final product}}{\text{Carbon molecles in natural gas feed}} \times 100\% \tag{E.1}$$

From the Unisim simulation the molar flow in $\frac{kmol}{h}$ can be obtained for all components in feed and product. In order to calculate the molecules of each component the relation in Equation E.2 was applied.

$$\text{Molecules of component i} = \text{Molar flow component i } \times 1000\frac{mol}{kmol} \times N_A \tag{E.2}$$

The carbon molecules for Equation E.1 is on mass basis and hence the number of molecules as calculated from Equation E.2 is to be multiplied with the molecular mass of the sum of carbon atoms in the respective component. The complete calculation procedure is illustrated for butane in Equations E.3, E.4 E.5 below.

Molar flow of C_4H_{10}: $17.5832\frac{kmol}{h}$
Number of C-atoms: 4

$$\begin{aligned} \mathrm{C_4H_{10}}\text{ molecules } &= 17.5382\ \frac{kmol}{h} \times 1000\ \frac{mol}{kmol} \times 6.023 \cdot 10^{23}\ \frac{molecules}{mol} \\ &= 5.025 \cdot 10^{27} \end{aligned} \tag{E.3}$$

$$\text{Molar mass of carbon atoms} = 4 \times 12 \frac{g}{mol} = 48 \frac{g}{molecule} \tag{E.4}$$

$$\begin{aligned} \text{Mass of carbon atoms} &= 1.06 \cdot 10^{28}\ \text{molecules} \times 48 \frac{g}{molecule} \\ &= 844\ \frac{kg}{h} \end{aligned} \tag{E.5}$$

This procedure is then carried out for all components and the carbon efficiency can be calculated by adding all these values in the feed and product stream respectively.

Appendix F

Calculation of Thermal Efficiency

As outlined in Section 7.1 the thermal efficiency was calculated after Equation F.1

$$\text{Thermal efficiency, (TE)} = \frac{\text{LHV of liquid final products}}{\text{LHV of natural gas feed}} \times 100\% \quad \text{(F.1)}$$

To be able to calculate the thermal efficiency, the lower heating value, LHV, for all components have to be calculated first. This is achieved by calculating the enthalpy of reaction when the respective component is combusted as shown in Equation F.2. When the LHV values is calculated it is multiplied with the respective molar flow of the component to get the LHV value in $\frac{kJ}{h}$

$$\text{Component } (i) + O_2 \rightarrow CO_2 + H_2O\ (g) \quad \text{(F.2)}$$

By summing up all LHV values for the components in feed and final product respectively, the thermal efficiency can be calcluated from Equation F.1

Below is a calculation example for obtaining the LHV value for butane: Stoichiometric combustion of butane is given by Equation F.3

$$C_4H_{10} + 6\frac{1}{2}O_2 \rightarrow 4CO_2 + 5H_2O(g) \quad \text{(F.3)}$$

This gives the following expression for the enthalpy of reaction:

$$\begin{aligned}\Delta H_{rxn} &= \sum \Delta H_{products} - \sum \Delta H_{reactants} \\ &= 4\Delta_f H^{\circ}_{298}(\mathrm{CO_2}) + 5\Delta_f H^{\circ}_{298}(\mathrm{H_2O}) \\ &- \Delta_f H^{\circ}_{298}(\mathrm{C_4H_{10}}) - 6\frac{1}{2}\Delta_f H^{\circ}_{298}(\mathrm{O_2}) \\ &= 4(-393.51) + 5(-241.814) - (-125.79) - 6\frac{1}{2}(0) \\ &= -2657.32\frac{kJ}{mol} \end{aligned} \tag{F.4}$$

From the Unisim simulation the molar flow of $\mathrm{C_4H_{10}}$ is reported to be $32.78\frac{kmol}{h}$. Multiplied with the enthalpy value obtained from Equation F.4 the LHV value of butane is found to be $-8.71 \cdot 10^{-7}\frac{kJ}{h}$

Appendix G

Optimizer in Unisim

This appendix list the complete changes, including changes in terms of numerical parameters such as tolerance and number of iterations, between each run for the optimizer. Table G.1 outlines the changes when flow to upgrading was applied as objective function while Table G.2 and Table G.3 outlines the changes when CE and TE were applied as objective functions respectively.

Table G.1 – Complete overview of the changes for the optimizer in Unisim when applied to flow to upgrading unit as objective function

Case	**Change from previous**
Optimizer base case	Based on case 8v2 from the case study optimization
1	number of iterations set to 100, tolerance set to 0.001, boundaries for optimization variables changed, see Table 8.4
2	tolerance set to 0.01
3	re-run
4	objective function changed to liquid volume flow at standard conditions
5	Number of iterations set to 200, tolerance set to $1 \cdot 10^{-5}$, maximum change per iteration set to 0.1, boundaries changes as shown in Table 8.4
6	Increased number of iterations and function evaluations to 500, lower bound reactor volume set to 1500
7	re-run
8	included temperature of boiling water to FTR in variables
9	re-run, adjust not solved
10	re-run, adjust not solved
11	re-run, adjust solved

Table G.2 – Complete overview of the changes for the optimizer in Unisim when applied to carbon efficiency as objective function

Case	Change from previous/Note
CE basecase	Based on case 11 from the product flow optimizer
CE2	tolerance set to $1 \cdot 10^{-5}$, maximum change per iteration set to 0.05
CE3	maximum iterations and function evalutaions set to 1200
CE4	tolerance set to $1 \cdot 10^{-6}$, maximum change per iteration set to 0.3

Table G.3 – Optimizer summary

Case	Change from previous
TE base case	Based on CE4 but tolerance set to $1 \cdot 10^{-5}$ and maximum change per iteration set to 0.1 in addition to the new bounds as given in Table
TE2	lower bounds as given in Table 8.8, penalty for $\frac{H_2}{CO}$ ratio set to 1000
TE3	Penalty value increased to 10000, tolerance set to $1 \cdot 10^{-4}$, maximum change per iteration set to 0.2
TE4	new start value for steam
TE5	New bounds for steam as given by Table 8.8, maximum change per iteration set to 0.3
TE6	maximum change per iteration set to 0.3
TE7	maximum change per iteration set to 0.5
Bypass	Liquid from V-101 bypassed V-102 and sent straight to upgrade, new bounds as given in Table 8.8, penalty value back to 50, tolerance set to $1 \cdot 10^{-5}$, maximum change per iteration set to 0.1

Appendix H

Composite curves

All values in Table H.1 and Table H.2 have been calculated based on values for the respective streams at the respective temperatures from Table 9.1 from section 9.1 in the main report.

The total enthalpy at each temperature was summed for the hot composite curve and plotted against the temperature resulting in Figure H.1. The same procedure was used to construct the cold composite curve as shown in Figure H.2

Table H.1 – Numerical basis for the construction of the hot composite curve

Temperature [°C]	$\mathbf{T_{interval}}$[°C]	$\mathbf{CP_{interval}}$ $[\frac{kW}{C}]$	$\mathbf{H_{interval}}$ [kW]	$\mathbf{H_{total}}$ [kW]
1030				443026.568
	806.2	395.27	318665.769	
223.8				124360.799
	185.8	669.33	124360.7986	
38				0

For the construction of the combined composite curve the hot composite curve was plotted as previously outlined and then the total enthalpy from Table H.1 at 1030 °C as starting point for the cold composite curve at 675 °C. From here the enthalpy for each temperature along the cold composite curve was obtained by deducting the cold enthalpy from the previous level, where the first level as mentioned was 443026.568 as given from Table H.1.

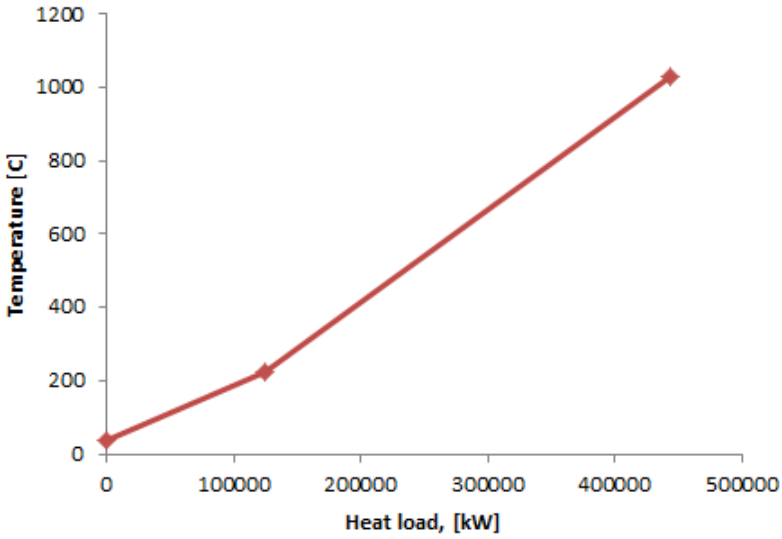

Figure H.1 – Plot of the hot composite curve, with temperature [°C] and heat-load [kW] on the vertical and horizontal axis respectively

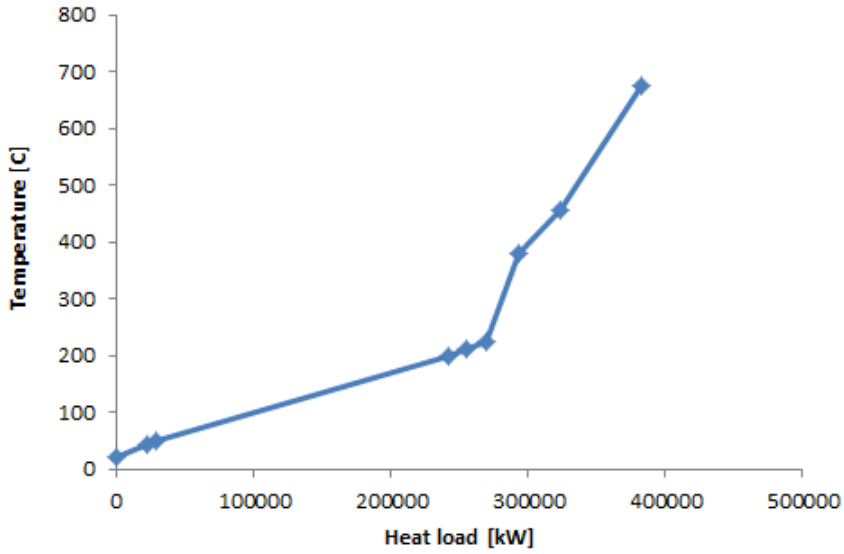

Figure H.2 – Plot of the cold composite curve, with temperature [°C] and heat-load [kW] on the vertical and horizontal axis respectively

Table H.2 – Numerical basis for the construction of the cold composite curve

Temperature [°C]	$\mathbf{T_{interval}}$[°C]	$\mathbf{CP_{interval}}$ $[\frac{kW}{C}]$	$\mathbf{H_{interval}}$ [kW]	$\mathbf{H_{total}}$ [kW]
675				382263.06
	220.00	266.10	58542.65	
455				323720.41
	74.89	414.14	31013.33	
380.11				292707.08
	156.31	148.04	23140.09	
223.80				269566.98
	13.80	1076.27	14852.57	
210				254714.42
	10.00	1353.58	13535.85	
200				241178.57
	151.60	1397.70	211892.10	
48.40				29286.47
	6.03	1249.66	7536.23	
42.37				21750.24
	22.37	972.35	21750.24	
20				0

This was done as the cascade indicated a threshold problem only needing a cold utility. The numerical values for this is outlined in Table H.3 and the curves are displayed in Figure H.3. The total cooling utility will be shown as the left over enthalpy for the last temperature.

Table H.3 – Numerical basis for the construction of the combined composite curve

Temperature [°C]	$\mathbf{T_{interval}}$[°C]	$\mathbf{CP_{interval}}$ $[\frac{kW}{C}]$	$\mathbf{H_{interval}}$ [kW]	$\mathbf{H_{total}}$ [kW]
675				443027
	220.00	266.10	58542.65	
455				384484
	74.89	414.14	31013.33	
380.11				353471
	156.31	148.04	23140.09	
223.80				330330
	13.80	1076.27	14852.57	
210				315478
	10.00	1353.58	13535.85	
200				301942
	151.60	1397.70	211892.10	
48.40				90050
	6.03	1249.66	7536.23	
42.37				82513.70
	22.37	972.35	21750.24	
20				60763.5

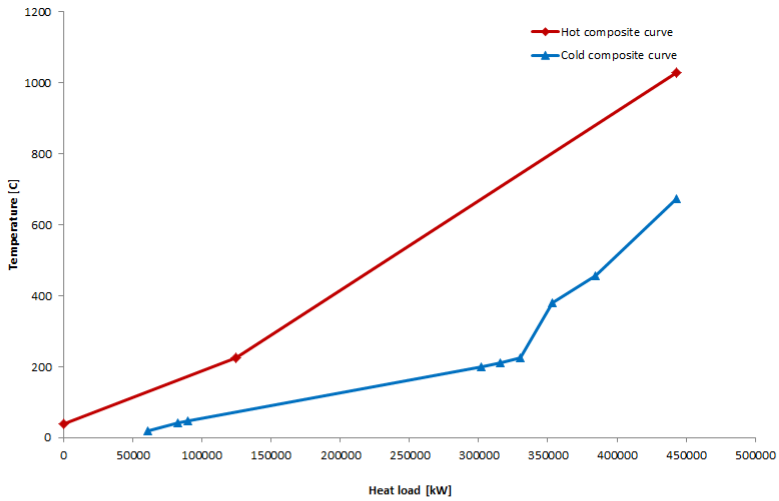

Figure H.3 – Plot of the combined composite curves for the pinch analysis for the GTL model simulated in Unisim. Temperature in °C is the unit for the vertical axis, while heat load in kW is given on the horizontal axis.

Appendix I

Calculation of heat exchanger area

The equation for the overall heat transfer coefficient is shown in Equation I.1

$$\frac{1}{U} = \frac{1}{h_o} + \frac{1}{h_{od}} + \frac{d_o\, ln\left(\frac{d_o}{d_i}\right)}{2k_w} + \frac{d_o}{d_i} \times \frac{1}{h_{id}} + \frac{d_o}{d_i} \times \frac{1}{h_i} \tag{I.1}$$

The inner and outer dirt coefficients, h_{od} an h_{id}, are set to zero in Unisim by default and were neglected in this work due to simplicity. Consequently Equation I.1 is now on the form shown in Equation I.2

$$\frac{1}{U} = \frac{1}{h_o} + \frac{d_o\, ln\left(\frac{d_o}{d_i}\right)}{2k_w} + \frac{d_o}{d_i} \times \frac{1}{h_i} \tag{I.2}$$

The thermal conductivity of the tube wall material and the inner and outer tube diameter are found directly from the rating page of the heat exchnagers in Unisim. These values are the default set by Unisim and this was not altered at any point. Table I.1 lists all the default values taken from unisim for this calculation.

Hence this leaves two unknown parameters in Equation I.2, h_o and h_i. These are the outside and inside fluid film coefficients and need to be calculated.

I.0.6 Outer film fluid coefficient

Calculation of this parameter was done after Kern's method [90]. First the cross-flow area of the hypothetical row of tubes at the shell equator is calculated as given in Equation I.3. D_s is the shell inside diameter, l_B is the baffle spacing and p_t is the tube pitch. all are found on the rating page of the heat exchanger in Unisim, and are the default ones set by Unisim. The specific default values are listed in Table I.1

$$A_s = \frac{(p_t - d_o)D_s l_B}{p_t} \tag{I.3}$$

Next the shell side mass velocity, G_s was calculated by dividing the fluid flow rate on the shell side by the cross flow area calculated in Equation I.3. This is shown in Equation I.4

$$G_s = \frac{W_s}{A_s} \tag{I.4}$$

Then the linear velocity was calculated as indicated by Equation I.5

Next the shell side equivalent diameter must be calculated and this is a function of the tube arrangement. A equilateral triangle pitch arrangement was chosen and gives the relationship in Equation I.6 for the calculation of the equivalent diameter.

$$u_s = \frac{G_s}{\rho} \tag{I.5}$$

$$d_e = \frac{1.10}{d_o}(p_t^2 - 0.917 d_o^2) \tag{I.6}$$

Now the Reynolds number can be calculated from Equation I.7.

$$Re = \frac{G_s d_e}{\mu} = \frac{u_s d_e \rho}{\mu} \tag{I.7}$$

The relationship for the caluclation of the Nusselt number as shown in Equation I.8 can consequently be used to calculate the outer film fluid coefficient.

$$Nu = \frac{h_s d_e}{k_f} = j_h Re Pr^{0.33} \left(\frac{\mu}{\mu_w}\right)^{0.14} \tag{I.8}$$

The last part of Equation I.8 is a viscosity correction term this was omitted from teh equation due to simplicity. Even though this is left out

of the equation there are still three unknown parameter in Equation I.8, j_h, k_f and Pr.

The thermal conductivity of the shell side fluid, k_f is obatined from Unisim while the Prandlt number and heat transfer factor, j_h must be calculated. The Prandtl number is given by Equation I.9 and all values are obatined from the respective stream in Unisim.

$$Pr = \frac{C_p \mu}{k_f} \tag{I.9}$$

Normally the heat transfer factor is read of a table, but due to the need of constant updating in the iterations in Unisim a relation was needed for this parameter. The one shown in Equation I.10 were used, again neglecting the viscosity correction term.

$$j_h = StPr^{0.67} \left(\frac{\mu}{\mu_w} \right)^{-0.14} \tag{I.10}$$

For this equation the Stanton, St, number is needed and is calculated by the use of Equation I.11 and E is given by Equation I.12

$$St = ERe^{-0.205} Pr^{-0.505} \tag{I.11}$$

$$E = 0.0225 \exp(-0.0225(lnPr)^2) \tag{I.12}$$

By then inserting the values for Re, Pr, equivalent diameter, thermal conductivity of fluid and heat transfer factor in Equation I.8, the outer film transfer coefficient can be found.

Table I.1 – Default values from unisim used in the calculation of the heat exchanger area.

Parameter	Default value [mm]
d_o	20
d_i	16
D_s	739.05
l_B	800
p_t	50

I.0.7 Inner film fluid coefficient

The inner film fluid coefficient, h_i can also be calculated based on Equation I.8. For the inner film coefficient and neglecting the viscosity correction term, it can be written as in Equation I.13

$$\frac{h_i d_i}{k_f} = j_h RePr^{0.33} \tag{I.13}$$

As for the outer film coefficient the linear velocity is needed when calculating the Reynolds number as shown in Equation I.7. This is calculated by dividing the fluid mass velocity by the fluid density as outlined in Equation I.5. However the mass velocity is a function of the cross sectional flow area as given by Equation I.4. This calculation is done a bit differently for the tube side than it was on the shell side. The total flow area is equal to the number of tubes times the cross sectional area per tube.

Equation I.14 gives the cross sectional area of each tube.

$$A_t = \frac{\pi}{4} \times d_i^2 \tag{I.14}$$

In each heat exchanger the number of tube passes per shell was set to two by default and the total number of tubes set to 160. This gives 80 tubes per pass and hence the total flow area is given by Equation I.15

$$\text{Total flow area} = 80 \times \frac{\pi}{4} \times d_i^2 \tag{I.15}$$

By the same procedure as for the inner film coefficient the Prandtl number can be calculated for the tube side by inserting values from the respective stream in Unisim. This enables the calculation of the Stanton number on the tube side and consequently the heat transfer factor, j_h. Inserting these values in Equation I.13 gives the inner film fluid coefficient.

By calculating h_i and h_o the overall heat transfer coeffiient can be calculated from Equation I.2 and the heat exchanger area can be found by dividing the value for UA, given by Unisim.

Appendix J

Result multi variable economic optimization

Table J.1 gives the data resulting from the multivariable case study for the econmics.

Table J.1 – Data obtained through the multi variable case study for economic optimization

Reactor volume [m^3]	Oxygen[$\frac{kmol}{h}$]	Steam[$\frac{kmol}{h}$]	Production cost [$\frac{USD}{bbl}$]
1200	7000	5331.86752096054	18.0873305257247
1200	7000	5306.89584997468	18.1271184107054
1200	7000	5303.29510046274	17.9539794594521
1200	7000	5307.36426727102	18.0695635105403
1200	7000	5334.94330084251	18.1695954501845
1200	7000	5280.30036509676	17.805431488331
1200	7000	5307.44396352012	17.9916717665863
1200	7000	5315.93779860787	18.2554965217841
1200	7000	5326.48139798788	18.1788086796692
1200	7300	5259.77605966441	17.4900328967578
1200	7300	5310.32491350151	18.0020273423884
1200	7300	5247.43188203358	16.0365529059081
1200	7300	5313.54562260899	18.0083452231577
1200	7300	5313.80056602966	18.0223594486748
1200	7300	5274.40094777028	17.6588865983933
1200	7300	5293.97734045282	17.9158305785465
1200	7300	5351.0574496327	18.2776796478578
1200	7300	5343.81632524825	18.1861559127729
1200	7600	5279.51372429104	17.8249067031741
1200	7600	5349.63034038824	18.0245282523507
1200	7600	5338.1446080803	18.0275882292833
1200	7600	5311.8733716642	17.9280337604269
1200	7600	5353.12922829132	18.0922896581852
1200	7600	5228.27814364178	17.4402559876671
1200	7600	5294.51526047883	17.8400426273258
1200	7600	5356.16972701213	18.1995720716046
1200	7600	5330.7919766183	17.9724249776307
1200	7900	5308.43062875241	17.6692660427164
1200	7900	5347.54713357894	17.9766368654161
1200	7900	5289.20470089388	17.6608258045775
1200	7900	5299.85738513723	17.7803363960996
1200	7900	5287.27103138187	17.5807445501007
1200	7900	5235.22215747228	17.3857261848242
1200	7900	5310.32107341383	17.7772863271627
1200	7900	5353.69254068909	18.0512589965699
1200	7900	5287.63481935257	17.5471984862114
1200	8200	5289.1234685435	17.6064494991606
1200	8200	5297.47274268671	17.7787885943054
1200	8200	5283.49311516814	17.5867761846169
1200	8200	5311.12929098078	17.8010849713767
1200	8200	5343.11328581729	17.8886332316106
1200	8200	5284.56023654878	17.4963953463729
1200	8200	5308.5496132631	17.6984196532361
1200	8200	5301.75659185541	17.7483205115676
1200	8200	5301.75659185541	17.6407996162017
1200	8500	5347.02148858417	17.7554804583085
1200	8500	5341.376195125	17.7997451877341
1200	8500	5283.8812540983	17.4908074357401
1200	8500	5307.70595564979	17.6199000997163
1200	8500	5299.12062580385	17.4103368472343
1200	8500	5283.88909609325	17.3898229013281
1200	8500	5287.42062082282	17.4069301862947
1200	8500	5264.96257181097	17.4233765653895
1200	8500	5348.19417238952	17.864420297855

Reactor volume [m^3]	Oxygen[$\frac{kmol}{h}$]	Steam[$\frac{kmol}{h}$]	Production cost [$\frac{USD}{bbl}$]
1200	8800	5308.36217888988	17.5245689175145
1200	8800	5254.12619348378	17.4056090273657
1200	8800	5339.01143302718	17.7389407152242
1200	8800	5282.46226764397	17.29367147119
1200	8800	5298.63731945811	17.3342565823118
1200	8800	5284.50534977072	17.3158256733466
1200	8800	5312.53247042082	17.5526150230174
1200	8800	5380.32739939502	17.9596940103639
1200	8800	5324.09549782749	17.6853097644049
1400	7000	5179.53177071598	16.9506060292602
1400	7000	5170.5156572162	16.8517645112649
1400	7000	5173.9200251665	16.9252512161992
1400	7000	5182.43789733897	16.9420978895244
1400	7000	5128.11936247741	16.7231759805372
1400	7000	5163.26213105445	16.9248102702113
1400	7000	5147.92755290374	16.7966008308491
1400	7000	5181.00114274561	16.9555502652457
1400	7000	5176.7379375428	16.9149678459155
1400	7300	5155.30141419571	16.6366341301503
1400	7300	5163.25154467954	16.7298583007607
1400	7300	5170.20458077663	16.7938950236489
1400	7300	5181.78632830669	16.9062227834173
1400	7300	5188.64941479013	16.8927560694918
1400	7300	5164.71685406376	16.8313422661477
1400	7300	5169.66547384918	16.7745628662125
1400	7300	5193.14545299003	17.0448422318039
1400	7300	5186.11401474218	16.9069870499856
1400	7600	5279.51372429104	17.1790161227724
1400	7600	5349.63034038824	17.5787855529464
1400	7600	5201.34628928499	16.7657152510003
1400	7600	5183.13007010165	16.7970990194948
1400	7600	5183.09076090447	16.8508524759904
1400	7600	5167.70059868978	16.7604952525249
1400	7600	5159.03712485985	16.5773384459003
1400	7600	5195.563773038	17.0010778377062
1400	7600	5170.39049184561	16.7960614777427
1400	7900	5175.87588727205	16.6884322299606
1400	7900	5180.74755645906	16.82020282877
1400	7900	5175.29572031906	16.7444002187559
1400	7900	5182.29079165368	16.7649481193852
1400	7900	5178.36385000438	16.6908299064824
1400	7900	5166.66460142846	16.6774239186507
1400	7900	5176.52038846529	16.7554068633796
1400	7900	5176.00054831904	16.7042865665806
1400	7900	5176.88901221449	16.7314326884962
1400	8200	5182.68025306766	16.6952175212807
1400	8200	5186.78507094469	16.6420463656306
1400	8200	5177.8160268712	16.7264153995637
1400	8200	5182.37673432569	16.7000062416992
1400	8200	5186.76914579293	16.7370018194059
1400	8200	5179.15298240958	16.7153430351307
1400	8200	5184.6877935003	16.7251029435209
1400	8200	5301.75659185541	17.153276646966
1400	8200	5169.63590705616	16.5358106263719

Reactor volume [m^3]	Oxygen[$\frac{kmol}{h}$]	Steam[$\frac{kmol}{h}$]	Production cost [$\frac{USD}{bbl}$]
1400	8500	5183.87104389782	16.5340810942069
1400	8500	5181.74679169807	16.590189224374
1400	8500	5185.3175775288	16.6353546785676
1400	8500	5181.01659270059	16.6613069053229
1400	8500	5178.3771417918	16.6465367231694
1400	8500	5175.7987657814	16.6214309703069
1400	8500	5166.07560120359	16.5514847687939
1400	8500	5264.96257181097	17.0264815058681
1400	8500	5234.71898341839	16.8342844181253
1400	8800	5177.75899477324	16.4839938509332
1400	8800	5192.88922626031	16.6702318124888
1400	8800	5198.41820612459	16.7180155292624
1400	8800	5175.36910422211	16.5648462711028
1400	8800	5181.32267957382	16.6070836431692
1400	8800	5179.93659179046	16.553636880055
1400	8800	5186.32096746356	16.6260608968428
1400	8800	5167.9739383843	16.5123983024927
1400	8800	5196.17042763305	16.6952417458741
1600	7000	5105.23513185419	16.5555172345017
1600	7000	5114.01462051398	16.6705033336535
1600	7000	5173.9200251665	16.8177550758054
1600	7000	5108.14857468642	16.6829358827724
1600	7000	5095.70521183244	16.5396583717822
1600	7000	5115.29886526726	16.6998621065091
1600	7000	5107.11309845451	16.6187338238125
1600	7000	5105.27236933838	16.5393719609985
1600	7000	5116.00383252769	16.6359448316866
1600	7300	5109.2830887425	16.6232130949601
1600	7300	5120.31119438594	16.5382042306624
1600	7300	5114.42577886983	16.6336360313351
1600	7300	5109.3262691122	16.6606328681343
1600	7300	5112.32393090704	16.6437782213544
1600	7300	5116.49215164906	16.6249317679155
1600	7300	5117.16301022447	16.6308856250482
1600	7300	5105.67477404593	16.6673103102628
1600	7300	5109.60080842069	16.495025003999
1600	7600	5279.51372429104	17.0856446751012
1600	7600	5349.63034038824	17.418872649583
1600	7600	5201.34628928499	16.772147079979
1600	7600	5122.88078018519	16.6060943629151
1600	7600	5115.86888266902	16.6376632578551
1600	7600	5118.75505629075	16.6122506459702
1600	7600	5118.13969518082	16.5637678567046
1600	7600	5119.30637768475	16.625101989331
1600	7600	5114.52314152957	16.6026805187025
1600	7900	5125.35893171763	16.5904305194098
1600	7900	5122.11271744054	16.5817178655972
1600	7900	5131.37519186416	16.6241128839023
1600	7900	5182.29079165368	16.7359137095001
1600	7900	5125.1172954604	16.5679400558485
1600	7900	5166.66460142846	16.6505292583978
1600	7900	5127.92512094329	16.6122148409042
1600	7900	5125.80490935182	16.6032671687706
1600	7900	5126.47444329302	16.585282238297

Reactor volume [m^3]	Oxygen[$\frac{kmol}{h}$]	Steam[$\frac{kmol}{h}$]	Production cost [$\frac{USD}{bbl}$]
1600	8200	5132.03827022984	16.5919306124033
1600	8200	5131.9003921281	16.5749726955202
1600	8200	5130.28211954203	16.5940092024659
1600	8200	5134.06389637224	16.5802299969179
1600	8200	5125.20183755823	16.4778475059524
1600	8200	5130.6909241177	16.5957366031936
1600	8200	5131.60775827174	16.5065614180401
1600	8200	5301.75659185541	17.1096952346473
1600	8200	5127.90899662341	16.5332385276603
1600	8500	5125.89482269328	16.5529892945386
1600	8500	5142.22146310494	16.5472351516399
1600	8500	5139.15750819967	16.5830611475325
1600	8500	5137.31658568623	16.5790521443457
1600	8500	5142.97063753111	16.5632743996656
1600	8500	5175.7987657814	16.5962587403574
1600	8500	5137.53281290182	16.5701763225181
1600	8500	5264.96257181097	16.8899876178411
1600	8500	5234.71898341839	16.7815127771808
1600	8800	5144.52648966719	16.5688861767495
1600	8800	5135.12715981559	16.5182738995649
1600	8800	5129.5747158293	16.5823067782844
1600	8800	5142.83210629842	16.5392440274736
1600	8800	5148.14637979397	16.5553788793217
1600	8800	5147.12305462452	16.5436813351152
1600	8800	5148.72537115915	16.5579635103278
1600	8800	5143.46170086615	16.5233453761459
1600	8800	5130.42059779161	16.5240062534387
1800	7000	5092.46954686974	16.8257382732263
1800	7000	5091.86336545466	16.8532712335595
1800	7000	5173.9200251665	17.0889354972955
1800	7000	5097.34433905459	16.8668852132737
1800	7000	5083.99145626615	16.8573038131308
1800	7000	5101.61409216161	16.8827728821047
1800	7000	5094.2837904866	16.8238007774213
1800	7000	5092.24808768053	16.8236408044577
1800	7000	5097.8866434812	16.8494393709525

Bibliography

[1] BP. Bp statistical review of world energy june 2012. June 2012.

[2] International Energy Agency and (IEA). World energy outlook 2010. 2010.

[3] Steve Sorrell, Jamie Speirs, et al. Global oil depletion: A review of the evidence. *Energy Policy*, 38(9):5290 – 5295, 2010. Special Section on Carbon Emissions and Carbon Management in Cities with Regular Papers.

[4] Rajab Khalilpour and I.A. Karimi. Evaluation of utilization alternatives for stranded natural gas. *Energy*, 40(1):317 – 328, 2012.

[5] Jerome Ellepola, Nort Thijssen, et al. Development of a synthesis tool for gas-to-liquid complexes. *Computers & Chemical Engineering*, 42(0):2 – 14, 2012. European Symposium of Computer Aided Process Engineering - 21.

[6] Magne Hillestad Ahmad Rafiee. Optimal design and operation of a gas-to-liquid process. *Chemical Engineering Transactions*, 21:1393–1398, 2010.

[7] X. Hao, M. Djatmiko, et al. Simulation analysis of a gtl process using aspen plus. *Chemical Engineering & Technology*, 31(2):188–196, 2008.

[8] Bipin Patel. Gas monetisation: A techno-economic comparison of gas-to-liquid and lng. Technical report, Foster Wheeler Energy Limited, 2005.

[9] R. Guettel, U. Kunz, et al. Reactors for fischer-tropsch synthesis. *Chemical Engineering & Technology*, 31(5):746–754, 2008.

[10] Buping Bao, Mahmoud M. El-Halwagi, et al. Simulation, integration, and economic analysis of gas-to-liquid processes. *Fuel Processing Technology*, 91(7):703 – 713, 2010.

[11] David A. Wood, Chikezie Nwaoha, et al. Gas-to-liquids (gtl): A review of an industry offering several routes for monetizing natural gas. *Journal of Natural Gas Science and Engineering*, 9(0):196 – 208, 2012.

[12] Mike Nel. Gtl - a window of opportunity. `http://www.sasol.com/sites/default/files/presentations/downloads/GTL_A_Window_Opportunity_XTLConference_London_7%2520June2011_1308044026713.pdf`, 2011.

[13] Mark E Dry. The fischer tropsch process: 1950-2000. *Catalysis Today*, 71:227 – 241, 2002.

[14] David Wood and Saeid Mokhatab. Gas monetization technolgies remain tantalizingly on the brink. *World Oil*, 229(1), January 2008.

[15] Alternative Fuels Data Center. Natural gas fuel basics. `http://www.afdc.energy.gov/fuels/natural_gas_basics.html`, 2013.

[16] Statoil. What is natural gas? `http://www.statoil.com/en/OurOperations/Gas/Pages/AboutNaturalGas.aspx`, 2012.

[17] NaturalGas.Org. Background. `http://naturalgas.org/overview/background.asp`.

[18] Vivek Chandra. Gas formation. `http://www.natgas.info/html/gasformation.html`.

[19] National Geographic Education. Natural gas. `http://education.nationalgeographic.com/education/encyclopedia/natural-gas/?ar_a=1`.

[20] A. Rojey et. al. *Natural Gas: Production, Processing, Transport*. Institut Francais du Petrole Publications, 1997.

[21] NaturalGas.Org. Unconventional natural gas resources. `http://www.naturalgas.org/overview/unconvent_ng_resource.asp`.

[22] Vivek Chandra. What is natural gas? http://www.natgas.info/html/whatisnaturalgas.html.

[23] Resources. http://naturalgas.org/overview/resources.asp.

[24] Country comparison :: Natural gas - proved reserves. https://www.cia.gov/library/publications/the-world-factbook/rankorder/2253rank.html.

[25] IndexMundi. Natural gas - proved reserves - world. http://www.indexmundi.com/map/?t=0&v=98&r=xx&l=en, 2012.

[26] Dr. Xiuli Wang. Marine cng trade: The time has come. http://www.coselle.com/resources/news/marine-cng-trade-time-has-come, March 2011.

[27] Dong Lichun, Wei Shun'an, et al. Gtl or lng: Which is the best way to monetize "stranded" natural gas. *Pet. Sci.*, 5:388–394, 2008.

[28] Center For Liquefied Natural Gas. Basics. http://www.lngfacts.org/about-lng/basics/.

[29] MEO Australia. About lng.

[30] J.S. Gudmundsson and M. Mork. Stranded gas to hydrate for storage and transport. http://www.ipt.ntnu.no/~ngh/library/paper11/Amsterdam2001Stranded.htm, November 2001.

[31] Mehdi Panhi, Ahmad Rafiee, et al. A natural gas to liquid process model for optimal operation. *Industrial & Engineering Chemistry Research*, 51:425–433, 2012.

[32] P.L. Spath and D.C. Dayton. Preliminary screening - technical and economic assessment of synthesis gas to fuels and chemicals with emphasis on the potential for biomass-derived syngas. Technical report, National Renewable Energy Laboratory, 2003.

[33] Yong Heon Kim, Ki-Won Jun, Hyunku Joo, Chonghun Han, and In Kyu Song. A simulation study on gas-to-liquid (natural gas to fischerï£ · ï£ · ï£ · tropsch synthetic fuel) process optimization. *Chemical Engineering Journal*, 155(1ï£ · ï£ · ï£ · 2):427 – 432, 2009.

[34] Energy Tribune. Compressed natural gas: Monetizing stranded gas. October 2007.

[35] Global Economic Monitor (GEM) Commodities. World data bank. http://databank.worldbank.org/data/views/variableselection/selectvariables.aspx?source=global-economic-monitor-(gem)-commodities#, 2013.

[36] Gas2. Stranded gas. http://www.gas-2.com/applications/stranded-gas/.

[37] The National Archives. The blockade of germany. http://www.nationalarchives.gov.uk/pathways/firstworldwar/spotlights/blockade.htm.

[38] (NETL) The National Energy Technology Laboratory. Introduction to gasification - history of gasification. http://www.netl.doe.gov/technologies/coalpower/gasification/gasifipedia/1-introduction/1-2-2_history-liquid-fuels.html.

[39] James G. Speight. Chapter 8 - hydrocarbons from synthesis gas. In *Handbook of Industrial Hydrocarbon Processes*, pages 281 – 323. Gulf Professional Publishing, Boston, 2011.

[40] (NETL) The National Energy Technology Laboratory. Supporting technologies. http://www.netl.doe.gov/technologies/coalpower/gasification/gasifipedia/5-support/5-11_ftsynthesis.html.

[41] EIA U.S Energy Information Administration. South africa. Technical report, U.S Energy Information Administration, EIA, January 2013.

[42] Sunita Dubey. Coal-to-liquids (ctl) - misplaced solution for oil starved world.

[43] South africa - the economy. http://www.mongabay.com/reference/country_studies/south-africa/ECONOMY.html.

[44] The Bancroft Library. Slaying the dragon of debth, fiscal politics &policy from the 1970s to the present: Oil crisis 1973-74. http://bancroft.berkeley.edu/ROHO/projects/debt/oilcrisis.html.

[45] Catherine Barnes. International isolation and pressure for change in south africa. *Accord*, pages 36–39, 2008.

[46] Kevin Halstead. Oryx gtl from conception to reality. *Nitrogen+Syngas*, 292:43–50, March-April 2008.

[47] H. Alfadala, G.V. Rex Reklaitis, et al., editors. *Shell GTL, from Bench scale to World scale*, 1st annual Gas Processing Symposium. Elsevier, 2009.

[48] Shell. Pearl gtl - an overview.

[49] Sasol. Sasol annual review 2005. `http://www.sasol.com/sasol_internet/downloads/sasol_ar_2005_review_1129643198214.pdf`, 2005.

[50] T.H. Fleisch, R.A. Sills, et al. 2002 - emergence of the gas-to-liquids industry: a review of global gtl developments. *Journal of Natural Gas Chemistry*, 11:1–14, 2002.

[51] Kevin Halstead. Oryx gtl - a case study. *Petrochemicals*, pages 34–36, 2006.

[52] Sasol. Sasol facts 2011 - your blueprint to the world of sasol. `http://www.sasol.com/sasol_internet/downloads/11029_Sasol_Facts_2011_1309786765289.pdf`.

[53] Ahmad Rafiee. *Optimal design issues of a gas-to-liquid process*. PhD thesis, Norwegian University of Science and Technology, 2012.

[54] Hydrocarbons-technology.com. Escravos gas-to-liquids project, niger delta, nigeria.

[55] K. Aasberg-Petersen, T S. Christensen, et al. Recent developments in autothermal reforming and pre-reforming for synthesis gas production in gtl applications. *Fuel Processing Technology*, 83:253 – 261, 2003. Advances in {C1} Chemistry in the Year 2002.

[56] Haldor TopsÃÿe. Prereforming catalyst. `http://www.topsoe.com/business_areas/synthesis_gas/~/media/PDF%20files/Prereforming/Topsoe_%20prereforming%20_cat_%20brochure.ashx`.

[57] Mehdi Panahi, Sigurd Skogestad, et al. Steady state simulation for optimal design and operation of a gtl process. In Farid Benyahia and Fadwa Eljack, editors, *Proceedings of the 2nd Annual Gas Processing Symposium*, pages 275 – 285. Elsevier, Amsterdam, 2010.

[58] Sarah LÃűgdberg and Hugo A. Jakobsen. Natural gas conversion. the reforming and fischer-tropsch processes.

https://www.google.no/url?sa=t&rct=j&q=&esrc=s&source=web&cd=3&cad=rja&ved=0CEMQFjAC&url=http%3A%2F%2Fwww.nt.ntnu.no%2Fusers%2Fjakobsen%2FTKP4145%2FNatural_Gas_Conversion.doc&ei=r72UUf_CDsbasgbogoCwDQ&usg=AFQjCNHG8O2EuiXYI9Ejiu5pSbrF9tDbIQ&sig2=GPize-UnMHThsx9cObz--A&bvm=bv.46471029,d.Yms.

[59] D.J Wilhelm, D.R Simbeck, et al. Syngas production for gas-to-liquids applications: technologies, issues and outlook. *Fuel Processing Technology*, 71:139 – 148, 2001. Fuel science in the year 2000: Where do we stand and where do we go from here.

[60] Lars J Christiansen Jens Rostrup-Nielsen. *Concepts in Syngas Manufacture*. Imperial College Press, July 2011.

[61] Hydrogen production and purification. http://www.eajv.ca/english/h2, 2012.

[62] A. Rafiee and M. Hillestad. Synthesis gas production configurations for gas-to-liquid applications. *Chemical Engineering & Technology*, 35(5):870–876, 2012.

[63] Anton C Vosloo. Fischer tropsch: a futuristic view. *Fuel Processing Technology*, 71:149 – 155, 2001. Fuel science in the year 2000: Where do we stand and where do we go from here.

[64] Roads2hycom. On-site hydrogen generators from hydrocarbons. http://www.ika.rwth-aachen.de/r2h/index.php/On-site_Hydrogen_Generators_from_Hydrocarbons.

[65] H. A. Wright, J. D. Allison, et al. Conocophillips gtl technology: The copoxâĎć process as the syngas generator. *American Chemical Society*, 48:791–792, 2003.

[66] Ib DybkjÃęr. Synthesis gas technology. *Hydrocarbon Engineering*, July 2006.

[67] Per K. Bakkerud. Update on synthesis gas production for gtl. *Catalysis Today*, 106:30–33, 2005.

[68] Henrik Surrow Larsen. Heat exchange reforming in gas synthesis. *Gas*, page 1, 2012.

[69] Hadi Ebrahimi, Alireza Behroozsarand, et al. Arrangement of primary and secondary reformers for synthesis gas production. *Chemical Engineering Research and Design*, 88(10):1342 – 1350, 2010.

[70] Lurgi GmbH. Lurgi megamethanol. `http://lurgi.com/website/fileadmin/user_upload/1_PDF/1_Broshures_Flyer/englisch/0312e_MegaMethanol.pdf`, 2010.

[71] DeVan, J.H. Tortorelli, et al. Carbon formation and metal dusting in advanced coal gasification processes - 1997. 1997.

[72] H.J. Grabke, R. Krajak, et al. Metal dusting of high temperature alloys. *Materials and Corrosion*, 44(3):89–97, 1993.

[73] A. AgÃijero, M. GutiÃIrrez, et al. Metal dusting protective coatings. a literature review. *Oxidation of Metals*, 76(1-2):23–42, 2011.

[74] C. M Chun, F. Hershkowitz, et al. *Materials Challenges in Syngas Production From Hydrocarbons*, pages 129–142. John Wiley & Sons, Inc., 2008.

[75] Hilde Venvik. Metal dusting corrosion initiation in conversion of natural gas to synthesis gas. In *2nd Trondheim Gas Technology Conference*, 2011.

[76] Y.Nishiyama et. al. Improved metal dusting resistance of new sumitomo 696 ni-base alloy for synthesis gas environments. In *Nitrogen+Syngas 2011 International Conference*, pages 129–138, 2011.

[77] Hilde Venvik. Personal communication.

[78] M.L. Holland and H.J. De Bruyn. Metal dusting failures in methane reforming plant. *International Journal of Pressure Vessels and Piping*, 66:125 – 133, 1996.

[79] Ben Jager. Fischer-tropsch reactors. *AICHE Mtg*, 2003.

[80] B Jager. Development of fischer tropsch reactors. In *Prepared for Presentation at the AIChE 2003 Spring National Meeting, New Orleans, LA*, 2003.

[81] Hans Schulz. Short history and present trends of fischer tropsch synthesis. *Applied Catalysis A: General*, 186:3 – 12, 1999.

[82] PhD Iraj Isaac Rahmim. Gas–to–liquid technologies: Recent advances, economics, prospects. In *26th IAEE Annual International Conference PragueâĂŤJune 2003*, 2003.

[83] I Puskas and R.S Hurlbut. Comments about the causes of deviations from the anderson-schulz-flory distribution of the fischer-tropsch reaction products. *Catalysis Today*, 84:99 – 109, 2003. Syngas Generation and Conversion to Fuels and Chemicals, {AIChE} Spring Meeting.

[84] Arend Hoek. The shell gtl process: Towards a world scale project in qatar: the pearl project. In *DGMK-Conference âĂIJSynthesis Gas ChemistryâĂİ October 4-6, 2006, Dresden*, 2006.

[85] Honeywell. *Simulation Basis Reference Guide*. November 2010.

[86] Magne Hillestad. Modelling the fischer-tropsch product distribution and model implementation. *Unpublished*, -:–, 2011.

[87] Robin Smith. *Chemical Process Design and Integration*. Wiley, 2008.

[88] Honeywell. *UniSim Design Operations Guide*. 2010.

[89] Gordon Aylward & Tristan Findlay. *SI Chemical Data*. Wiley, 6th edition, 2008.

[90] Ray Sinnott and Gavin Towler. *Chemical Engineering Design*. Elsevier, 2009.

[91] Max S. Peters, Klaus Timmerhaus, et al. *Plant Design and Economics for Chemical Engineers*. McGraw Hill, 5th edition, 2003.

[92] Richard Turton; Richard C. Bailie; Wallace B. Whiting; Joseph A. Shaeiwitz; Debangsu Bhattacharyya. *Analysis, Synthesis and Design of Chemical Processes*. Prentice Hall, 4th edition, 2012.

[93] S.M Walas. *Chemical Process Equipment - Selection and Design*. Elsevier, 1990.

[94] Gavin P. Towler and Raymond K. Sinnott. *Chemical Engineering Design: Principles, Practice, and Economics of Plant and Process Design*. Elsevier, 2013.

[95] (Statoil) Jostein Sogge. personal communication.

[96] https://www.dnb.no/bedrift/markets/valuta-renter/valutakurser-og-renter/historiske/hovedvalutaer/2013.html.

[97] Charles Butcher. Economic indicators. *Chemical Engineering*, 120(4):71–71, 2013. Copyright - Copyright Access Intelligence LLC Apr 2013; Last updated - 2013-05-04; DOI - 2958085271; 77849972; 29283; CEG; INODCEG0008525981.

[98] E.G. Derouane, Valentin Parmon, et al. *Sustainable Strategies ofor the Upgrading of Natural Gas: Fundamentals, Challenges and Opportunities: Proceedings of the NATO Advanced Study Institute, Held in Vilamoura, Portugal, July 6 - 18, 2003*. Springer, 2005.

[99] Chemlink Australia Acted Consultants. Gas to liquids.

[100] (IEA) International Energy Agency. Natural gas weekly update. http://www.eia.gov/naturalgas/weekly/#tabs-prices-1, 2013.

[101] Edd Blekkan. Personal communication.

[102] London Metal Exchange. Minor metals. http://www.lme.com/metals/minor-metals/, June 2013.

[103] Magne Hillestad. Personal communication.

[104] EIA US Energy Information Administration. Electric power monthly :table 5.3. average retail price of electricity to ultimate customers:. March 2013.